

Hepatocyte-specific role of the deubiquitinating enzyme OTUB1 during inflammatory liver diseases

Dissertation

zur Erlangung des akademischen Grades

doctor rerum naturalium

(Dr. rer. nat.)

genehmigt durch die Fakultät für Naturwissenschaften
der Otto-von-Guericke Universität Magdeburg

von: M. Sc. Josephin Koschel

geboren am: 12.12.1990 in Schönebeck (Elbe)

Gutachter: Prof. Dr. med. Dirk Schlüter
Prof. Dr. rer. nat. Hans-Willi Mittrücker

eingereicht am: 23.06.2020

verteidigt am: 18.12.2020

PUBLICATIONS

Schmid U, Stenzel W, Koschel J, Raptaki M, Wang X, Naumann M, Matuschewski K, Schlüter D, Nishanth G. (2016) The Deubiquitinating Enzyme Cylindromatosis Dampens CD8⁺ T Cell Responses and Is a Critical Factor for Experimental Cerebral Malaria and Blood-Brain Barrier Damage. *Front Immunol.* Feb 1;8:27. doi: 10.3389/fimmu.2017.00027.

Kummer A, Nishanth G, Koschel J, Klawonn F, Schlüter D, Jänsch L. (2016) Listeriosis downregulates hepatic cytochrome P450 enzymes in sublethal murine infection. *Proteomics Clin Appl.* Oct;10:1025-1035. doi: 10.1002/prca.201600030.

ABSTRACT

Both infectious and sterile liver inflammation may trigger death of the hepatocytes. In particular, in acute hepatitis, liver failure may develop due to an excessive hepatocellular death as a consequence of an imbalanced survival and death signaling. Both survival and death signaling are tightly regulated by post-translational modifications, including ubiquitination and deubiquitination. Here, we investigated the hepatocyte-specific function of the deubiquitinating enzyme OTUB1 during infection with the intracellular bacterium *Listeria monocytogenes* and acute liver injury induced by DGal/TNF using conditional OTUB1 knockout mice (OTUB1^{LPC-KO}). Upon both *Listeria* infection and DGal/TNF challenge, the OTUB1^{LPC-KO} mice developed severe liver damage and synthesized increased TNF levels in the liver as compared to the OTUB1^{FL} control mice. The aggravated liver damage resulted in liver failure and ultimately in death of OTUB1^{LPC-KO} mice. The enhanced liver damage in the absence of OTUB1 expression in hepatocytes was a consequence of an augmented TNF-driven necroptotic hepatocellular death which was further amplified by the enhanced hepatocyte-intrinsic production of TNF. Death of OTUB1-deficient hepatocytes could be prevented by Necrostatin-1s treatment and genetic ablation of MLKL, the executioner of necroptosis, respectively. Consequently, *Listeria*-infected OTUB1^{LPC-KO} mice treated with Necrostatin-1s or deficient for MLKL survived listeriosis with minimal liver damage equivalent to OTUB1^{FL} control mice. Mechanistically, hepatocyte-specific OTUB1 prevented cell death by protecting c-IAP1 from proteasomal degradation by reducing its K48-linked polyubiquitination. This stabilized c-IAP1 in turn conjugated K63-linked polyubiquitin chains RIPK1, thereby acting as scaffold for survival NF- κ B activation while inhibiting its kinase activity required for the induction of necroptosis. In the absence of OTUB1, the kinase active RIPK1 further amplified the hepatocyte-intrinsic TNF production in a RIPK1/ERK-dependent manner which augmented the hepatocellular death in these mice. Taken together, our studies identified OTUB1 as a hepatocyte-intrinsic inhibitor of necroptosis and TNF-production in both bacterial- and TNF-induced inflammation.

TABLE OF CONTENTS

PUBLICATIONS	II
ABSTRACT	III
TABLE OF CONTENTS	IV
LIST OF TABLES	VII
LIST OF FIGURES	VIII
ABBREVIATIONS	X
1 INTRODUCTION	1
1.1 Cell death programs in liver	1
1.2 Listeriosis - bacterial hepatitis.....	2
1.3 D-Galactosamine as experimental model for acute toxin-induced hepatitis.....	6
1.4 TNF as a regulator of cell survival and cell death.....	7
1.5 The ubiquitin system	10
1.5.1 Ubiquitination.....	10
1.5.2 Deubiquitinating enzymes.....	12
1.6 Post-translational regulation of TNFR1 signaling by the ubiquitin system.....	15
2 AIM OF THIS STUDY	19
3 MATERIAL AND METHODS	20
3.1 Materials.....	20
3.1.1 Chemicals	20
3.1.2 Buffers and cell culture media	21
3.1.3 Stimulation reagents	21
3.1.4 Reagents for cell culture.....	22
3.1.5 Reagents for transfection of HepG2 cells with siRNA	22
3.1.6 Inhibitors	23
3.1.7 Reagents for molecular biology	23
3.1.8 Reagents for protein analyses.....	24
3.1.9 Antibodies for Western blot	24
3.1.10 Antibodies for flow cytometry	26
3.1.11 Antibodies for Immunofluorescence	27
3.1.12 Kits	27

3.1.13	PCR primers	28
3.1.14	TaqMan gene expression assay probes	28
3.1.15	Consumables	29
3.1.16	Instruments	30
3.1.17	Software	31
3.1.18	Animals	31
3.2	Methods	32
3.2.1	Mouse genotyping	32
3.2.2	Cell culture	33
3.2.3	Transfection of HepG2 cells with small interfering RNA (siRNA).....	34
3.2.4	Protein analyses by Western Blotting	34
3.2.5	Immunoprecipitation	36
3.2.6	Quantitative real-time PCR (qRT-PCR)	37
3.2.7	Infection with <i>Listeria monocytogenes</i>	38
3.2.8	D-Galactosamine shock model.....	39
3.2.9	Histology	39
3.2.10	Serology	39
3.2.11	Immune cell characterization by flow cytometry.....	40
3.2.12	Inhibitor experiments	42
3.2.13	Immunofluorescence	42
4	RESULTS.....	44
4.1	Hepatocyte-specific expression of OTUB1 is dispensable for liver homeostasis....	44
4.2	OTUB1 protects mice from bacterial-and inflammation-induced lethality	46
4.2.1	OTUB1 prevents hepatic failure during infection with <i>Listeria monocytogenes</i>	46
4.2.2	OTUB1 prevents hepatic failure during toxin-induced liver injury	50
4.3	OTUB1 regulates TNF-induced signaling pathways	54
4.3.1	OTUB1 regulates TNF-triggered ERK but not NF- κ B activation.....	54
4.3.2	OTUB1 blocks TNF-induced necroptotic cell death.....	55
4.4	Inhibition of necroptosis but not of apoptosis rescues OTUB1 ^{LPC-KO} mice from <i>Listeria</i> -induced mortality	58
4.4.1	RIPK1 inhibition preserves liver function in Lm-infected OTUB1 ^{LPC-KO} mice	58
4.4.2	Deletion of MLKL prevents Lm-induced liver damage in OTUB1 ^{LPC-KO} mice	60
4.5	OTUB1 prevents TNF-triggered necroptosis via c-IAP1 stabilization.....	61
4.5.1	OTUB1 interacts with c-IAP1 upon <i>Listeria</i> -infection and DGal/TNF challenge ..	61

4.5.2	OTUB1 cleaves K48-linked polyubiquitin chains from c-IAP1	62
4.5.3	OTUB1-mediated stabilization of c-IAP1 increases K63-linked polyubiquitination of RIPK1	63
4.6	Hepatocyte-intrinsic OTUB1 limits necroptosis and TNF production	64
4.6.1	OTUB1 exhibits a similar phenotype in human and mice	64
4.6.2	Hepatocyte TNF production is enhanced by the RIPK1/ERK axis in the absence of OTUB1	68
5	DISCUSSION.....	71
	REFERENCES	77
	DECLARATION OF ORIGINALITY	87
	DECLARATION OF CRIMINAL CONVICTIONS	88
	DECLARATION OF HONOR.....	89

LIST OF TABLES

Table 1: Proteins regulated by the catalytic activity of OTUB1	14
Table 2: Proteins regulated by OTUB1 in a non-catalytic fashion	15
Table 3: Chemicals.....	20
Table 4: Buffers and cell culture media	21
Table 5: Reagents <i>in vivo</i> and <i>in vitro</i> stimulation.....	21
Table 6: Reagents for cell culture	22
Table 7: Transfection reagents	22
Table 8: Inhibitors used <i>in vivo</i> and <i>in vitro</i>	23
Table 9: Reagents for molecular biology	23
Table 10: Reagents for protein analyses	24
Table 11: Antibodies used for Western blot.....	24
Table 12: Antibodies for flow cytometric analyses	26
Table 13: Antibodies used for immunofluorescence.....	27
Table 14: Kits used in this study	27
Table 15: Primers for PCR	28
Table 16: TaqMan gene assay probes for qRT-PCR.....	28
Table 17: Consumables used in this study	29
Table 18: Instruments used in this study.....	30
Table 19: Software for data analysis	31

LIST OF FIGURES

Figure 1: Transmission of <i>Listeria monocytogenes</i> to the liver, its primary replication site.....	3
Figure 2: <i>Listeria</i> -induced immune response in the liver.	5
Figure 3: Mechanism of DGal/LPS-induced acute hepatitis.....	6
Figure 4: Basic scheme illustrating the TNF-regulated pathways.	9
Figure 5: The ubiquitin system.....	11
Figure 6: Schematic structure of the DUB OTUB1.	13
Figure 7: Polyubiquitination within TNFR1-signaling.	18
Figure 8: Deletion of OTUB1 in the liver did not disturb liver function.	45
Figure 9: OTUB1 protects from lethal listeriosis.....	46
Figure 10: Liver failure causes Lm-induced lethality in OTUB1 ^{LPC-KO} mice.	47
Figure 11: OTUB1 is dispensable for recruitment of leukocytes to Lm-infected livers.....	48
Figure 12: OTUB1 limits liver-intrinsic TNF production.....	48
Figure 13: OTUB1 dampens Lm-induced TNF expression in primary hepatocytes.	49
Figure 14: OTUB1 ^{LPC-KO} mice are highly to susceptible to DGal/LPS challenge.	51
Figure 15: OTUB1 ^{LPC-KO} mice develop acute hepatitis upon DGal/TNF challenge.	52
Figure 16: Augmented activation of ERK in OTUB1-deficient livers.	54
Figure 17: Accelerated degradation of c-IAP1 and enhanced necrosome formation in the absence of OTUB1.	56
Figure 18: Cell death in OTUB1 ^{LPC-KO} mice is RIPK1/RIPK3-mediated.....	57
Figure 19: Nec-1s but not zVAD limits liver failure and TNF production in Lm-infected OTUB1 ^{LPC-KO} mice.....	58
Figure 20: Improved survival of OTUB1 ^{LPC-KO} mice in the presence of Nec-1s.....	59
Figure 21: Genetic ablation of MLKL reduces liver damage in OTUB1 ^{LPC-KO} mice.....	60
Figure 22: <i>Listeria</i> - and DGal/TNF-induced interaction of OTUB1 and c-IAP1 in the liver.	61
Figure 23: OTUB1 deficiency causes accumulation of K48-linked polyubiquitination on c-IAP1.	62
Figure 24: Impaired K63-linked polyubiquitination of RIPK1 in the absence of OTUB1.....	63
Figure 25: Knockdown of OTUB1 destabilizes c-IAP1, augments ERK activation but does not affect NF-κB activation and caspase cleavage.....	65
Figure 26: Interaction of OTUB1 with c-IAP1 inhibits necroptosis in HepG2 cells.....	66
Figure 27: TNF/CHX-induced degradation of c-IAP1 and necroptosis in OTUB1-deficient HepG2 cells.	67

Figure 28: Augmented RIPK1-ERK interaction triggers TNF production in OTUB1-deficient HepG2 cells.	69
Figure 29: Interaction of RIPK1 and ERK mediates TNF mRNA expression.	70
Figure 30: Schematic summary of the present study.	76

ABBREVIATIONS

A

aa *Amino acid*
 ALT *Alanine aminotransferase*
 APS *Ammonium persulfate*
 ATP *Adenosine triphosphate*

B

Bax *Bcl-2-associated X protein*
 Bcl-2 *B cell lymphoma-2*
 BHI *Brain heart infusion*
 BID *BH3 interacting-domain death agonist*
 BSA *Bovine serum albumin*

C

CBA *Cytometric bead array*
 cDNA *complementary deoxyribonucleic acid*
 c-FLIP *Cellular FLICE-inhibitory protein*
 CFU *Colony forming unit*
 CHX *Cycloheximide*
 c-IAP *Cellular inhibitor of apoptosis*
 CYLD *Cylindromatosis*

D

DAPI *4',6-diamidino-2-phenylindole*
 DC *Dendritic cell*
 DEPTOR *DEP domain-containing mTOR-interacting protein*
 DGal *D-Galactosamine*
 DMEM *Dulbecco's Modified Eagle Medium*
 DMSO *Dimethyl sulfoxide*
 DNA *Deoxyribonucleic acid*
 dNTP *Deoxyribonucleotide triphosphate*
 DPBS *Dulbecco's phosphate buffered Saline*
 DTT *Dithiothreitol*
 DUB *Deubiquitinating enzyme*

E

EDTA *Ethylendiaminetetraacetic acid*
 ERK *Extracellular signal-regulated kinase*

F

FCS *Fetal calf serum*
 FOXM1 *Forkhead box protein M1*

G

GRAIL *Gene related to anergy in lymphocytes*

H

H&E *Hematoxylin & eosin*
 HBSS *Hank's balanced salt solution*
 HEPES *(4-(2-Hydroxyethyl)-1-piperazine-ethanesulfonic acid*
 HepG2 *Human hepatocellular carcinoma cells*
 HPRT *Hypoxanthine guanine phosphoribosyl*

HRP *Horseradish peroxidase*

I

i.p. *Intraperitoneal*
 i.v. *Intravenous*
 IFN *Interferon*
 IgG *Immunoglobulins*
 IKK *Inhibitor of kappa B kinase*
 IL *Interleukin*
 Inl *Internalin*
 iNOS *Inducible nitric oxide synthase*
 IκB *Inhibitor of kappa B*

J

JAMM *JAB1/MPN/MOV34*

L

LDH *Lactate dehydrogenase*
 LLO *Listeriolysin*
 Lm *Listeria monocytogenes, Listeria*
 LPS *Lipopolysaccharides*
 LUBAC *Linear ubiquitin chain assembly complex*

M

MAPK *Mitogen-activated kinase*
 MCP-1 *Monocyte chemotactic protein-1*
 MEM *Minimal essential medium*
 MINDY *Motif interacting with ubiquitin-containing novel DUB family*
 MLKL *Mixed lineage kinase domain-like protein*
 MOI *Multiplicity of infection*

N

NEAA *Non-essential amino acid*
 Nec-1s *Necrostatin-1s*
 NF-κB *Nuclear factor-'kappa-light-chain-enhancer' of activated B cells*
 NIK *Nuclear factor-'kappa-light-chain-enhancer' of activated B cells-inducing kinase*
 NK *Natural killer*

O

OTU *Ovarian tumor protease*
 OTUB1 *Ovarian tumor domain-containing, ubiquitin aldehyde-binding protein 1*

P

PCR *Polymerase chain reaction*
 PFA *Paraformaldehyde*
 PKB *Protein kinase B*
 Plc *Phospholipase*
 PMSF *Phenylmethanesulfonyl fluoride*
 PRR *Pattern recognition receptor*
 PVDF *Polyvinylidene fluoride*

Q

qRT-PCR *Quantitative real-time polymerase chain reaction*

R

RIG-I *Retinoic acid-inducible gene I*
RIPA *Radioimmunoprecipitation assay*
RIPK *Receptor-interacting serine/threonine kinase*
RNA *Ribonucleic acid*
ROS *Reactive oxygen species*
RT *Room temperature*

S

SDS *Sodium dodecyl sulfate*
SEM *Standard error of the mean*
Ser *Serine*
siRNA *Small interfering ribonucleic acid*
SOCS1 *Suppressor of cytokine signaling 1*

T

TAB *TAK1-binding protein*
TAK1 *Transforming growth factor-beta-activated kinase 1*
TBE *Tris-borate-EDTA*
TEMED *Tetramethylethylenediamine*
TGF *Transforming growth factor*

Thr *Threonine, Threonine*
TNF *Tumor necrosis factor*
TNFAIP3 *Tumor necrosis factor alpha-induced protein 3*
TNFR *Tumor necrosis factor receptor*
TRADD *Tumor necrosis factor receptor type 1-associated death domain protein*
TRAF *Tumor necrosis factor-associated factor*
TRAIL *Tumor necrosis factor-related apoptosis-inducing ligand*
TWEAK *Tumor necrosis factor related weak inducer of apoptosis*
Tyr *Tyrosine*

U

Ub *Ubiquitin*
UBE *Ubiquitin-conjugating enzyme*
UCH *Ubiquitin C-terminal hydrolase*
UDP *Uridine diphosphate*
USP *Ubiquitin-specific protease*

W

WB *Western blot*

Z

zVAD *Z-VAD-FMK*

1 INTRODUCTION

The liver is a highly metabolic active organ with a privilege for regeneration (Tacke *et al.*, 2009). Hepatocytes are the predominant type of liver-resident cells comprising around 80 % of the organ mass (Bogdanos *et al.*, 2013; Dara *et al.*, 2016). Beside its metabolic function in detoxification and nutrient supply, the liver is immunologically important, since the hepatocytes are frequently exposed to food-borne derived bacterial peptides, viral particles or other toxic metabolites which originate from the gastrointestinal tract (Tacke *et al.*, 2009). Exposure to these pathogens or toxic substances can trigger inflammation as well as cell death of the hepatocytes. Notably, liver homeostasis and regeneration, in part, require a basal inflammation in order to replace non-functional or aged hepatocytes by programmed cell death (Brenner *et al.*, 2013; Luedde *et al.*, 2014; Robinson *et al.*, 2016).

1.1 Cell death programs in liver

Apart from the functional importance of programmed cell death in liver regeneration, programmed cell death under inflammatory conditions may also be hepatoprotective as it is part of the host defense machinery against invading pathogens (Brenner *et al.*, 2013; Luedde *et al.*, 2014). Hepatocytes have been shown to undergo several modes of cell death, including necrosis, apoptosis and necroptosis as the classical mechanisms. Likewise, autophagic cell death, pyroptosis and ferroptosis have gained growing attention (Schwabe & Luedde, 2018; Macías-Rodríguez *et al.*, 2020). Among these cell death mechanisms, apoptosis is considered as the most prevalent form of cell death in hepatocytes. Morphologically, apoptotic cells are defined by a shrinkage in cell size and membrane blebbing which are accompanied by nuclear condensation or fragmentation (Schwabe & Luedde, 2018). With the progression of apoptosis, the whole cellular content is fragmented and incorporated in apoptotic bodies, a process which maintains the membrane integrity while destroying the cell structure (Macías-Rodríguez *et al.*, 2020). On a molecular level, apoptotic cell death involves the cleavage of the initiator caspase-8 and thereafter the cleavage of effector caspases. Importantly, in type II cells as the hepatocytes are, apoptosis is amplified via the intrinsic mitochondrial pathway (Luedde *et al.*, 2014). In contrast to apoptosis, necrosis was originally considered as an accidental cell death mechanism which is mainly caused by a metabolic break down leading to cell swelling and ultimately to membrane rupture. However, studies on necrosis identified that necrosis can occur in a regulated manner, the term necroptosis evolved (Luedde *et al.*, 2014; Schwabe & Luedde, 2018). Necroptosis is mediated by the Receptor-interacting serine/threonine kinases (RIPK),

RIPK1 and RIPK3 as well as the Mixed lineage kinase domain-like protein (MLKL) (Luedde *et al.*, 2014). A key feature of necroptosis is the loss of membrane integrity and late stage chromatin condensation (Macías-Rodríguez *et al.*, 2020). Membrane rupture leads to the release of the cellular content which accounts for its highly immunogenic capacity, similar to necrosis but contrary to apoptosis (Luedde *et al.*, 2014; Schwabe & Luedde, 2018; Kondylis & Pasparakis, 2019; Macías-Rodríguez *et al.*, 2020). However, necroptosis induction and its inducing factors are critically discussed, especially in context of hepatocytes. The discrepancy mainly arose from two observations (i) necroptosis induction was only observed upon inhibition of caspase-8 and (ii) hepatocytes are considered as RIPK3 low-expressing cells (Dara *et al.*, 2016; Kondylis & Pasparakis, 2019). However, several groups, including Wang *et al.* and Ramachandran *et al.*, clearly demonstrated the expression of hepatic RIPK3 and its contribution to toxin-induced liver injury (Ramachandran *et al.*, 2013; Wang, Ni, *et al.*, 2016). Despite different underlying molecular mechanisms, both programmed cell death programs can be initiated in response to extrinsic or intrinsic factors. Extrinsic stimuli such as bacterial peptides (e.g. Lipopolysaccharides, LPS) or pro-inflammatory cytokines (e.g. Tumor necrosis factor, TNF) trigger the activation of death receptors such as Tumor necrosis factor receptor (TNFR) 1 (Schwabe & Luedde, 2018). Of note, these stimuli normally do not induce hepatocyte death unless the counterregulatory survival signaling is impaired (Feltham *et al.*, 2017; Schwabe & Luedde, 2018). In addition, both pathways crossregulate each other. However, an imbalance in cell death signaling can result in excessive cell death of the hepatocytes which may manifest in an acute hepatitis and eventually in liver failure.

1.2 Listeriosis - bacterial hepatitis

Listeriosis is a foodborne infectious disease which is mainly transmitted via contaminated food. Although infections with the Gram-positive, facultative intracellular bacteria *Listeria monocytogenes* (*Listeria*, Lm) are usually clinically asymptomatic, in immunosufficient individuals, in particular, immunocompromised patients, elderly people (> 60 years), fetuses, and newborns are at high risk of an invasive listeriosis with life-threatening symptoms including meningoencephalitis, septicemia or even fetal abortion in pregnant women (Stavru *et al.*, 2011; Schlech, 2019). As *Listeria* is a foodborne pathogen, its route of transmission starts with the digestion of contaminated food in the gastrointestinal tract where it rapidly transmigrates the intestinal barrier, thereby entering the lymphatic system and subsequently the blood stream. Via the blood stream, *Listeria monocytogenes* spreads to the liver and spleen, the primary targets of infection (Figure 1) (Cossart, 2011).

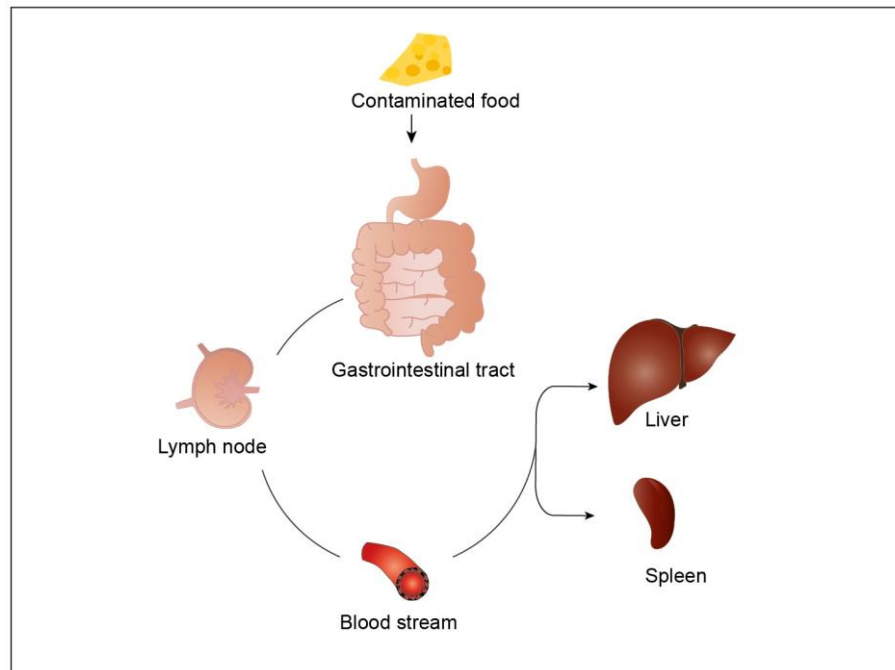


Figure 1: Transmission of *Listeria monocytogenes* to the liver, its primary replication site.

Following consumption of contaminated food, *Listeria* is digested in the gastrointestinal tract, where it crosses the intestinal barrier, thereby reaches the bloodstream and disseminates to other organs, in particular to the liver and the spleen (adapted and modified from (Cossart, 2011)).

Function of hepatocytes during acute listeriosis The ability to employ the cellular signaling and endocytic pathway of the host cell ensures *Listeria*'s invasion and intracellular spreading (Hamon *et al.*, 2006). *Listeria* actively invade non-professional phagocytic cells such as epithelial cells and hepatocytes by utilizing internalins (InlA and InlB) which bind to the host cell (Stavru *et al.*, 2011). In hepatocytes, *Listeria* induces endocytosis by binding of the InlB to the c-Met receptor tyrosine kinase expressed on hepatocytes (Shen *et al.*, 2000). Following internalization, *Listeria* secretes listeriolysin O (LLO) and phospholipases (PlcA, PlcB) to lyse the phagosome (Hamon *et al.*, 2006). Once in the cytoplasm, *Listeria* starts replicating and spreading. As the major cell type in the liver, the hepatocytes have been identified as primary site for *Listeria* multiplication. Intravenous infection of mice with *Listeria* results in a rapid localization and exponential proliferation of the bacteria within the hepatocytes during the first three days after infection (Gregory *et al.*, 1992). During infection, the hepatocytes contribute to the resolution of the pathogen as they upregulate antilisterial mechanisms in response to inflammatory cytokines. Beside their antilisterial activity, *Listeria*-infected or cytokine-stimulated hepatocytes themselves can synthesize TNF probably to recruit immune cells to the site of infection and to activate macrophages (Szalay *et al.*, 1995; Santos *et al.*, 2011). In addition, death of the *Listeria*-infected hepatocytes may serve as defense

mechanism by exposing the pathogen to innate immune cells (Cousens & Wing, 2000; Santos *et al.*, 2011).

Immune cell response to *Listeria monocytogenes* in the liver Detection of *Listeria*-derived antigens such as peptidoglycan and muramyl-dipeptides by professional phagocytic and non-professional phagocytic cells through pattern recognition receptors (PRR) activate the innate and adaptive immune system. Liver-resident macrophages, i.e. Kupffer cells, are considered as the first pathogen-immune cell contact, since they function at the liver sinusoids, thereby bridging the blood stream and the hepatocytes (Cousens & Wing, 2000). *Listeria* adhere to Kupffer cells in the blood which in turn secrete Interleukin (IL)-6, IL-12, IL-1 β and TNF (Cousens & Wing, 2000) (Figure 2). In particular, the release of TNF is triggered by LLO-secreting *Listeria* to restrict bacterial growth (Vazquez *et al.*, 1995). However, Kupffer cells are highly susceptible to *Listeria* and die from necroptosis (Blériot *et al.*, 2015), thus providing *Listeria* a niche for the entry into the liver and further migration to hepatocytes. The Kupffer cell-derived cytokines mainly function in attracting other innate immune cells, including neutrophils, Natural killer (NK) cells, monocytes and Dendritic cells (DCs). Early killing of the bacteria is mediated by Reactive oxygen species (ROS). Activated monocytes differentiate into inflammatory monocytes, monocyte-derived macrophages and TNF/inducible nitric oxide synthase (iNOS)-producing DCs (Pamer, 2004; Blériot *et al.*, 2015). TNF secretion by these cell populations along with Interferon (IFN) γ synthesized by NK cells trigger the rapid proliferation of monocyte-derived macrophages, probably in order to replace dying Kupffer cells, and to enhance their antibacterial potential (Stavru *et al.*, 2011; Blériot *et al.*, 2015; D’Orazio, 2019). While innate immune cells play an important role in restricting bacterial growth early after infection, efficient clearance of the bacteria as well as the development of a memory response require a functional, adaptive T cell response (Zenewicz & Shen, 2007). Upregulation of co-stimulatory factors on DCs activate cytotoxic CD8⁺ T cells which lyse infected cells through perforin and granzyme B secretion (Zenewicz & Shen, 2007). Together with CD4⁺ T cells, a pool of memory CD8⁺ T cells is formed (Sun & Bevan, 2003).

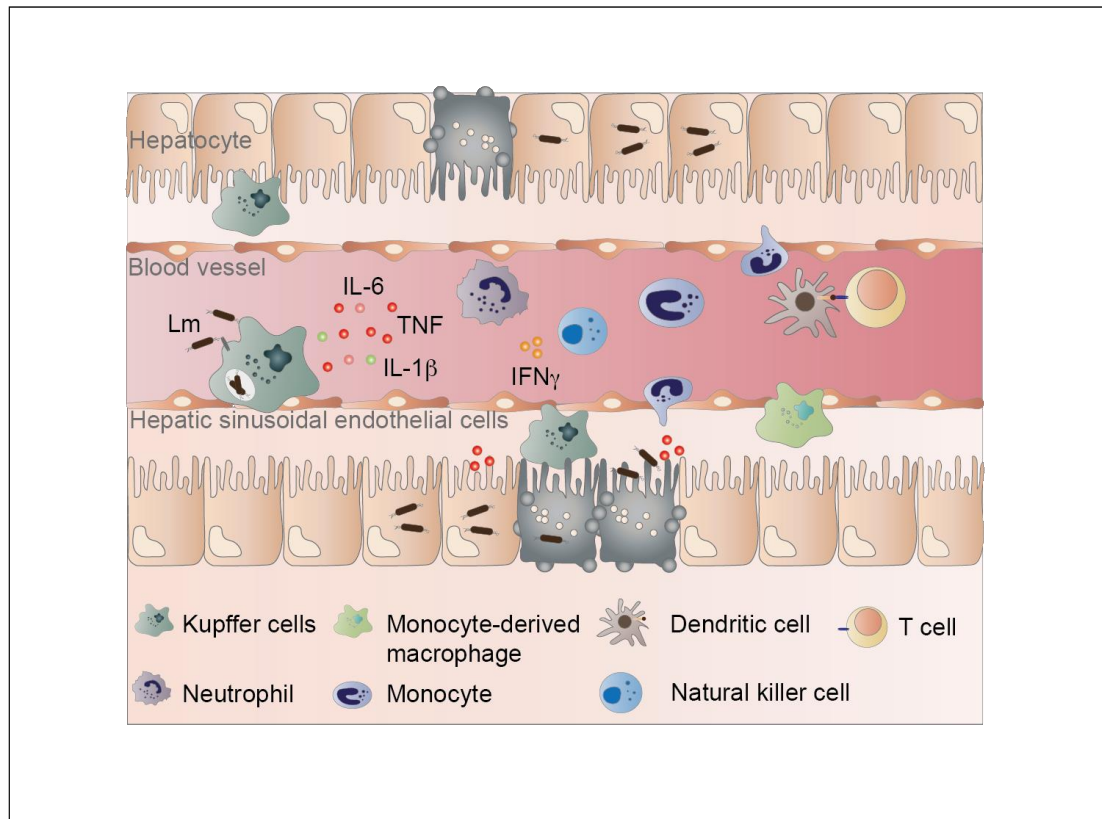


Figure 2: *Listeria*-induced immune response in the liver.

Cellular invasion of *Listeria* into Kupffer cells stimulates the release of pro-inflammatory cytokines and induces necroptosis of the Kupffer cells. Consequently, *Listeria* infects hepatocytes, where the bacteria further replicate and may induce cell death of the infected hepatocytes. Activated hepatocytes release TNF. In response to the cytokine secretion, neutrophils, monocytes, NK cells and DCs are recruited in order to kill the bacteria. T cells as part of the adaptive immune response are primed by DCs leading to a protective immunity against *Listeria*.

1.3 D-Galactosamine as experimental model for acute toxin-induced hepatitis

In addition to pathogens, toxins are potential triggers for liver inflammation. Experimentally, toxin-induced acute hepatitis is often mimicked by the combined administration of D-Galactosamine (DGal) and LPS into mice. In this model, all pathological features of an acute hepatitis as seen in humans, including fulminant hepatic failure, are reproduced by the combined effect of transcriptional arrest through DGal and the subsequent sensitization to the endotoxic effects of LPS (Keppler *et al.*, 1968). In the liver, DGal is rapidly metabolized to Uridine diphosphate (UDP)-galactosamine. Of note, the strong tropism for the liver is attributed to the high contents of galactokinase and galactose-1-phosphate-uridylyltransferase in the liver (de Oliveira *et al.*, 1992). Conversion to these UDP-sugar derivatives reduces the pool of free uracil nucleotides, which accounts for the blockage in Ribonucleic acid (RNA) synthesis (Keppler D., Rudigier J.F.M., Bischoff E., 1970). While LPS in low doses per se is only a moderate liver inflammatory stimulus, in context of transcriptional arrest by DGal, low doses of LPS are sufficient to induce fulminant hepatic failure (Wu *et al.*, 2014).

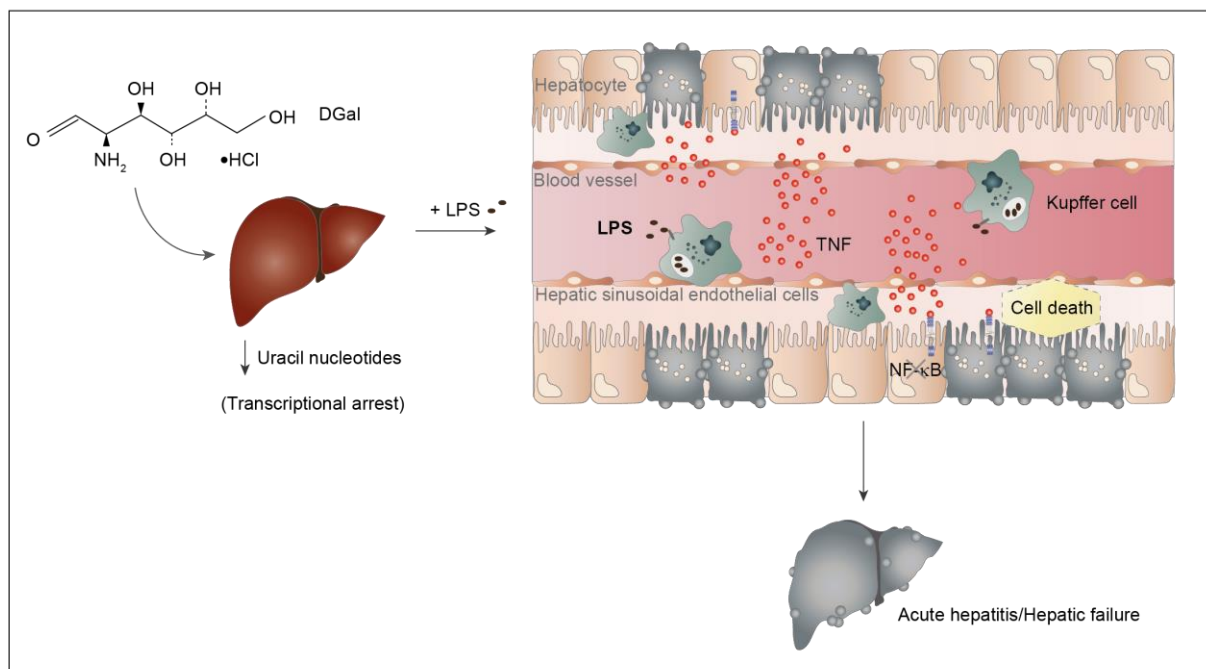


Figure 3: Mechanism of DGal/LPS-induced acute hepatitis.

Metabolized DGal causes the reduction uracil nucleotides required for RNA transcription in the liver. This transcriptional arrest sensitizes the hepatocytes to LPS challenge. LPS is recognized by Kupffer cells which in turn secrete TNF. In response to TNF, the hepatocytes undergo cell death due to the lack of NF-κB activation resulting in hepatic failure.

Similar to bacterial infections, recognition of the bacteria-derived antigen LPS by the PRR-expressing Kupffer cells stimulate the Kupffer cells to secrete TNF which serves as activating signal for immune system. However, due to transcriptional arrest, the hepatocytes fail to activate the pro-survival Nuclear factor-‘kappa-light-chain-enhancer’ of activated B cells (NF- κ B) signaling in response to TNF resulting in the activation of the cell death program and culminating in hepatic failure (Muriel *et al.*, 2017). Although cell death under these conditions has been widely accepted to rely on the pro-inflammatory cytokine TNF and to occur in an apoptotic fashion (Tiegs *et al.*, 1989; Josephs *et al.*, 2000; Wu *et al.*, 2014), recent evidence that necroptosis inhibition improved survival in DGal/LPS-treated mice by preventing necrosome formation implicated necroptosis as an alternative cell death program upon DGal/LPS challenge (Kim & Lee, 2017). However, it is still controversially discussed whether DGal/LPS can in fact induce necroptosis, since proximal components of the apoptosis and necroptosis pathways are identical.

1.4 TNF as a regulator of cell survival and cell death

Inflammatory responses are mediated by the release of cytokines and chemokines. TNF is a pro-inflammatory cytokine of central importance due to its ability to promote both cell survival and cell death. TNF signals are transduced via two TNF receptors, TNFR1 and TNFR2. While the TNFR1 is commonly expressed on all mammalian cell types, the expression of TNFR2 seems to be regulated on immune cells and certain other cell types, including hepatocytes (Schümann *et al.*, 2003; Wajant *et al.*, 2003). Upon binding of TNF to TNFR1, the TNFR signaling complex I consisting of TNFR1-associated death domain protein (TRADD), TNFR-associated factor (TRAF) 2/5, RIPK1 and the cellular inhibitor of apoptosis (c-IAP) 1/2 is engaged (Figure 4). Assembly of the TNFR-signaling complex I functions as adaptor allowing the recruitment of the linear ubiquitin chain assembly complex (LUBAC) and the TAK1-binding protein (TAB) 2, 3-containing transforming growth factor (TGF)- β -activated kinase 1 (TAK1) complex. The TAK1 complex subsequently activates the mitogen-activated kinases (MAPKs) and the inhibitor of κ B (I κ B) kinase (IKK) complex (Holbrook *et al.*, 2019). The latter facilitates the release of the NF- κ B from its inhibitory protein, I κ B α . As a result, NF- κ B translocates to the nucleus driving the gene transcription of the anti-apoptotic molecules B cell lymphoma-2 (Bcl-2) and cellular FLICE-inhibitory protein (c-FLIP) as well as the gene transcription of pro-inflammatory cytokines such as TNF and IL-6 (Luedde *et al.*, 2014; Feltham *et al.*, 2017; Schwabe & Luedde, 2018; Kondylis & Pasparakis, 2019). In contrast to

TNFR1, TNFR2 utilizes a simplified signaling complex consisting of TRAF1/2 and c-IAP1/2 for activating NF- κ B (Wajant & Siegmund, 2019). In addition to the canonical NF- κ B, TNFR2 activation can also promote the NF- κ B-inducing kinase (NIK)-dependent processing of the p100/RelB to p52/RelB, thus activating the non-canonical NF- κ B pathway (Rauert *et al.*, 2010; Wajant & Siegmund, 2019). However, only TNFR1 harbors a cytoplasmic death domain which permits cell death signaling (Brenner *et al.*, 2015). Therefore, cell death programs are initiated either through direct binding of TNF to the TNFR1 or in context of TNFR2 by transactivating the TNFR1 (Schümann *et al.*, 2003). In hepatocytes, downregulation of TNFR2 has been suggested as a protective mechanism against TNF-TNFR1-mediated cell death during toxin-induced hepatitis (Schümann *et al.*, 2003). Cell death signaling is initiated by the assembly of an alternative cytosolic complex (complex II) which either directs towards apoptosis (complex IIa, IIb) or necroptosis (complex IIc) (Holbrook *et al.*, 2019). As caspase-dependent form of cell death, apoptosis involves first the autocleavage of the initiator caspase-8 and second the caspase-8-mediated cleavage of its downstream targets, the effector caspases, caspase-3, -6 and -7. Of note, in type II cells such as hepatocytes, caspase-8 also induces apoptosis indirectly by cleaving BH3 interacting-domain death agonist (BID) to tBID (truncated BID) which induces the dimerization of the Bcl-2-associated X protein (Bax) (Feltham *et al.*, 2017). Activated Bax promotes mitochondrial membrane permeabilization leading to the release of cytochrome c and the activation of the effector caspases-3, -6 and -7 (Schwabe & Luedde, 2018). Since c-FLIP and Bcl-2 as NF- κ B-regulated proteins act inhibitory on caspase-8 autocleavage and the caspase-8-mediated processing of BID, respectively, apoptosis execution is often associated with defects in NF- κ B signaling (Bentires-alj *et al.*, 2001; Yi *et al.*, 2003; Luedde *et al.*, 2014; Peltzer *et al.*, 2016). However, in conditions of caspase-8 inhibition accompanied with the loss of c-IAP1, a complex referred to as necrosome (complex IIc) is formed (Feltham *et al.*, 2017). The necrosome comprises of RIPK1, RIPK3 and the pseudokinase MLKL (Kondylis & Pasparakis, 2019). Upon activation, phosphorylated MLKL undergoes conformational changes required for its translocation to the plasma membrane and the subsequent rupture of the membrane (Chen *et al.*, 2014; Hildebrand *et al.*, 2014).

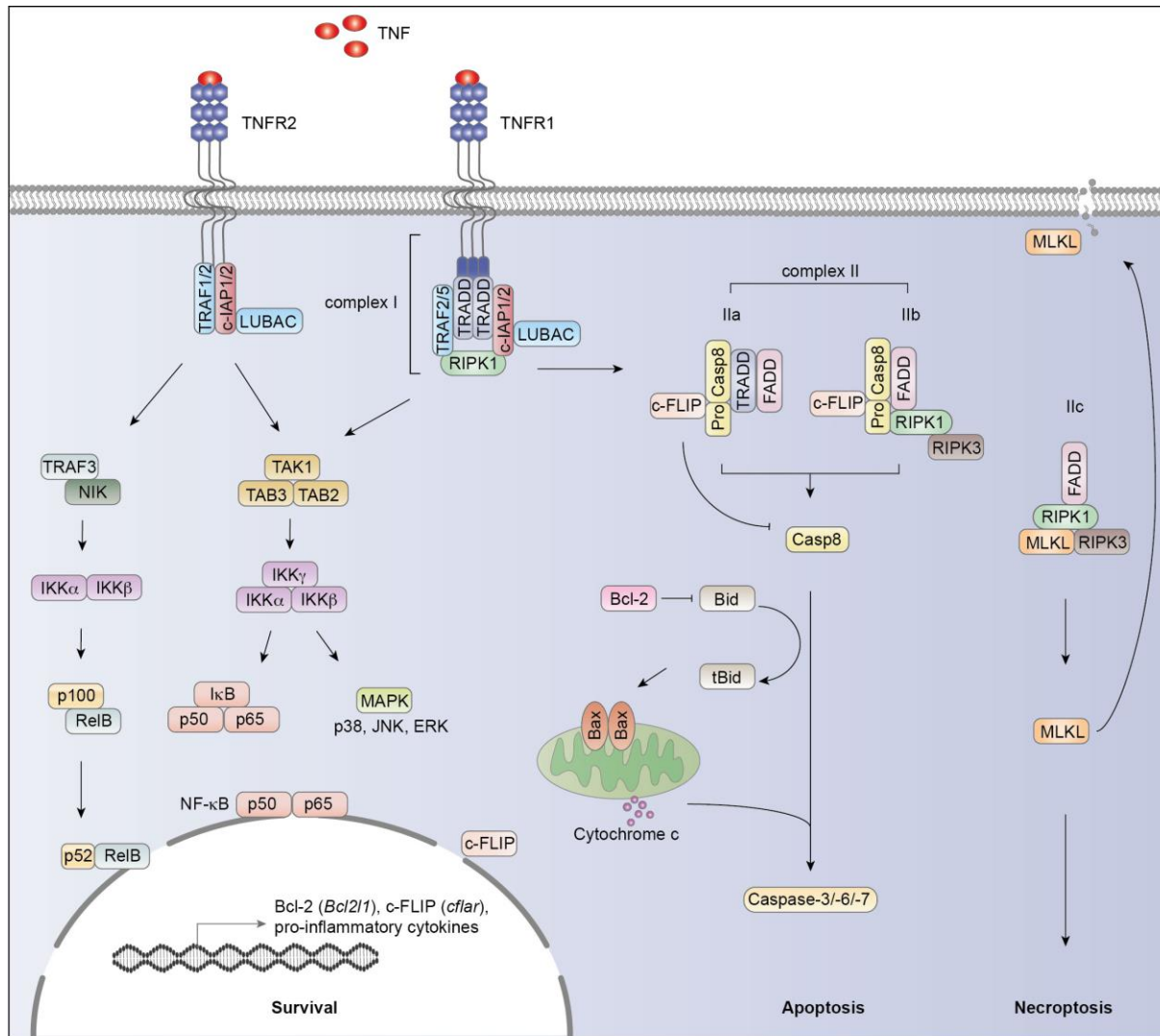


Figure 4: Basic scheme illustrating the TNF-regulated pathways.

Activation of TNFR1 or TNFR2 by TNF initiates the recruitment of TRADD, TRAF2, c-IAP1/2 and RIPK1 or TRAF1/2 and c-IAP1/2 in context of TNFR2 to form the NF- κ B-activating signaling complex I. Following association of LUBAC to the TNFR signaling complex I, the TAB2/3-TAK1 complex is attracted which fosters the release of the transcription factor NF- κ B from I κ B α by activating the IKK complex (canonical NF- κ B). Translocation of the NF- κ B subunit p50/p65 induces survival genes and pro-inflammatory cytokines. In addition, TNFR2 promotes the release of NIK, thereby inducing the processing of p100 to p52/RelB (non-canonical NF- κ B). Due to its death domain, TNFR1 is capable of inducing the cell death signaling cascade which involves the assembly of complex II comprising procaspase-8, TRADD, FADD (complex IIa) and possibly RIPK1 and RIPK3 (complex IIb) in the cytoplasm. This complex primarily triggers caspase-dependent apoptosis via direct caspase-8-mediated cleavage of the effector caspases, caspase-3, -6 and -7 or indirectly through conversion of BID to tBID followed by Bax-induced cytochrome release from the mitochondria and the activation of the effector caspases. Inhibition of caspase-8 leads to engagement of RIPK1 and RIPK3 to MLKL (complex IIc) driving the translocation of MLKL to the plasma membrane.

1.5 The ubiquitin system

1.5.1 Ubiquitination

The complex interplay of inflammation, cell survival and cell death is precisely coordinated by post-translational modifications, including ubiquitination and deubiquitination. Ubiquitination is the reversible attachment of small ubiquitin molecules comprising 76 amino acids (aa) to signaling molecules, thereby modulating their stability, localization or signal transduction. The process of ubiquitination is a multi-step enzymatic cascade which is catalyzed by three distinct enzymes, the ubiquitin (Ub)-activating enzyme (E1), the ubiquitin-conjugating enzyme (E2) and the ubiquitin-ligating enzyme (E3). The cascade starts with the activation of the ubiquitin molecule (Figure 5 A). In this step, E1 forms a C-terminal ubiquitin adenylate upon consumption of Adenosine triphosphate (ATP) which is thereafter coupled to the cysteine residue in E1 by a thioester bond (Pickart & Eddins, 2004). Following activation, the ubiquitin molecule is conjugated to a cysteine residue in the E2 through a thioester bond. The E3, finally, ligates with the E2-Ub complex and the target substrate leading to the transfer of the Ub to the ϵ -amino group of a lysine residue in the substrate (monoubiquitination). By repeating the cycle of ubiquitination, either single ubiquitin molecules are attached at multiple sites (multiple monoubiquitination) or ubiquitin chains are formed (polyubiquitination) (Figure 5 B). Noteworthy, the substrate specificity is primarily conferred by E3 whereas linkage specificity and type of linkages are dedicated by the targeted complexing to an E2 (Pickart & Eddins, 2004; Ye & Rape, 2009). Considering the variety of substrates, the increasing numbers from two identified E1s to at least 600 identified E3s encoded in the human genome are not surprising (Ye & Rape, 2009). As the ubiquitin molecule itself harbors seven lysine (K) residues (K6, K11, K27, K29, K33, K48 and K63) through which ubiquitin molecules can be conjugated, several polyubiquitin chains at each lysine can be assembled. In addition, ubiquitin molecules can be linked through the N-terminal amino group (M1, linear) and each lysine residue can serve as branching site, further enlarging the diversity of ubiquitin modifications (Nijman *et al.*, 2005). Polyubiquitin chains at K6, K11, K27, K29, K33 and K48 are associated with protein targeting for proteasomal degradation (Dammer *et al.*, 2011). However, since its discovery as signal for proteasomal degradation, the knowledge about ubiquitination and its biological functions expanded to various non-degradative functions, including endocytosis (monoubiquitination, K63), Deoxyribonucleic acid (DNA) damage response (monoubiquitination, K63), protein interactions (monoubiquitination, K63) and protein activity (M1, K11, K63). Notably, K48- and K63-linked polyubiquitin chains are the most prominent ubiquitin modifications in human and mice (Dammer *et al.*, 2011).

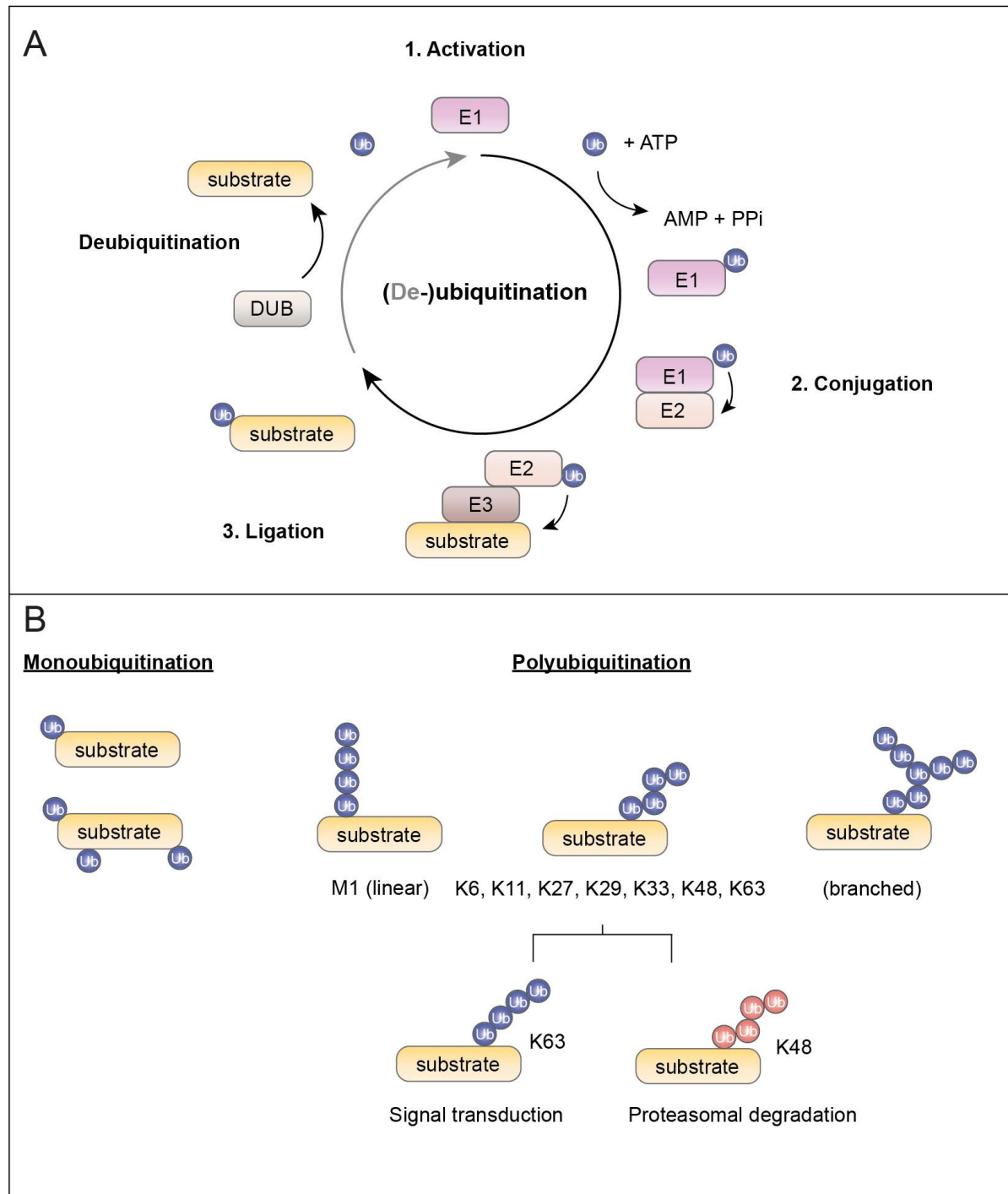


Figure 5: The ubiquitin system.

(A) The three-step process of ubiquitination involves (1) the activation of the ubiquitin molecule and subsequent transfer of the ubiquitin molecule to the ubiquitin-activating enzyme (E1), (2) the ubiquitin conjugation to the ubiquitin-conjugating enzyme (E2) and (3) the ligation of the ubiquitin molecule to the substrate with the help of the ubiquitin-ligating enzyme (E3). The process of ubiquitination is counterbalanced by the enzymatic activity of DUBs. (B) Depending on the number of ubiquitination cycles and the kind of ubiquitin linkage, proteins can be modified with a single ubiquitin molecule or multiple ubiquitin molecules (multiple monoubiquitination, polyubiquitination) determining the fate of the substrate.

1.5.2 Deubiquitinating enzymes

Ubiquitin modifications can be reversed by the activity of deubiquitinating enzymes (DUBs). Due to their ubiquitin editing capacity, DUBs such as OTUB1 are crucial regulators of several cellular processes. Based on their structural and catalytic characteristics, DUBs are categorized in six subfamilies: the ubiquitin-specific proteases (USPs), the ovarian tumor proteases (OTUs), ubiquitin C-terminal hydrolases (UCHs), the Josephin family, the recently discovered motif interacting with ubiquitin-containing novel DUB family (MINDYs) and the JAB1/MPN/MOV34 (JAMMs) as exclusive metalloprotease (Mevisen & Komander, 2017). With 54 members the USPs represent the largest family of DUBs, followed by the OTUs and JAMMs which count 16 members and the UCHs, Josephins and MINDYs with each 4 members, making up to 98 currently identified DUBs in the human genome (Mevisen & Komander, 2017).

Mode of action All DUBs are proteases, in particular cysteine proteases with an exception for JAMMs which are metalloproteases. As proteases, DUBs are able to cleave ubiquitin molecules from their target substrates catalytically by hydrolyzing the peptide bond. Beside their catalytic activity, DUBs also act in a non-catalytic fashion by interfering with ubiquitination cascade, thus inhibiting the ubiquitination of a target substrate. The latter mechanism relies on the active binding of DUBs to either E2s or E3s which prevents the generation of the E2-Ub thioesters or the transfer of ubiquitin molecules to the substrate, respectively (He *et al.*, 2016). However, removal of ubiquitin by DUBs is involved in ubiquitin homeostasis as DUBs maintain a constant pool of free ubiquitin (Komander *et al.*, 2009; He *et al.*, 2016).

OTU domain-containing, ubiquitin aldehyde binding protein 1 (OTUB1) OTUB1 is a member of the OTU domain protease family, the second largest subfamily of DUBs (Mevisen & Komander, 2017). The *otub1* gene is located on chromosome 11 in the human genome and on chromosome 19 in the mouse genome. OTUB1 is expressed in various human tissues including the liver (Balakirev *et al.*, 2003). Structurally, OTUB1 comprises an amino sequence of 270 aa (Figure 6). Given that OTUB1 is a cysteine protease, the catalytic activity of OTUB1 for cleaving iso-peptide bonds is substantiated by three catalytic residues: an aspartate (D) residue positioned at 88 aa, a cysteine (C) residue at 91 aa and a histidine (H) residue at the position of 265 aa (Edelmann *et al.*, 2009; Komander *et al.*, 2009; Saldana *et al.*, 2019). In addition, OTUB1 harbors a Ub-E2 binding motif for proximal Ub-binding. This motif confers linkage specificity, a feature conserved among most of the OTU domain and several

other DUB families. In fact, OTUB1 was shown to possess a strong tropism for cleaving K48-linked polyubiquitin chains whereas Tumor necrosis factor alpha-induced protein 3 (TNFAIP3, A20), another member of the OTU domain family, specifically cleaves K63-linked polyubiquitin chains (Edelmann *et al.*, 2009; Wang *et al.*, 2009).

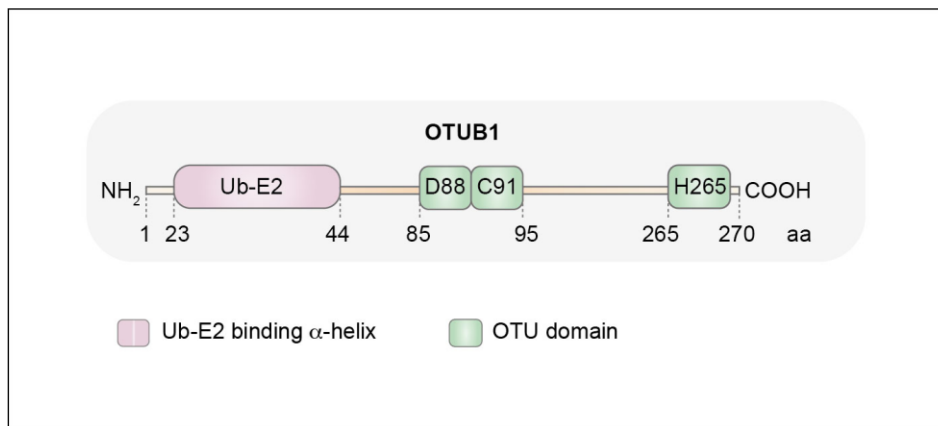


Figure 6: Schematic structure of the DUB OTUB1.

The OTUB1 protein comprises of an amino sequence of 270 aa with an Ub-E2 binding site and three catalytic residues D88, C91 and H265 within the OTU domain (adapted and modified from Saldana *et al.*, 2019).

In this regard, OTUB1 has been demonstrated to stabilize various signaling molecules related to inflammatory responses, autoimmunity, cell survival and cancer development (Table 1). For instance, in murine DCs, OTUB1 hydrolyzes K48-linked polyubiquitin chains from the ubiquitin-conjugating enzyme E2 N (UBE2N, UBC13) upstream of the IKK complex. Consequently, stabilization of UBC13 fosters the NF- κ B dependent activation of DCs which contributes to a protective inflammatory response against the parasite *Toxoplasma gondii* but also causes immunopathology upon LPS challenge *in vivo* and *in vitro* (Mulas *et al.*, 2020). Likewise, astrocyte-specific OTUB1 dampens neuronal hyperinflammation in a murine model of multiple sclerosis. Here, OTUB1 disassembles K48-linked polyubiquitin chains from the suppressor of cytokine signaling 1 (SOCS1), an inhibitor of IFN γ signaling (Wang *et al.*, 2019). In addition, OTUB1 critically regulates cell death. Upon stimulation with the TNF related weak inducer of apoptosis (TWEAK), OTUB1 stabilizes c-IAP1 in human cell lines, thereby blocking TNF-induced cell death *in vitro* (Goncharov *et al.*, 2013). The importance of OTUB1 in regulating cell death and survival was further supported by the observation that OTUB1 knock out mice are embryonic lethal (Pasupala *et al.*, 2018). Of note, cancer development is often associated with an overexpression of OTUB1 as seen in hepatocellular carcinoma, prostate cancer and ovarian cancer. In the latter case, OTUB1 targets Snail for removing its K48-conjugated polyubiquitin chains. Interestingly, OTUB1 seems to be crucial for the cellular

invasion and survival of these cancer cells since knock-down of OTUB1 not only restricted their invasive potential but also induced apoptotic cell death, at least in context of hepatocellular carcinoma (Iglesias-Gato *et al.*, 2015; Ni *et al.*, 2017; Zhou *et al.*, 2018). Given that carcinogenesis can arise from dysregulated DNA damage responses, it is not surprising that OTUB1 is also involved in DNA damage-induced apoptosis by increasing the half-life of p53 and Forkhead box protein M1 (FOXO1) in a catalytic fashion (Sun *et al.*, 2012; Karunarathna *et al.*, 2016).

Table 1: Proteins regulated by the catalytic activity of OTUB1

Target	Ub-linkage	Cellular context
UBC13 (UBE2N)	K48	NF- κ B signaling (Mulas <i>et al.</i> , 2020)
SOCS1	K48	IFN γ signaling (Wang <i>et al.</i> , 2019)
c-IAP1	K48	TNF-induced apoptosis (Goncharov <i>et al.</i> , 2013)
p53	K48	DNA damage (Sun <i>et al.</i> , 2012)
FOXO1	K48	DNA damage, Ovarian cancer (Karunarathna <i>et al.</i> , 2016; Wang, Zhou, <i>et al.</i> , 2016)
Snail	K48	Ovarian cancer (Zhou <i>et al.</i> , 2018)

Importantly, OTUB1 also curtails ubiquitination independent of its catalytic activity by complexing to ubiquitin-conjugating enzymes (E2) resulting in the blockage of ubiquitin transfer to target substrates. Binding of OTUB1, for instance, to the ubiquitin-conjugating enzyme E2 D1 (UBE2D1, UBCH5) in response to DNA damage serves as an alternative mechanism to stabilize p53 (Sun *et al.*, 2012) (Table 2). Accordingly, OTUB1 acts inhibitory on the synthesis of K63-linked polyubiquitin chains at DNA double strand breaks by binding to UBC13 (Nakada *et al.*, 2010; Wiener *et al.*, 2012). In T cells, OTUB1 inhibits the autoubiquitination of the Gene related to anergy in lymphocytes (GRAIL) through trapping the E2 USP8, thus affecting T cell proliferation (Soares *et al.*, 2004). However, although the corresponding E2s are incompletely identified, several studies with OTUB1 mutants uncovered its non-catalytic activity on p100, protein kinase B (PKB, AKT) and Smad2/3 (Herhaus *et al.*, 2013; Li *et al.*, 2019; Zhou *et al.*, 2019). In particular, stabilization of the NF- κ B precursor p100 crucially regulates B cell homeostasis. OTUB1-deficient B cells display an autoimmune phenotype which is characterized by an abnormal NF- κ B activation (Li *et al.*, 2019).

Table 2: Proteins regulated by OTUB1 in a non-catalytic fashion

Interaction partner	Target	Ub	Cellular context
UBC13 (UBE2N)	chromatin	K63	DNA damage response (Nakada <i>et al.</i> , 2010; Wiener <i>et al.</i> , 2012)
UBCH6 (UBE2E1)	UBE2E1	K48	Embryogenesis (Pasupala <i>et al.</i> , 2018)
UBCH5 (UBE2D)	p53	K48	DNA damage response (Sun <i>et al.</i> , 2012)
UBCH5 (UBE2D)	DEPTOR	K48	mTORC1 signaling (Zhao <i>et al.</i> , 2018)
USP8	GRAIL	K48	T cell anergy (Soares <i>et al.</i> , 2004)
AKT	AKT	K63	T cell, NK cell activation (Zhou <i>et al.</i> , 2019)
Smad2/3	Smad2/3	K48	TGF- β signaling (Herhaus <i>et al.</i> , 2013)
p100	p100	K48	NF- κ B signaling (Li <i>et al.</i> , 2019)

More interestingly, the group of Jahan *et al.* recently uncovered that OTUB1 participates in virus-triggered immune responses by employing both catalytic and non-catalytic functions. The authors propose a dual function of OTUB1 in (i) removing K48-linked polyubiquitin chains catalytically and (ii) inhibiting the transfer of K48-linked polyubiquitin chains by binding to UBCH5 which ensures the Retinoic acid-inducible gene I (RIG-I)-mediated antiviral response (Jahan *et al.*, 2020).

1.6 Post-translational regulation of TNFR1 signaling by the ubiquitin system

Ubiquitination as post-translational modification is a key regulator in the fine tuning of cellular signaling events such as inflammation and cell death. Especially, M1-, K11-, K48- and K63-linked polyubiquitinations have been implicated in signal transduction required for TNF-induced activation of the pro-survival NF- κ B pathway (Brenner *et al.*, 2015; Dondelinger *et al.*, 2016). Within the TNFR1 signaling, ubiquitination of RIPK1 is considered as the point of decision since defects in the ubiquitination status of RIPK1 favors death signaling prior to survival NF- κ B signaling. With the assembly of the TNFR1 signaling complex, the E3 ligases TRAF2 and c-IAP1 are recruited to RIPK1. While the function of TRAF2 in ubiquitinating RIPK1 is still under debate, it was clearly demonstrated that c-IAP1 rapidly induces its K63-linked autoubiquitination and thereafter conjugates K63-, K11- and K48-linked polyubiquitin chains on RIPK1 (Dynek *et al.*, 2010; Liu *et al.*, 2016; Zhang *et al.*, 2019). In addition to its activation, autoubiquitination of c-IAP1 serves as an adaptor for the recruiting LUBAC which in turn adds additional M1-linked polyubiquitin chains on RIPK1. These

ubiquitin-linkages provide docking sites for the TAB2/3-containing TAK1 and the IKK complex, thus bringing both complexes into proximity to ensure the phosphorylation of the IKK complex (Brenner *et al.*, 2015; Ting & Bertrand, 2016; Annibaldi & Meier, 2018). Importantly, phosphorylation and ubiquitination strongly affect each other. Phosphorylation of the NF- κ B inhibitor I κ B α by IKK β is a prerequisite for its K48-dependent proteasomal degradation and the ultimate release of the transcription factor NF- κ B (Wertz & Dixit, 2008). Beside its adaptor function, ubiquitination of RIPK1 also retains RIPK1 in the NF- κ B activating TNFR1 signaling complex I (Peltzer *et al.*, 2016). Thus, deubiquitination of RIPK1 by DUBs such as TNFAIP3 (A20), OTUD7B (Cezanne) or Cylindromatosis (CYLD) allows RIPK1 to translocate from complex I to complex II, the cell death-activating complex which fosters apoptosis (complex IIa, b) or necroptosis (complex IIc) (Harhaj & Dixit, 2011; Liu *et al.*, 2016). Of note, caspase-8-mediated apoptosis can occur in the absence (complex IIa) or in the presence of RIPK1 (complex IIb). Mice with RIPK1-deficient hepatocytes are highly susceptible to TNF-induced RIPK1-independent apoptotic cell death in an experimental model of immune-mediated liver injury (Suda *et al.*, 2016). Consistently, targeting of RIPK1 for K48-dependent proteasomal degradation by the ubiquitin-editing enzyme A20 promotes RIPK1-independent apoptosis via complex IIa. The TNF-induced signaling complexes are tightly regulated by the kinase activity of RIPK1. While the kinase activity of RIPK1 is dispensable for the complexes I and IIa, it is indispensable for the complexes IIb and IIc (Dondelinger *et al.*, 2016). Studies with RIPK1 mutants further revealed that in particular the c-IAP1-mediated K63-linked polyubiquitin chains on RIPK1 at K376 prevents its kinase activity as well as its autophosphorylation (Zhang *et al.*, 2019). The same group showed that RIPK1 mutant mice are consequently highly sensitive to TNF-triggered apoptosis and necroptosis due to the enhanced complex II formation. Accordingly, Tenev *et al.* hypothesized that kinase active RIPK1 spontaneously triggers the cytosolic formation of complex IIb, irrespective of a receptor activation, in conditions of genotoxic stress-induced c-IAP1 depletion (Tenev *et al.*, 2011). Notably, the stability of c-IAP1 itself is also regulated by ubiquitination and deubiquitination. In this line, the DUB OTUB1 has been shown to block TNF-induced apoptosis by maintaining c-IAP1 levels through constant cleavage of its K48-linked polyubiquitin chains (Goncharov *et al.*, 2013). Kinase active RIPK1 recruits RIPK3 in order to trigger necroptosis. Apart from c-IAP1, inhibition of caspase-8 seems to be required for the execution of necroptosis as revealed by experimental blockage and genetic ablation (Feltham *et al.*, 2017). Beside its function in driving apoptosis, caspase-8 also cleaves RIPK1 and RIPK3, thus preventing necrosome formation (Liu *et al.*, 2016). Activation and autocleavage of caspase-8 have been

shown to underly the regulation of ubiquitination, at least in context of CD95L- or TNF-related apoptosis-inducing ligand (TRAIL)-induced cell death signaling. Here, K63-linked polyubiquitin chains along with K48-linked polyubiquitin chains on procaspase-8 facilitate the autocatalytic cleavage, a process which is counterbalanced by the action of A20 (Jin *et al.*, 2009; Lim *et al.*, 2017). In contrast, attachment of K48-linked polyubiquitin chains on the caspase-8 cleavage products terminate apoptosis (Gonzalvez *et al.*, 2012). Similarly, the caspase-8 inhibitory protein c-FLIP is stabilized in a ubiquitin-dependent manner (Wertz & Dixit, 2008; Tang *et al.*, 2018). However, the mechanism of necroptosis and its inducing factors are still intensively discussed. Studies with overexpression of RIPK3 revealed that the expression of RIPK3 per se is sufficient to trigger necroptosis (Feoktistova *et al.*, 2011; Orozco *et al.*, 2014). In addition, it is generally believed that RIPK1 and RIPK3 undergo (i) autophosphorylation and (ii) phosphorylate each other upon activation. However, up to date, there is no direct evidence that RIPK1 phosphorylates other substrates except for itself arguing against the phosphorylation of RIPK3 by RIPK1 within the necrosome (Delanghe *et al.*, 2020). More recently, ubiquitination of RIPK1 and RIPK3 within the necrosome has been uncovered. Both M1- and K63-linked polyubiquitin chains have been reported for RIPK1 while only K63-linked polyubiquitin chains have been reported for RIPK3 (Dondelinger *et al.*, 2016). According to De Almagro *et al.*, M1- and K63-linked polyubiquitin chains assembled on RIPK1 at K115 stabilize its kinase activity to ensure necroptosis (de Almagro *et al.*, 2017).

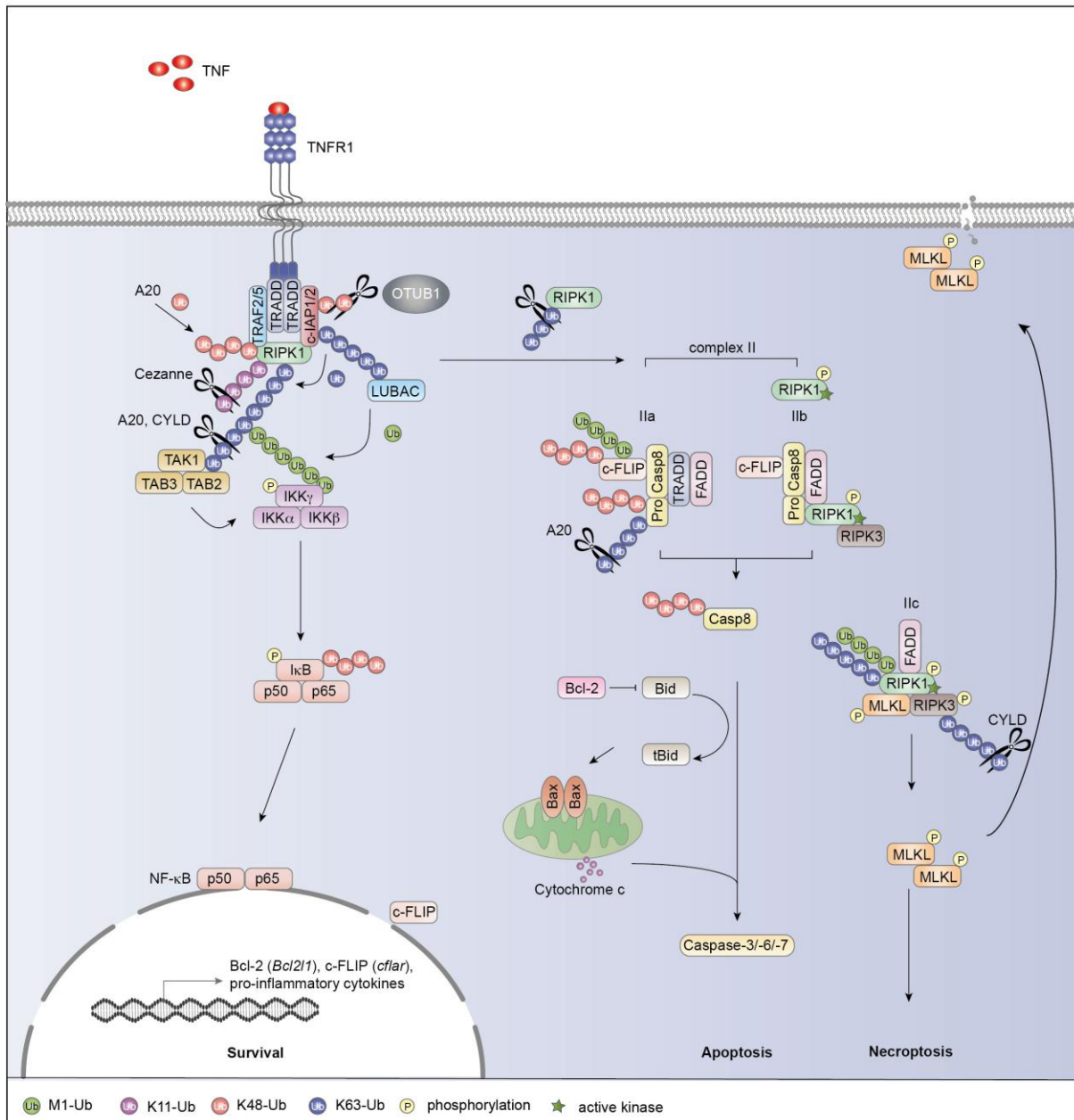


Figure 7: Polyubiquitination within TNFR1-signaling.

TNFR1-signaling is controlled by the two counterregulatory processes, ubiquitination and deubiquitination. Upon TNFR1 activation, K63-linked autoubiquitination of c-IAP1 and the subsequent c-IAP1-mediated conjugation of K63-, K11- and K48-linked polyubiquitin chains to RIPK1 initiates the recruitment of LUBAC adding M1-linked polyubiquitin chains to RIPK1. Consequently, the TAK1-TAB2/3 and the IKK complex attach to these ubiquitin chains trigger the translocation of NF- κ B to the nucleus by phosphorylating and thereby targeting I κ B α for K48-dependent proteasomal degradation. The polyubiquitin chains linked to RIPK1 are targeted by DUBs such as A20, CYLD or Cezanne. In addition, A20 can function as E3 ligase by adding K48-linked polyubiquitin chains to RIPK1. Deubiquitination of RIPK1 initiates its entry into complex II which is assembled in the cytosol and triggers caspase-8-mediated apoptosis. In conditions of reduced c-IAP1 stability, RIPK1 exhibits kinase activity leading to the formation of complex IIb. Depending on the caspase-8 activity, either RIPK1-dependent apoptosis or RIPK1/RIPK3/MLKL-mediated necroptosis is initiated. Both caspase-8 and the RIPK1/RIPK3-containing necrosome underly the control of the ubiquitin system. Caspase-8 is regulated by K48- and K63-linked polyubiquitin chains while the necrosome is mainly regulated by K63- but also M1-linked polyubiquitin chains.

2 AIM OF THIS STUDY

The deubiquitinating enzyme OTUB1 has been shown to control the activity and the stability of several signaling molecules, thus regulating a number of cellular processes. However, most of these studies were carried out using *in vitro* systems. Therefore, less is known about the *in vivo* function of OTUB1, especially in the context of the liver. This study aims to address the hepatocyte-specific function of OTUB1 under inflammatory conditions by using conditional OTUB1 knockout mice (OTUB1^{LPC-KO} mice). In particular, we determined:

Role of OTUB1 in liver homeostasis OTUB1-deficient mice are embryonically lethal. Moreover, OTUB1-deficient hepatocellular cancer cells possess defects in cell survival and proliferation. Therefore, we characterized the livers of OTUB1^{LPC-KO} mice for functionality, architecture as well as for their immune cell repertoire under physiological conditions. To clarify whether the deficiency of OTUB1 in hepatocytes yields in the development of an age-dependent autoimmune phenotype, we further analyzed one-year old OTUB1^{LPC-KO} mice.

Impact of OTUB1 on the course of bacterial hepatitis OTUB1 has been shown to regulate protective inflammatory responses against parasitic and viral infections. In this study, we elucidated whether hepatocyte-specific OTUB1 expression might regulate the outcome of bacterial infections. Therefore, we infected OTUB1^{LPC-KO} and OTUB1^{FL} mice with *Listeria monocytogenes*, a Gram-positive bacterium infecting and replicating in hepatocytes. In addition to survival, liver architecture and the immune response for an effective pathogen clearance, we studied the functional importance of OTUB1 in regulating pro-inflammatory as well as cell death signaling.

Role of OTUB1 during toxin-induced hepatitis To study whether OTUB1 might regulate immune responses in a pathogen-dependent manner, we induced acute liver injury in the OTUB1^{LPC-KO} mice by administration of DGal in combination with LPS or TNF, respectively.

Hepatocyte-intrinsic function of OTUB1 To further decipher the molecular mechanism how OTUB1 might influence signaling, we analyzed inflammatory signaling as well as cell death signaling in human HepG2 cells, in which OTUB1 was stably knocked down using lentiviral transduction.

3 MATERIAL AND METHODS

3.1 Materials

3.1.1 Chemicals

Table 3: Chemicals

Chemicals	Company
Agarose	Biozym (Hessisch Oldendorf, Germany)
Ammonium chloride (NH ₄ Cl)	Carl Roth (Karlsruhe, Germany)
Ammonium persulfate (APS)	Carl Roth (Karlsruhe, Germany)
Boric acid	Merck (Darmstadt, Germany)
Bovine serum albumin (BSA), Fraction V	Capricorn Scientific GmbH (Ebsdorfergrund, Germany)
Calcium chloride (CaCl ₂)	Merck (Darmstadt, Germany)
Dimethyl sulfoxide (DMSO)	Sigma-Aldrich (Steinheim, Germany)
Ethanol (99 %)	AppliChem (Darmstadt, Germany)
Ethylendiaminetetraacetic acid (EDTA)	Sigma-Aldrich (Steinheim, Germany)
Glucose	Sigma-Aldrich (Steinheim, Germany)
Glycine	Carl Roth (Karlsruhe, Germany)
Heparin (5000 U/ml)	Biochrom AG (Berlin, Germany)
Isoflurane (Forene)	Baxter (Unterschleißheim, Germany)
Magnesium chloride (MgCl ₂)	Qiagen (Hilden, Germany)
Methanol	J. T. Baker (Deventer, Netherlands)
Paraformaldehyde (PFA)	Carl Roth (Karlsruhe, Germany)
Percoll	GE Healthcare (Uppsala, Sweden)
Potassium chloride (KCl)	Merck (Darmstadt, Germany)
Potassium hydrogen carbonate (KHCO ₃)	Merck (Darmstadt, Germany)
Powdered milk	Carl Roth (Karlsruhe, Germany)
Rotiphorese Gel 30 (37.5:1) (Acrylamide)	Carl Roth (Karlsruhe, Germany)
Sodium Chloride (NaCl)	Carl Roth (Karlsruhe, Germany)
Sodium dodecyl sulfate (SDS)	Carl Roth (Karlsruhe, Germany)
Sucrose	Sigma-Aldrich (Steinheim, Germany)
Tetramethylethylenediamine (TEMED)	Sigma-Aldrich (Steinheim, Germany)

Chemicals	Company
Tris base, Tris HCl	Carl Roth (Karlsruhe, Germany)
Triton-X-100	Sigma-Aldrich (Steinheim, Germany)
Trypan blue	Sigma-Aldrich (Steinheim, Germany)
Tween 20	Sigma-Aldrich (Steinheim, Germany)

3.1.2 Buffers and cell culture media

Table 4: Buffers and cell culture media

Description	Company
Dulbecco's phosphate buffered saline (DPBS)	Gibco by Thermo Fisher Scientific (Waltham, USA)
Dulbecco's modified eagle medium (DMEM)	Gibco by Thermo Fisher Scientific (Waltham, USA)
Hank's balanced salt solution (HBSS)	Gibco by Thermo Fisher Scientific (Waltham, USA)
Opti-Minimal essential medium (MEM)	Gibco by Thermo Fisher Scientific (Waltham, USA)

3.1.3 Stimulation reagents

Table 5: Reagents *in vivo* and *in vitro* stimulation

Description	Specification	Company
LPS	<i>Salmonella enterica</i>	Sigma-Aldrich (Steinheim, Germany)
Cytokines		
human TNF	recombinant	PeptoTech (London, UK)
murine TNF	recombinant	PeptoTech (London, UK)

3.1.4 Reagents for cell culture

Table 6: Reagents for cell culture

Description	Company
Fetal calf serum (FCS)	Capricorn Scientific GmbH (Ebsdorfergrund, Germany)
Collagen solution from calf skin	Sigma-Aldrich (Steinheim, Germany)
Collagenase from <i>clostridium histolyticum</i>	Sigma-Aldrich (Steinheim, Germany)
Gentamicin solution	Sigma-Aldrich (Steinheim, Germany)
(4-(2-Hydroxyethyl)-1-piperazine-ethanesulfonic acid (HEPES)	Biochrom AG (Berlin, Germany)
L-Glutamine	Gibco by Thermo Fisher Scientific (Waltham, USA)
Non-essential amino acid (NEAA, 100 x)	Gibco by Thermo Fisher Scientific (Waltham, USA)
Penicillin/streptomycin (100 x)	Gibco by Thermo Fisher Scientific (Waltham, USA)
Trypsin-EDTA (0.5 %)	Gibco by Thermo Fisher Scientific (Waltham, USA)

3.1.5 Reagents for transfection of HepG2 cells with siRNA

Table 7: Transfection reagents

Description	Company
Lipofectamine RNAiMAX Transfection Reagent	Invitrogen by Thermo Fisher Scientific (Waltham, USA)
OTUB1 Silencer Select Validated siRNA	Ambion by Thermo Fisher Scientific (Waltham, USA)
Silencer Select Negative Control #1 siRNA	Ambion by Thermo Fisher Scientific (Waltham, USA)

3.1.6 Inhibitors

Table 8: Inhibitors used *in vivo* and *in vitro*

Description	Target	Company
Cycloheximide (CHX)	protein translation	Sigma-Aldrich (Steinheim, Germany)
D-Galactosamine	protein transcription	Carl Roth (Karlsruhe, Germany)
MG132	proteasome inhibitor	Sigma-Aldrich (Steinheim, Germany)
Necrostatin-1s (Nec-1s) (7-Cl-O-Nec1)	RIPK1	BioVision, Inc. (Milpitas, USA)
SCH772984	ERK1/2	Selleck Chemicals (Houston, USA)
Z-VAD-FMK (zVAD)	Pan-caspase	Enzo Life Sciences (Farmingdale, USA)

3.1.7 Reagents for molecular biology

Table 9: Reagents for molecular biology

Description	Company
Dithiothreitol (DTT)	Qiagen (Hilden, Germany)
Deoxyribonucleotide triphosphates (dNTPs)	Invitrogen by Thermo Fisher Scientific (Waltham, USA)
First Strand Buffer (5 x)	Invitrogen by Thermo Fisher Scientific (Waltham, USA)
HotStar Taq DNA Polymerase	Qiagen (Hilden, Germany)
Oligo(dT) ₁₂₋₁₈ Primer	Invitrogen by Thermo Fisher Scientific (Waltham, USA)
Polymerase chain reaction (PCR) Buffer (10 x)	Qiagen (Hilden, Germany)
SuperScript II Reverse Transcriptase	Invitrogen by Thermo Fisher Scientific (Waltham, USA)

3.1.8 Reagents for protein analyses

Table 10: Reagents for protein analyses

Description	Company
GammaBind G Sepharose Beads	GE Healthcare (Uppsala, Sweden)
Lane Marker Reducing Sample Buffer (5 x)	Thermo Fisher Scientific (Waltham, USA)
PageRulerPrestained Protein Ladder (10 - 180 kDa)	Thermo Fisher Scientific (Waltham, USA)
Phenylmethanesulfonylfluoride (PMSF)	Cell Signaling Technology (Danvers, USA)
PhosSTOP	Roche Diagnostics (Mannheim, Germany)
Protease Inhibitor Cocktail (25 x)	Sigma-Aldrich (Steinheim, Germany)
Protein Assay Dye Reagent Concentrate	Bio-Rad (California, USA)
Radioimmunoprecipitation assay (RIPA) buffer (10 x)	Cell Signaling Technology (Danvers, USA)

3.1.9 Antibodies for Western blot

Table 11: Antibodies used for Western blot

Description	Specification	Company
Primary antibodies		
α - β -Actin	D6A8	Cell Signaling Technology (Danvers, USA)
α -caspase-3	polyclonal	Cell Signaling Technology (Danvers, USA)
α -Bax	6A7	Novus Biologicals (Centennial, USA)
α -Bcl-2	polyclonal	Cell Signaling Technology (Danvers, USA)
α -BID	polyclonal	Cell Signaling Technology (Danvers, USA)
α -BID Cleavage Site	polyclonal	Abcam (Cambridge, UK)
α -caspase-8	1C12	Cell Signaling Technology (Danvers, USA)
	D35G2	Cell Signaling Technology (Danvers, USA)
	Asp387	Cell Signaling Technology (Danvers, USA)
α -c-IAP1	polyclonal	Abcam (Cambridge, UK)
α -ERK1/2	polyclonal	Cell Signaling Technology (Danvers, USA)
α -I κ B α	44D4	Cell Signaling Technology (Danvers, USA)
α -K63 TUBE	Biotin	LifeSensors (Malvern, USA)

Description	Specification	Company
α -OTUB1	polyclonal	Novus Biologicals (Centennial, USA)
α -p-ERK1/2	Thr202/Tyr204	Cell Signaling Technology (Danvers, USA)
α -p-I κ B α	Ser32	Cell Signaling Technology (Danvers, USA)
α -p-p38	Thr180/Tyr182 (3D7)	Cell Signaling Technology (Danvers, USA)
α -p-p65	Ser536 (93H1)	Cell Signaling Technology (Danvers, USA)
α -p-SAPK/JNK	Thr183/Tyr185	Cell Signaling Technology (Danvers, USA)
α -p100/p52	polyclonal	Cell Signaling Technology (Danvers, USA)
α -p38	polyclonal	Cell Signaling Technology (Danvers, USA)
α -p65	D14E12	Cell Signaling Technology (Danvers, USA)
α -RIPK1	D94C12	Cell Signaling Technology (Danvers, USA)
α -RIPK3	polyclonal	Abcam (Cambridge, UK)
α -SAPK/JNK	polyclonal	Cell Signaling Technology (Danvers, USA)
α -ubiquitin	Lys48-specific (Apu2)	Merck Millipore (Darmstadt, Germany)
Secondary antibodies		
Rabbit Anti-Mouse IgG/HRP (polyclonal)		Dako (Glostrup, Denmark)
Swine Anti-Rabbit IgG/HRP (polyclonal)		Dako (Glostrup, Denmark)
Goat Anti-Rat IgG/HRP (polyclonal)		Abcam (Cambridge, UK)
Mouse Anti-Rabbit IgG, light chain specific		Jackson ImmunoResearch Europe Ltd. (Cambridge, UK)

3.1.10 Antibodies for flow cytometry

Table 12: Antibodies for flow cytometric analyses

Fluorochrome	Antibody	Clone	Company
APC	CD11c	N418	Biolegend (San Diego, USA)
	Ly-6C	HK1.4	eBioscience by affymetrix (San Diego, USA)
	TNF	MP6-XT22	Biolegend (San Diego, USA)
	IgG1, κ	RTK2071	Biolegend (San Diego, USA)
APC-Cy7	CD11b	M1/70	Biolegend (San Diego, USA)
BV421	CD45R/B220	RA3-6B	BD Biosciences (San Jose, USA)
	F4/80	BM8	Biolegend (San Diego, USA)
BV510	CD3	145-2C11	BD Biosciences (San Jose, USA)
	CD8	53-6.7	Biolegend (San Diego, USA)
	CD45	30-F11	Biolegend (San Diego, USA)
FITC	Ly-6G	1A8	Biolegend (San Diego, USA)
	CD3	145-2C11	eBioscience by affymetrix (San Diego, USA)
PE	CD4	RM4-5	BD Biosciences (San Jose, USA)
	CD19	MB19-1	eBioscience by affymetrix (San Diego, USA)
	NK1.1	PK136	BD Biosciences (San Jose, USA)
PeCy7	CD3	145-2C11	Biolegend (San Diego, USA)
	CD11b	M1/70	Biolegend (San Diego, USA)
PerCP	CD45	30-F11	Biolegend (San Diego, USA)
PerCP/Cy5.5	Ly-6C	HK1.4	Biolegend (San Diego, USA)

Non-specific binding sites were blocked with α -CD16/32 (Clone 93) from Invitrogen by Thermo Fisher Scientific (Waltham, USA). Cells were stained with Fixable Viability Dye eFluor 506 or eFluor 780 from eBioscience by affymetrix (San Diego, USA) to exclude dead cells.

3.1.11 Antibodies for Immunofluorescence

Table 13: Antibodies used for immunofluorescence

Antibody	Specification	Company
Primary Antibodies α -p-MLKL	Ser358	Abcam (Cambridge, UK)
Secondary Antibody Goat Anti-Rabbit IgG, Alexa Fluor Plus 594	polyclonal	Thermo Fisher Scientific (Waltham, USA)

The nucleus was stained with ProLong Diamond Antifade Mountant with 4',6-diamidino-2-phenylindole (DAPI) which was purchased from Invitrogen by Thermo Fisher Scientific (Waltham, USA).

3.1.12 Kits

Table 14: Kits used in this study

Description	Company
ALT Activity Assay Kit	Sigma-Aldrich (Steinheim, Germany)
BD CBA Mouse Inflammation Kit	BD Biosciences (San Jose, Germany)
Intracellular Fixation & Permeabilization Buffer Set	eBioscience by affymetrix (San Diego, USA)
KAPA Mouse Genotyping Kit	KAPA Biosystems (Wilmington, USA)
KAPA PROBE FAST qPCR Master Mix (2x) Kit	KAPA Biosystems (Wilmington, USA)
Pierce LDH Cytotoxicity Assay Kit	Thermo Fisher Scientific (Waltham, USA)
Pierce ECL 2 Western Blotting Substrate	Thermo Fisher Scientific (Waltham, USA)
QIAshredder Kit	Qiagen (Hilden, Germany)
RNeasy Mini Kit	Qiagen (Hilden, Germany)

3.1.13 PCR primers

Table 15: Primers for PCR

Primer	Sequence (5'→3')	
Alb-Cre	sense	5'-ACC TGA AGA TGT TCG CGA TTA TCT-3'
	antisense	5'-ACC GTC AGT ACG TGA GAT ATC TT-3' (Amplicon size: 450 bp)
OTUB1	sense	5'-GAG GTA GGT GAT GCT CAG GTG-3'
	antisense	5'-CTT ACT GGG AAA GAA GCT TGC-3' (Amplicon size: OTUB1 ^{wt/wt} = 216 bp, OTUB1 ^{fl/fl} = 376 bp)
MLKL	sense	5'-CAT CAA GTT AGG CCA GCT CA-3'
	antisense	5'-TCT GCT GGT TAG CCT CCT TC-3' (Amplicon size: MLKL ^{wt/wt} = 204 bp; MLKL ^{del/del} = 173 bp)
HPRT	sense	5'-GCT GGT GAA AAG GAC-3'
	antisense	CCA GTT TCA CTA ATG (Amplicon size: genomic DNA = 945 bp; complementary DNA = 145 bp)

All primers were purchased from Eurofins MWG (Ebersberg, Germany).

3.1.14 TaqMan gene expression assay probes

Table 16: TaqMan gene assay probes for qRT-PCR

TaqMan Assay probe	Gene	Assay ID	Amplicon Length
Bax	<i>Bax</i>	Mm00432051_m1	84
Bcl-2	<i>Bcl2l1</i>	Mm00437783_m1	65
c-FLIP	<i>Cflar</i>	Mm01255576_m1	83
c-IAP1	<i>Birc2</i>	Mm00431811_m1	90
HPRT	<i>Hprt</i>	Mm01545399_m1	81
IFN γ	<i>Ifng</i>	Mm00801778_m1	101
IL-1 β	<i>Il1b</i>	Mm00434228_m1	90
IL-6	<i>Il6</i>	Mm00446190_m1	78
OTUB1	<i>Otub1</i>	Mm00506597_m1	93
TNF	<i>Tnf</i>	Mm00443258_m1	81

All TaqMan Assay probes were purchased from Thermo Fisher Scientific (Waltham, USA).

3.1.15 Consumables

Table 17: Consumables used in this study

Description	Company
Cell strainer (40 µm, 70 µm, 100 µm)	Falcon (Durham, USA)
Cell culture plates (6 well, 12 well, 96 well, flat bottom)	Greiner Bio-One (Frickenhausen, Germany)
Cuvettes	Sarstedt AG & Co. (Nümbrecht, Germany)
Eppendorf tubes (0.2 ml, 1.5 ml, 2 ml)	Eppendorf (Hamburg, Germany)
Filter Paper 583 Gel Dryer	Bio-Rad (California, USA)
5 ml Polystyrene Round-Bottom Tube	Falcon (Durham, USA)
Needles (26G)	B. Braun Melsungen AG (Melsungen, Germany)
Petri dishes	Sarstedt AG & Co. (Nümbrecht, Germany)
Polyvinylidene fluoride (PVDF) membrane	Roche Diagnostics (Mannheim, Germany)
Serological Pipette (5 ml, 10 ml, 25 ml)	Greiner Bio-One (Frickenhausen, Germany)
Lightcycler plates 480 Plate 96 white	Roche Diagnostics (Mannheim, Germany)
Stericup Filter Units	Merck Millipore (Darmstadt, Germany)
Syringes (1ml, 2 ml)	BD Biosciences (San Jose, USA)

3.1.16 Instruments

Table 18: Instruments used in this study

Instrument	Company
Agagel Midi-wide	Biometra Analytik (Jena, Germany)
BD FACS Canto II Flow Cytometer	BD Biosciences (San Jose, Germany)
Bio Photometer B30	Eppendorf (Hamburg, Germany)
Biotek Microplate Reader	BioTek (Vermont, USA)
Centrifuge Mikro 200R	Hettich (Tuttlingen, Germany)
Centrifuge Rotanta 460R	Hettich (Tuttlingen, Germany)
Chemo Cam Luminescent	INTAS (Göttingen, Germany)
Image Analysis System	
Incubator Heraeus Cytosperm2	Heraeus (Hanau, Germany)
Incubator shaker GFL 3032	GFL (Großburgwedel, Germany)
Laboratory Balance	Sartorius (Göttingen, Germany)
Laminar Flow Hood	Heraeus (Hanau, Germany)
Lightcycler 480 II	Roche Diagnostics (Mannheim, Germany)
Microscope Olympus CX-41	Olympus (Hamburg, Germany)
Microscope Axio Imager Z1	Carl Zeiss AG (Oberkochen, Germany)
Mini-PROTEAN tetra vertical electrophoresis	Bio-Rad (California, USA)
NanoDrop ND-1000 Spectrophotometer	Thermo Fisher Scientific (Waltham, USA)
Neubauer Counting chamber (improved)	LO Laboroptik (Lancing, UK)
pH meter	Schott (Mainz, Germany)
Pipettes (10 µl, 20 µl, 200 µl, 100 µl, 1000 µl)	Eppendorf (Hamburg, Germany)
Pipetting aid	Eppendorf (Hamburg, Germany)
PowerPac HC	Bio-Rad (California, USA)
Roller Mixer SRT9	Stuart (Staffordshire, UK)
Professional Gel Documentation System	PHASE (Lübeck, Germany)
Thermomixer	Eppendorf (Hamburg, Germany)
Trans-Blot Turbo Transfer System	Bio-Rad (California, USA)
Vortex Genius 3	IKA (Staufen, Germany)
Water bath	Thermo Fisher Scientific (Waltham, USA)

3.1.17 Software

Table 19: Software for data analysis

Software	Description	Company
BD FACSDiva Software	Data acquisition on BD Fluorescent activated cell sorter (FACS) Canto II	BD Biosciences (San Jose, USA)
FlowJo vX software	FACS data analysis	Tree Star (Ashland, USA)
FCAP Array v3.0	CBA data analysis	Soft Flow Inc. (St. Louis Park, USA)
GraphPad Prism 8	Statistical analysis	GraphPad Software (San Diego, USA)
LabImage	Western blot analysis, Quantification of protein intensity	Intas Science Imaging Instruments GmbH (Göttingen, Germany)

3.1.18 Animals

C57BL/6 OTUB1^{FL} as previously described (Wang *et al.*, 2019) were crossed with C57BL/6 Alb-Cre mice to generate Alb-Cre OTUB1^{FL} mice (OTUB1^{LPC-KO}) which lack the expression of OTUB1 specifically in liver parenchymal cells. C57BL/6 OTUB1^{FL} mice were used as control throughout all experiments. The MLKL^{del/del} mice were kindly provided by Prof. Dr. Manolis Pasparakis (CECAD Research Center, Institute for Genetics, University of Cologne) (Lin *et al.*, 2016). MLKL^{del/del} mice were crossed with OTUB1^{LPC-KO} mice to obtain MLKL^{del/del} OTUB1^{LPC-KO} mice. For experiments, age and sex matched mice were used. All experiments were performed in accordance to the German Animal Welfare Act (Deutsches Tierschutzgesetz) and approved by local authorities (Landesverwaltungsamt, Sachsen-Anhalt, Germany; file number: 42502-2-1440).

3.2 Methods

3.2.1 Mouse genotyping

Mice strains were genotyped by conventional polymerase chain reaction (PCR) using the KAPA Mouse Genotyping Kit. Genomic DNA extraction from tail biopsies of four-week-old mice and the subsequent PCR were performed according to the manufacturer's protocol with the primers listed in Table 15. PCR products were separated on a 1.5 % agarose gel in Tris-borate-EDTA (TBE) buffer.

TBE buffer (10 x)

100	mM	Boric acid
100	mM	Tris base
2.5	mM	EDTA
ad 1	l	distilled water
		pH 8.3

PCR reaction mix

25	mM	MgCl ₂
1	x	2 x KAPA2G Fast HotStart Genotyping Mix
1	μM	Primer (sense)
1	μM	Primer (antisense)
1	μl	genomic DNA
ad 25	μl	PCR-grade water

PCR cycling protocol

Step	Temperature	Time	Cycles
Initial denaturation	95 °C	3 min	1
Denaturation	95 °C	15 s	} 35
Annealing	60 °C	15 s	
Extension	72 °C	15 s	
Final Extension	72 °C	10 min	1

3.2.2 Cell culture

Isolation of primary hepatocytes Primary hepatocytes were isolated from mouse liver by a two-step perfusion method. The mice were anesthetized with isoflurane and the liver was perfused with perfusion buffer I via the inferior vena cava. In a second step, the liver was perfused with pre-warmed (37 °C) perfusion buffer II containing 0.9 mg/ml collagenase for additional 3 min. Thereafter, the liver was dissected and passed through a 100 µm cell strainer. Viable hepatocytes were enriched by percoll gradient centrifugation (3.2.11) and determined by trypan blue staining. Subsequently, the hepatocytes were seeded on collagen-coated plates in Dulbecco's modified eagle medium (DMEM) supplemented with 10 % fetal calf serum (FCS), 1 % penicillin/streptomycin, 1 % L-Glutamine and 1 % non-essential amino acids (NEAA). To remove non-adherent cells, the cells were washed twice and the medium was changed to DMEM supplemented with 20 % FCS, 1 % penicillin/streptomycin, 1 % L-Glutamine and 1 % NEAA after 4 h of cultivation.

Perfusion buffer I

0.2	mM	EDTA
5	mM	Glucose
10	mM	HEPES
0.05	%	KCl
ad 500	ml	DPBS
	pH	7.4

Perfusion buffer II

1	mM	CaCl ₂
5	mM	Glucose
20	mM	HEPES
0.05	%	KCl
ad 500	ml	DPBS
	pH	7.4

Cultivation of human hepatocellular carcinoma cells (HepG2) OTUB1-sufficient and OTUB1- deficient HepG2 cells were kindly provided by Prof. Dr. habil. Andrea Kröger (Institute of Medical Microbiology and Hospital Hygiene, Otto von Guericke University,

Magdeburg). OTUB1 was stably knocked down in these cells using lentiviral transduction. The cells were cultured in DMEM supplemented with 10 % FCS and 1 % penicillin/streptomycin.

3.2.3 Transfection of HepG2 cells with small interfering RNA (siRNA)

HepG2 cells were transfected with OTUB1 siRNA or negative control siRNA as indicated in Table 7. Transfection was performed with the Lipofectamine RNAiMAX Transfection Reagent according to the manufacturer's instructions for 24 h in a 6-well format. Knockdown efficiency was controlled by western blotting (WB).

3.2.4 Protein analyses by Western Blotting

Protein extraction Liver tissue was minced through a 100 µm cell strainer in radioimmunoprecipitation assay (RIPA) lysis buffer, aliquoted and stored at -80 °C. For western blotting, protein stocks were diluted 1:10 in RIPA lysis buffer, incubated for 30 min on ice and thereafter centrifuged at 13 000 x g at 4 °C for 15 min. Protein extracts from cultured hepatocytes or HepG2 cells were obtained by lysing the cells in RIPA lysis buffer, followed by an incubation for 30 min on ice and a centrifugation at 13 000 x g at 4 °C for 15 min. Supernatants were collected and the protein concentrations were measured with Bradford assay.

RIPA lysis buffer

1	mM	PMSF
1	x	PhosSTOP (10 x)
1	x	Protease Inhibitor cocktail (25 x)
1	x	RIPA (10 x)

Western Blotting Protein lysates prepared as described above were denatured for 5 min at 99 °C after adding 1 x Lane Marker Reducing Sample Buffer. Equal amounts of protein were fractionated on an 8 - 15 % SDS-polyacrylamide gel and subsequently blotted on a polyvinylidene fluoride (PVDF) membrane in a semi-dry transfer. To block non-specific bindings, the membrane was blocked at room temperature with 5 % bovine serum albumin (BSA) or 5 % milk, respectively, for 1 h. Proteins were probed with the primary antibodies as listed Table 11 at 4 °C overnight, washed for three times with TBST and thereafter probed with the corresponding secondary antibodies as listed in Table 11 at RT for 1 h. Blots were developed using Pierce ECL 2 Western Blotting Substrate and captured with Chemo Cam Luminescent

Image Analysis system (INTAS Science Imaging Instruments, Göttingen, Germany). For quantification, the LabImage Platform software (Kapelan Bio-Imaging, Leipzig, Germany) was used.

Resolving gel (%)				
8	10	12	15	Reagents
46 % (v/v)	40 % (v/v)	33 % (v/v)	23 % (v/v)	distilled water
27 % (v/v)	33 % (v/v)	40 % (v/v)	50 % (v/v)	Acrylamide (30 %)
25 % (v/v)	25 % (v/v)	25 % (v/v)	25 % (v/v)	Tris-HCl (1.5 M, pH 8.8)
0.1 % (v/v)	0.1 % (v/v)	0.1 % (v/v)	0.1 % (v/v)	SDS
0.1 % (v/v)	0.1 % (v/v)	0.1 % (v/v)	0.1 % (v/v)	APS
0.04 % (v/v)	0.04 % (v/v)	0.04 % (v/v)	0.04 % (v/v)	TEMED

Stacking gel (5 %)

68 % (v/v)	distilled water
17 % (v/v)	Acrylamide (30 %)
13 % (v/v)	Tris-HCl (1 M, pH 7.4)
0.1 % (v/v)	SDS
0.1 % (v/v)	APS
0.1 % (v/v)	TEMED

Gel running buffer (10 x)

30.2 g	Tris
144 g	Glycine
10 g	SDS
ad 1 l	distilled water
	pH 8.3

Transfer buffer

3 g	Tris
14.5 g	Glycine
1 g	SDS
20 % (v/v)	Methanol
ad 1 l	distilled water
	pH 8.4

TBS (10 x)

24.2 g	Tris
80 g	NaCl
ad 1 l	distilled water
	pH 7.6

TBST (10 x)

add 0.1 % (v/v)	Tween 20
-----------------	----------

3.2.5 Immunoprecipitation

Protein lysates prepared as described in 3.2.4 were pre-cleared with GammaBind G Sepharose Beads at 4 °C for 1 h with agitation. Protein samples were centrifuged for 10 min at 10 000 x g at 4 °C to remove the beads. Equal amounts of protein were incubated with antibodies against OTUB1, c-IAP1, RIPK1 or ubiquitin (Lys48-specific) at 4 °C overnight with agitation, followed by an additional incubation with beads at 4 °C for 2 h. The beads were collected by centrifugation at 10 000 x g at 4 °C for 30 s and subsequently washed three times with cold DPBS. Immune complexes were eluted with 2 x Lane Marker Reducing Sample Buffer for 5 min at 99 °C. To remove the beads, samples were centrifuged at 10 000 x g at 4 °C for 30 s. Western blot analyses were performed as described in 3.2.4.

3.2.6 Quantitative real-time PCR (qRT-PCR)

Total RNA was isolated from liver tissue or cultured cells using the QIAshredder kit for homogenization, followed by using the RNeasy Mini Kit. Concentration and purity of the isolated RNA was quantified with NanoDrop Spectrophotometer. First strand complementary DNA (cDNA) was synthesized from 1 µg of total RNA input with the Superscript Reverse Transcriptase Kit as follows:

cDNA synthesis		
	1 µg	Total RNA
	ad 50 µl	RNase free water
1. Annealing	2 µl	Oligo(dT) ₁₂₋₁₈ Primer
	5 µl	dNTPs
		5 min at 65°C, afterwards cool on ice
2. First strand cDNA synthesis	16 µl	First strand buffer (5x)
	8 µl	DTT
	1.5 µl	SuperScript II Reverse Transcriptase
	4.5 µl	RNase free water
		50 min at 42 °C
3. Inactivation	→	10 min at 70 °C

Prior to the qRT-PCR, a conventional PCR for the house keeping gene HPRT using the primers indicated in Table 15 was performed to exclude contaminations with genomic DNA.

PCR reaction mix

1	x	PCR Buffer (10x)
200	µM	dNTPs
0.4	µM	HPRT Primer (sense)
0.4	µM	HPRT Primer (antisense)
0.6	U	HotStarTaq DNA Polymerase
1.5	µl	Template (cDNA)
ad 25	µl	PCR-grade water

PCR cycling protocol

Step	Temperature	Time	Cycles
Initial denaturation	95 °C	15 min	1
Denaturation	94 °C	45 s	} 38
Annealing	53 °C	45 s	
Extension	72 °C	45 s	
Final Extension	72 °C	7 min	1

qRT-PCR was performed with the TaqMan Assay probes listed in Table 16 and the KAPA PROBE FAST qPCR Master Mix (2 x) Kit on a LightCycler 480 II according to manufacturer's protocol. Gene expression was normalized to the HPRT reference gene. Gene expression levels were calculated as ratio between the target gene and the reference gene based on the $2^{-\Delta\Delta CT}$ method (Livak & Schmittgen, 2001).

qRT-PCR reaction mix

10	μl	KAPA PROBE FAST qPCR Master Mix (2x)
0.5	μl	TaqMan gene expression assay probes
2	μl	cDNA
ad 20	μl	PCR-grade water

3.2.7 Infection with *Listeria monocytogenes*

Infection experiments were performed with *Listeria monocytogenes* wildtype (Lm, EGD strain). Lm was grown in Brain heart infusion (BHI) broth at 37 °C up to log-phase and aliquoted for storage at -80 °C.

***In vivo* infection with Lm** For infection of mice, a fresh log-phase culture was prepared from frozen Lm stock and adjusted to 5×10^4 colony forming units (CFU) of Lm in 200 μl of sterile pyrogen-free Dulbecco's phosphate buffered saline (DPBS, pH 7.4). Mice were infected intravenously (i.v.). Infection dose was monitored by plating an inoculum on BHI agar and counting the grown colonies after an overnight incubation at 37 °C.

Colony Forming Units To determine the bacterial loads in liver and spleen, mice were sacrificed at the indicated time points. After perfusion with 0.9 % NaCl, the organs were dissected and homogenized with sterile tissue grinders. Serial dilutions of the homogenate were plated on BHI agar and incubated at 37 °C for 24 h. Bacterial colonies were counted microscopically for calculating the CFUs per organ.

***In vitro* infection with Lm** Infection of primary hepatocytes or HepG2 cells *in vitro* was carried out at 37 °C for 1 h. Cells were starved overnight before infecting the cells with a multiplicity of infection (MOI) of 10 in DMEM supplemented with 10 % FCS and 1 % penicillin/streptomycin. After 1 h of infection, extracellular Lm were killed by adding 30 µg/ml gentamicin solution to the medium. Cells were harvested for protein isolation and total RNA isolation at the indicated time points. To determine the number of intracellular bacteria, the Lm-infected cells were lysed in 0.1 % Triton-X-100, diluted serially and thereafter plated on BHI agar. After an incubation of 24 h at 37 °C, the bacterial colonies were counted microscopically.

3.2.8 D-Galactosamine shock model

Mice received either 400 mg/kg DGal and 40 µg/kg TNF or 700 mg/kg DGal in combination with 2.5 µg/kg LPS dissolved in 200 µl of sterile pyrogen-free DPBS intraperitoneally. After 6 h and 24 h, mice were sacrificed for analysis.

3.2.9 Histology

For histology, the mice were anesthetized and were perfused with 0.9 % NaCl to remove blood contaminations. The liver was dissected and fixed with 4 % paraformaldehyde (PFA) at 4 °C. After 48 h, the liver was transferred to sterile DPBS for long-term storage at 4 °C. Paraffin sections were stained with Hematoxylin and eosin (H&E).

3.2.10 Serology

Mice were anesthetized with isoflurane and blood was sampled via cardiac puncture using a gauge needle (26 G) which was attached to a heparinized syringe. Serum was obtained after centrifugation and analyzed for cytokine levels, Alanine aminotransferase (ALT) activity and LDH release into the serum. Cytokine levels were measured by flow cytometry using Cytometric Bead Array (BD CBA Mouse Inflammation Kit). To determine the ALT activity in

serum, manufacturer's instructions for the ALT Activity Assay Kit were followed. LDH release was measured using the Pierce LDH Cytotoxicity Assay Kit.

3.2.11 Immune cell characterization by flow cytometry

Immune cell populations were characterized in livers and spleens of uninfected and Lm-infected mice by flow cytometry.

Leukocyte isolation from liver and spleen The anesthetized mice were perfused with 0.9 % NaCl intracardially before the organs were dissected and minced through a 70 μ m cell strainer in Hank's balanced salt solution (HBSS) supplemented with 3 % FCS. After erythrocyte lysis at 4 °C for 10 min, the cells were washed with HBSS supplemented with 3 % FCS at 300 x g at 4 °C for 6 min. The cell pellet was resuspended in an appropriate volume of HBSS containing 3 % FCS and passed through a 40 μ m cell strainer.

Erythrocyte lysis buffer

8.29	g	NH ₄ Cl
1	g	KHCO ₃
37.2	mg	Na ₂ EDTA
ad 1	l	distilled water
		pH 7.2 - 7.4

To isolate leukocytes from liver, an additional percoll gradient centrifugation was performed following the erythrocyte lysis. The cells were resuspended in 15 ml of 80 % percoll and then carefully overlaid with 15 ml of 40 % percoll. The created gradient was centrifuged at 1200 x g at 25 °C without rotor break for 20 min. Afterwards, the top layer was removed and the interface ring containing the leukocytes was collected. The cell suspension was washed once with HBSS supplemented with 3 % FCS at 300 x g at 4 °C for 6 min. The number of viable cells were determined in a Neubauer counting chamber using trypan blue staining.

Percoll stock solution (per liver)

25	ml	Percoll
2.7	ml	NaCl (1.5 M)
<hr/>		
80 %		40 %
15	ml	7.5 ml Percoll stock solution
3.75	ml	11.25 ml HBSS + 3 % FCS

Flow cytometry Single cell suspension was prepared as described above. For detection of surface antigens, 1×10^6 cells were transferred to a 5 ml polystyrene round bottom tube (FACS tube) and washed once with FACS buffer (DPBS supplemented with 3 % FCS) at $300 \times g$ at 4°C for 6 min. To prevent non-specific binding of the fluorochrome-conjugated antibodies, $1 \mu\text{g}$ of CD16/CD32 diluted in $30 \mu\text{l}$ of FACS buffer was added to the cells and incubated for 10 min in the dark before the cells were stained with the specific fluorochrome-conjugated antibodies diluted in $100 \mu\text{l}$ of FACS buffer at 4°C for 20 min protected from light. The fluorochrome-conjugated antibodies are indicated in Table 12. Afterwards, the cells were washed with FACS buffer at $300 \times g$ at 4°C for 6 min. Cells were stained with Fixable Viability Dye eFluor 506 or eFluor 780 to exclude dead cells and fixed in 1 % PFA at 4°C for 20 min. Staining of intracellular antigens was performed after restimulation with $1 \mu\text{l}$ of heat killed Lm at 37°C for 5 h in the presence of Brefeldin A solution (1x, Biolegend, San Diego, USA). Intracellular antigens were stained using the Intracellular Fixation & Permeabilization Buffer Set and the protocol for intracellular (cytoplasmic) proteins provided by eBioscience. Briefly, cells were fixed with $100 \mu\text{l}$ of IC Fixation buffer at RT for 20 min and washed two times with 1x Permeabilization buffer before the fluorochrome-conjugated antibodies diluted in $100 \mu\text{l}$ of 1x Permeabilization buffer were added. After an incubation of 20 - 60 min at RT, cells were washed two times with 1x Permeabilization buffer. Finally, cells were resuspended in $100 \mu\text{l}$ of FACS buffer. Samples were acquired on the BD FACS Canto II Flow Cytometer using BD FACSDiva Software (BD Biosciences, San Jose, USA) followed by data analysis with FlowJo vX software (Tree Star, Ashland, USA).

Heat killed Lm Heat killed Lm was prepared from a fresh log-phase Lm culture of frozen Lm stock. 1 ml of the log-phase culture was pelleted at 5000 x g for 10 min, washed twice with DPBS and thereafter resuspended in 500 µl of DPBS. For inactivation, Lm was incubated at 80 °C for 1 h. Restimulation was performed with 1 µl of heat killed Lm per 1 x 10⁶ cells.

3.2.12 Inhibitor experiments

***In vivo* inhibition of apoptosis and necroptosis** To investigate the mode of cell death, mice were injected with either 4 mg/kg Necrostatin-1s (Nec-1s) or 6 mg/kg or Z-VAD-FMK (zVAD) i.v. 90 min before the intravenous infection with 5 x 10⁴ CFU of Lm. Nec-1s or zVAD was injected daily up to day 2 p.i. At day 3 p.i., mice were sacrificed. For survival experiments, Nec-1s administration was continued until day 5 p.i. and survival rates were monitored daily.

***In vitro* inhibition of necroptosis** Cultured HepG2 cells were infected with Lm as described in 3.2.7. For inhibition of necroptosis, the infection with Lm was performed in the presence of 30 µM Nec-1s for the indicated timepoints. The inhibitor was added 30 min before infecting the cells.

***In vitro* inhibition of protein translation** For cell death induction *in vitro*, cultured HepG2 cells were starved overnight and thereafter stimulated with 20 ng/ml human recombinant TNF in combination with 10 µg/ml of the protein translation inhibitor, Cycloheximide (CHX) for the indicated timepoints.

***In vitro* inhibition of ERK activation** Activation of the Extracellular signal-regulated kinase (ERK) was blocked by adding 0.5 µM SCH772984 to the cells 30 min prior to the stimulation with TNF/CHX or infection with Lm.

3.2.13 Immunofluorescence

2.5 x 10⁵ HepG2 cells were plated on sterilized coverslips under starving conditions one day before infecting the cells with Lm as described in 3.2.7. Following infection, the cells were fixed with 4 % PFA at RT for 10 min. The cells were washed with DPBS three times and then permeabilized with 0.1 % Triton-X-100 at RT for 7 min. Thereafter, non-specific bindings were blocked by adding blocking solution at RT for 45 min. The cells were incubated with the primary antibody (α-p-MLKL, purchased from Abcam, Cambridge, UK) diluted 1:200 in

blocking solution overnight on a shaking platform. After three times of washing with DPBS, cells were incubated with the fluorophore-conjugated secondary antibody (Alexa Fluor 594 goat-anti-rabbit, purchased from Invitrogen by Thermo Fisher Scientific, Waltham, USA) at RT for 2 h protected from light. Cells were washed again three times with DPBS and finally mounted on a slide using ProLong Diamond Antifade with DAPI. Images were captured on Microscope Axio Imager Z1.

Blocking solution

0.5	%	BSA
10	%	FCS
5	%	Sucrose
0.3	%	Triton-X-100
		DPBS

4 RESULTS

4.1 Hepatocyte-specific expression of OTUB1 is dispensable for liver homeostasis

To investigate the hepatocyte-specific function of OTUB1, conditional OTUB1 knockout mice were generated using the Cre/loxP system. In brief, C57BL/6 OTUB1^{FL} mice as published by Wang et al. (Wang *et al.*, 2019) were crossed to C57BL/6 Alb-Cre mice expressing the Cre recombinase under control of the albumin promoter. Thus, activity of the Cre recombinase was restricted to liver parenchymal cells where it targeted the *Otub1* gene flanked with two loxP sequences (exon 2 and 3) for excision. The Alb-Cre OTUB1^{FL} (OTUB1^{LPC-KO}) mice showed an efficient deletion of OTUB1 in the liver as confirmed by Western blot (WB) analysis (Figure 8 A) and qRT-PCR (Figure 8 B). The OTUB1^{LPC-KO} mice were born in a normal mendelian ratio and developed normally without apparent phenotypical abnormalities. In particular, the liver architecture was similar between OTUB1^{LPC-KO} and OTUB1^{FL} mice as revealed by histological examinations of liver tissue from 10-week-old mice (Figure 8 C). At the age of one year, the livers from OTUB1^{LPC-KO} mice were normal without evidence for inflammation (Figure 8 B). Consistently, serological and flow cytometric analysis revealed a normal liver function in 10-week-old OTUB1^{LPC-KO} mice under physiological conditions as serum levels of the liver enzyme Alanine aminotransferase (ALT) and absolute numbers of hepatic leukocytes were comparable between 10-week-old OTUB1^{LPC-KO} and OTUB1^{FL} mice (Figure 8 D, E). Similarly, no alterations of liver function were detected in aging OTUB1^{LPC-KO} mice as indicated by equal serum ALT levels and the immune cell composition in the livers of naïve 52-week-old OTUB1^{LPC-KO} mice (Figure 8 F, G). These data suggest that hepatic OTUB1 expression is not required for liver homeostasis.

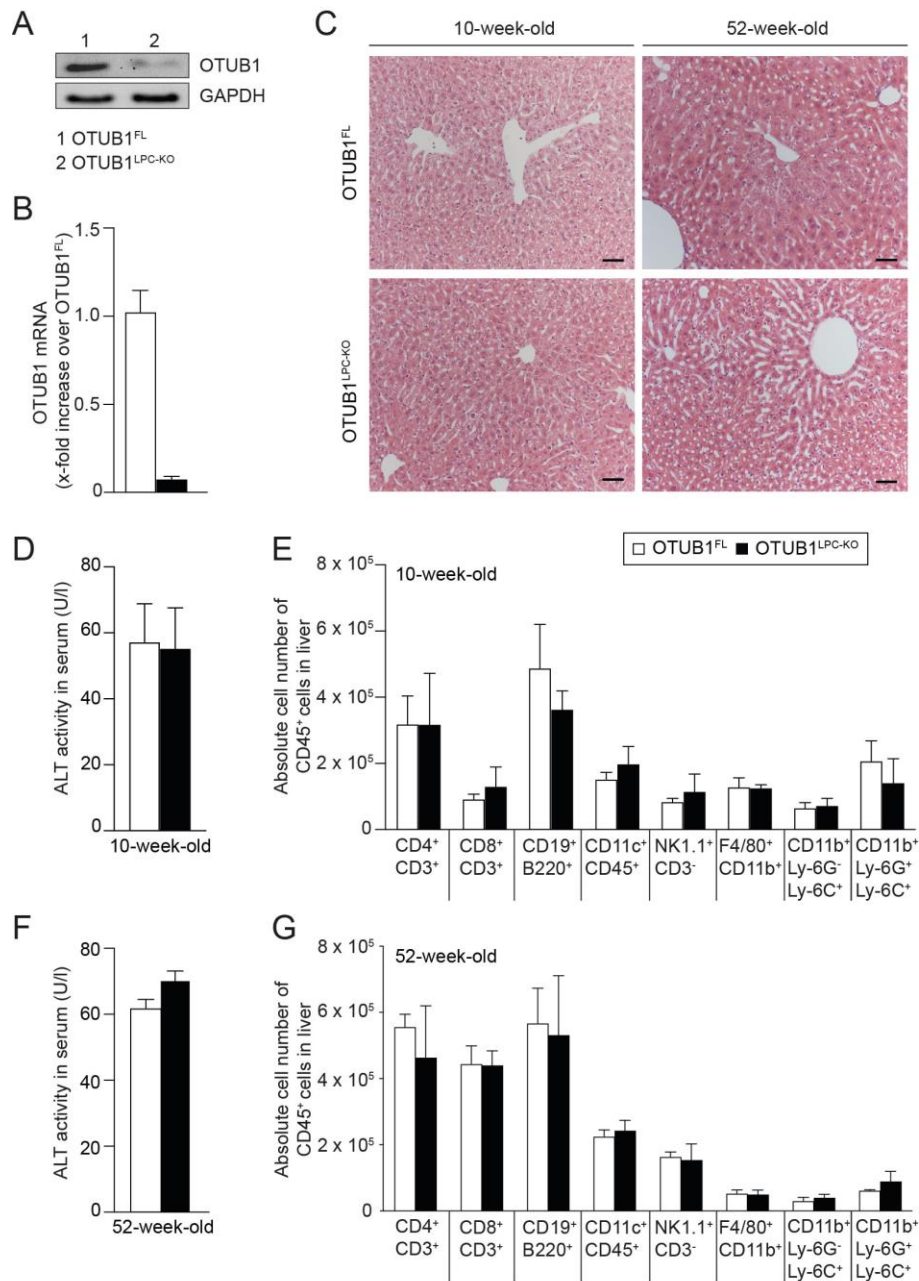


Figure 8: Deletion of OTUB1 in the liver did not disturb liver function.

(A) Total liver protein lysates isolated from naïve OTUB1^{LPC-KO} and OTUB1^{FL} control mice were analyzed for OTUB1 and GAPDH expression by WB. Representative blots are shown. (B) Quantitative RT-PCR analysis for the relative OTUB1 mRNA expression in the livers of naïve OTUB1^{LPC-KO} and OTUB1^{FL} mice (n = 4 per experimental group). (C) Liver sections from naïve 10- and 52-week-old OTUB1^{LPC-KO} and OTUB1^{FL} control mice were dissected and examined by histopathology. Representative images are depicted (H&E staining, scale bars indicate 50 μ m, n = 3 per experimental group). (D) ALT activity was measured in serum samples of 10-week-old OTUB1^{LPC-KO} and OTUB1^{FL} mice (n = 4 per experimental group) (E) Hepatic leukocytes were isolated from liver and analyzed by flow cytometry (n = 3 per experimental group). (F, G) Characterization of 52-week-old OTUB1^{LPC-KO} and OTUB1^{FL} mice (n = 3 per experimental group). (F) ALT activity was determined in serum. (G) Flow cytometric analysis of leukocyte populations in liver. Data are represented as mean + SEM, (B - F) Student's *t*-test.

4.2 OTUB1 protects mice from bacterial-and inflammation-induced lethality

4.2.1 OTUB1 prevents hepatic failure during infection with *Listeria monocytogenes*

The intracellular bacterium *Listeria monocytogenes* primarily targets the liver where it infects and replicates in the hepatocytes (Gregory *et al.*, 1992). To study whether OTUB1 expression in the liver might regulate the outcome of bacterial infections, OTUB1^{LPC-KO} and OTUB1^{FL} control mice were infected with *Listeria monocytogenes* (Lm) i.v. Upon low dose infection with 1×10^4 CFU of Lm, 20 % of OTUB1^{LPC-KO} mice succumbed to the infection within 6 days p.i., while all OTUB1^{FL} control mice survived (Figure 9 A). An increase in the dose of infection to 5×10^4 CFU of Lm caused 100 % mortality of OTUB1^{LPC-KO} mice but only 10 % mortality of OTUB1^{FL} control mice illustrating a protective role of hepatocyte-specific OTUB1 during infection with *L. monocytogenes* (Figure 9 B).

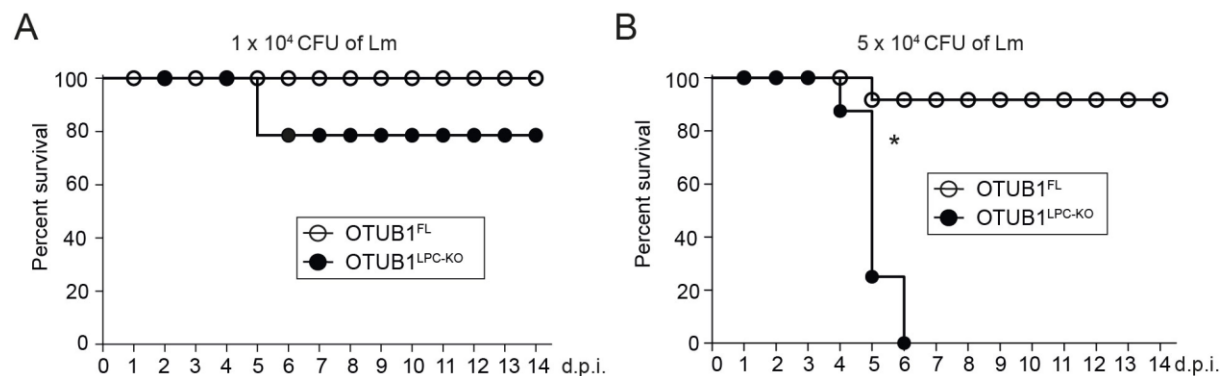


Figure 9: OTUB1 protects from lethal listeriosis.

OTUB1^{LPC-KO} and OTUB1^{FL} mice were infected intravenously with (A) 1×10^4 CFU of Lm and (B) 5×10^4 CFU of Lm. Survival of the mice was monitored daily up to day 14 after infection (n=16 -18), (A, B) Log-Rank test, * $p \leq 0.05$.

Histopathological examinations revealed a more severe liver pathology in OTUB1^{LPC-KO} mice which was characterized by large inflammatory foci with central necrosis as compared to OTUB1^{FL} at day 3 p.i. (Figure 10 A). In contrast to OTUB1^{LPC-KO} mice, only small inflammatory foci throughout the hepatic parenchyma without necrotic hepatocytes were detected in OTUB1^{FL} livers (Figure 10 A). Concomitantly, the severe liver pathology of OTUB1^{LPC-KO} mice resulted in disturbance of the liver function as indicated by the significantly elevated serum levels of ALT (Figure 10 B) and the increased release of Lactate dehydrogenase (LDH) into the serum at day 3 p.i. (Figure 10 C). Importantly, OTUB1^{LPC-KO} mice harbored only slightly higher numbers of bacteria in the livers but not in spleens at day 3 p.i. (Figure 10 D, E) These data demonstrate a protective function of hepatocyte-specific OTUB1 independent of pathogen control during listeriosis.

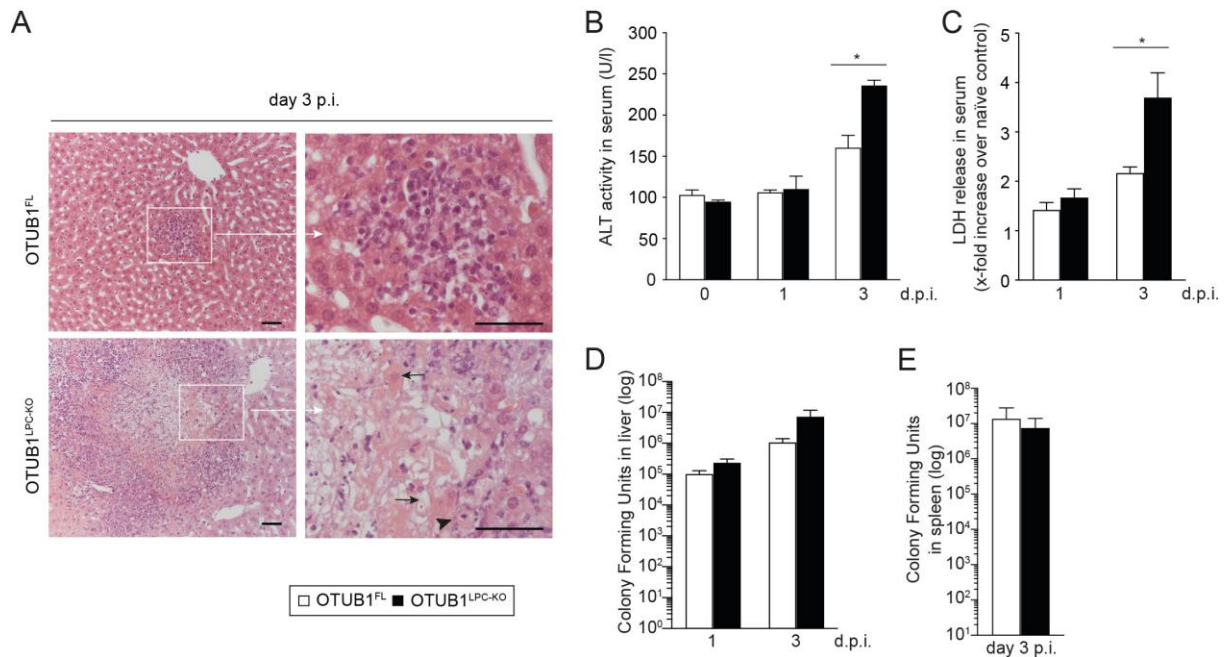


Figure 10: Liver failure causes Lm-induced lethality in OTUB1^{LPC-KO} mice.

OTUB1^{LPC-KO} and OTUB1^{FL} control mice were infected with 5×10^4 CFU of Lm i.v. (A) At day 3 p.i., liver sections were examined by histopathology. Histopathological analysis revealed a large inflammatory focus with central necrosis containing cellular debris and is surrounded by inflammatory cells in the liver of OTUB1^{LPC-KO} mice (white box marks the border of the necrotic lesion, lower left panel). A high-power magnification of the white box is shown in the lower right panel. Arrows indicate uninfected, swollen hepatocytes with pale nucleus lacking distinct chromatin and prominent eosinophilic cytoplasm. Arrowhead points to a dying hepatocyte with pale eosinophilic cytoplasm and condensed basophilic nucleus. In contrast, OTUB1^{FL} livers harbored viable hepatocytes with only small inflammatory foci (white box, upper left panel). In the upper right image, a high-power magnification of the small inflammatory lesion is shown (H&E staining, scale bars indicate 50 μ m). Representatives are shown (n = 3 per experimental group). (B, C) Serum samples of uninfected and Lm-infected OTUB1^{LPC-KO} and OTUB1^{FL} control mice were analyzed for (B) ALT activity and (C) LDH release at the indicated time points. Data represent one experiment out of three independent experiments with each 3 - 6 mice per group. (D) Bacterial loads in Lm-infected livers were determined at day 1 and day 3 p.i., respectively. Data are compiled of 3 independent experiments with 3 - 4 mice per experimental group. (E) Bacterial loads were determined in spleen at day 1 after Lm infection. Compiled data of three individually performed experiments are shown (n = 9 per experimental group). Bar graphs are depicted as mean + SEM, (B, C) Student's *t*-test, (D) Kruskal-Wallis-test, (E) Mann-Whitney *U*-test, * $p \leq 0.05$.

In listeriosis, different immune cells including NK cells, macrophages and CD8⁺ T cells are recruited to the liver to control and finally eliminate Lm from the liver by secreting various cytokines and chemokines (Pamer, 2004). Therefore, we further investigated the immune cell composition as well as the cytokine release following Lm infection. Interestingly, infiltration of leukocytes to the Lm-infected livers was not altered in the absence of OTUB1 as revealed by flow cytometry (Figure 11).

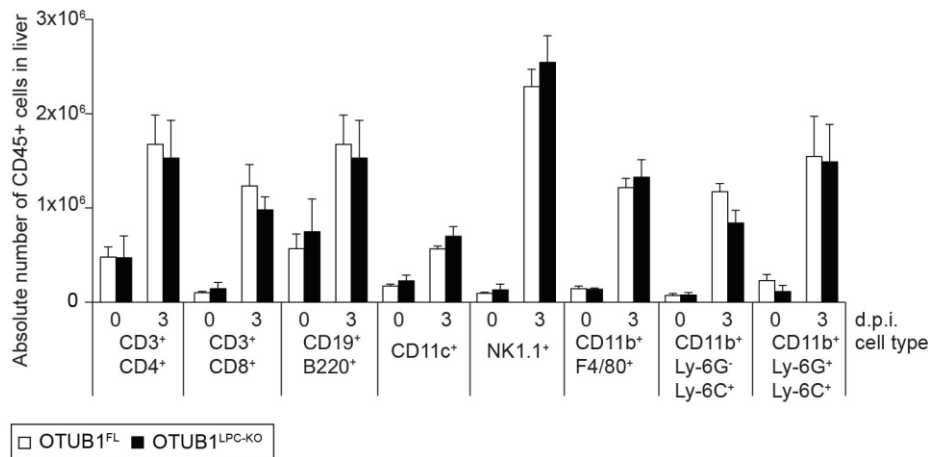


Figure 11: OTUB1 is dispensable for recruitment of leukocytes to Lm-infected livers.

Leukocyte populations were determined in livers of OTUB1^{LPC-KO} and OTUB1^{FL} control mice by flow cytometry 3 days after infection with 5×10^4 CFU of Lm i.v. Absolute numbers were calculated after gating on CD45⁺ cells. Data represents a combination of two independent experiments with 3 - 4 mice per experimental group. Bar graphs are depicted as mean value + SEM, Student's *t*-test.

Upon Lm infection, IL-6, IFN γ , TNF, IL-12, IL-10 and the monocyte chemotactic protein-1 (MCP-1) were released equally into serum of the OTUB1^{LPC-KO} mice and the OTUB1^{FL} control mice (Figure 12 A). Similarly, transcription of IL-6, IFN γ , IL-1 β and TNF were induced in both mouse strains but only the expression of TNF was significantly increased in the livers of OTUB1^{LPC-KO} mice as compared to OTUB1^{FL} mice at day 3 p.i. (Figure 12 B).

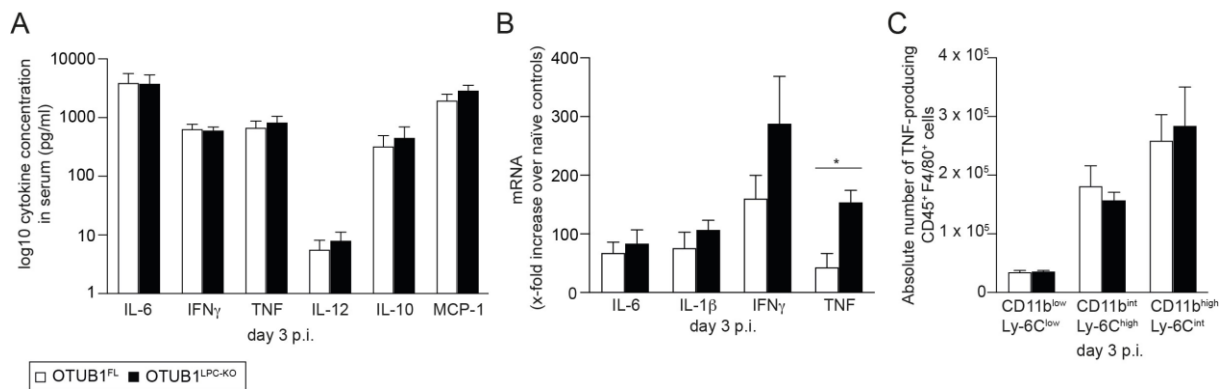


Figure 12: OTUB1 limits liver-intrinsic TNF production.

OTUB1^{LPC-KO} and OTUB1^{FL} mice were infected with 5×10^4 CFU of Lm i.v. (A) Cytokine levels were measured in serum harvested from Lm-infected OTUB1^{LPC-KO} and OTUB1^{FL} control mice at day 3 p.i. Three individual experiments with each 3 mice per group were compiled. (B) Relative gene expression of the indicated cytokines was quantified in liver tissue at day 3 p.i. Compiled data of three individual experiments are depicted ($n = 3$ for each experiment). (C) TNF-production by the indicated CD11b⁺ subpopulations were determined in Lm-infected livers of OTUB1^{LPC-KO} and OTUB1^{FL} control mice by flow cytometry. Absolute numbers were calculated after gating on CD45⁺/F4/80⁺ cells. One representative experiment is shown ($n = 3$ per experimental group). Bar graphs are shown as mean + SEM, (A-C) Student's *t*-test, * $p \leq 0.05$.

To further identify the source of TNF, we analyzed the TNF production of Kupffer cells ($CD45^+ F4/80^+ CD11b^{low} Ly-6C^{low}$), inflammatory monocytes ($CD45^+ F4/80^+ CD11b^{int} Ly-6C^{high}$) and monocyte-derived macrophages ($CD45^+ F4/80^+ CD11b^{high} Ly-6C^{int}$) in the liver by flow cytometry. As shown in Figure 12 C, the TNF production by these cell populations was comparable between both mouse strains.

Noteworthy, primary hepatocytes isolated from $OTUB1^{LPC-KO}$ mice expressed more TNF mRNA as compared to primary hepatocytes isolated from $OTUB1^{FL}$ mice when infected with *Lm in vitro*. Gene transcription for TNF mRNA was increased at 6 h as well as at 24 h after *Lm* infection, although the differences were only significant at the peak of TNF transcription (6 h.p.i.) (Figure 13 A). In addition, *Lm*-infected hepatocytes showed profound hepatocellular death in the absence of OTUB1 as determined by the LDH release into the supernatant but harbored comparable bacterial loads after 24 h of infection (Figure 13 B, C). Taken together, these findings suggest that OTUB1 is essential for restricting hepatocyte-intrinsic TNF production and hepatocellular death without affecting pathogen control.

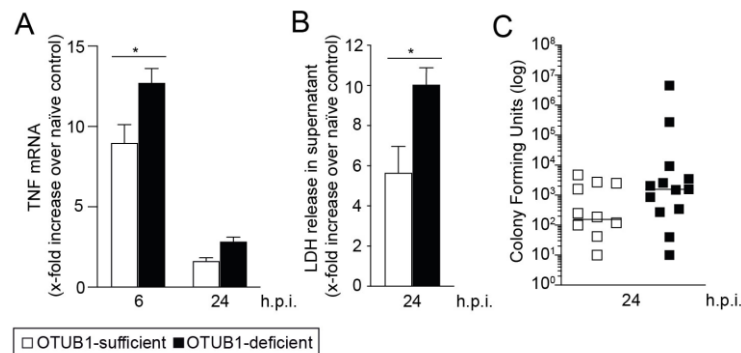


Figure 13: OTUB1 dampens *Lm*-induced TNF expression in primary hepatocytes.

Primary hepatocytes isolated from $OTUB1^{LPC-KO}$ and $OTUB1^{FL}$ control mice were infected with *Lm* (MOI of 10) for 6 and 24 h, respectively. (A) Cells were harvested at 6 and 24 h.p.i., respectively, and analyzed for the relative TNF mRNA expression by qRT-PCR ($n = 5 - 6$ per group). In (B) LDH release was measured in supernatant at 24 h.p.i. A representative experiment is shown with $n = 5$ per experimental group. (C) After 24 h of infection, numbers of intracellular bacteria were determined. Compiled data of three independent experiments are depicted ($n = 10 - 13$). Means + SEM are presented, (A, B) Student's *t*-test, (C) Mann-Whitney *U*-test, * $p \leq 0.05$.

4.2.2 OTUB1 prevents hepatic failure during toxin-induced liver injury

To validate whether OTUB1 possesses the capacity to limit TNF-dependent hepatocellular death, we induced acute liver injury by injecting DGal in combination with LPS intraperitoneally (i.p.) into the mice. In this model of experimental acute liver injury, blockage of hepatic gene transcription by DGal sensitizes the hepatocytes towards TNF-dependent cell death following LPS stimulation. After 24 h of DGal/LPS injection, 100 % of the OTUB1^{LPC-KO} mice died whereas 75 % of the OTUB1^{FL} control mice survived (Figure 14 A). Macroscopically, the OTUB1^{LPC-KO} mice displayed massive disturbance of the liver architecture with necrotic lesions already at 6 h post DGal/LPS administration (Figure 14 B). Additional histopathological examinations of DGal/LPS-treated liver tissue confirmed sharply demarcated liver necrosis in the OTUB1^{LPC-KO} mice which was absent in OTUB1^{FL} at 6 h post challenge (Figure 14 C). Similar to the infection with Lm, the more severe liver pathology in the OTUB1^{LPC-KO} mice yielded in significantly increased serum ALT levels as compared to the OTUB1^{FL} mice within 6 h of DGal/LPS challenge (Figure 14 D). Of note, as shown in Figure 14 E and F, expression of TNF mRNA was augmented in livers from OTUB1^{LPC-KO} mice whereas the levels of TNF and other cytokines circulating in the blood did not differ between both genotypes indicating an augmented pathogen-independent TNF production in the absence of OTUB1. These data suggest that OTUB1 may restrict (i) TNF-dependent hepatocellular death and (ii) hepatocyte TNF production.

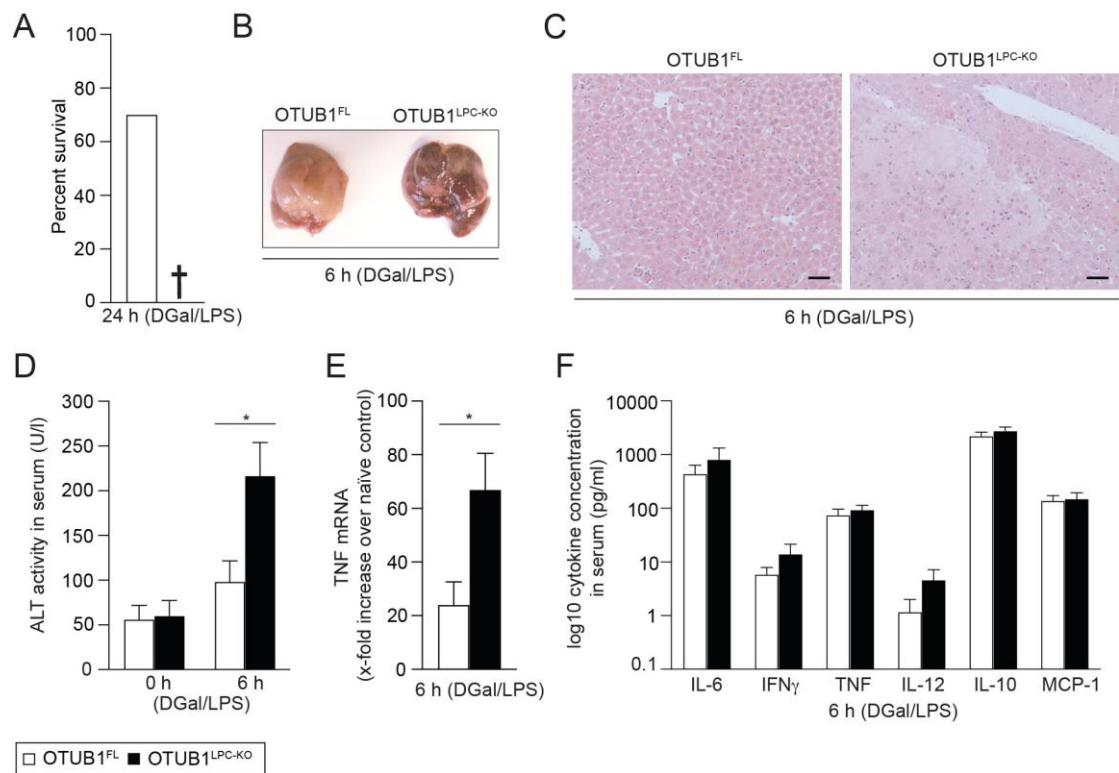


Figure 14: OTUB1^{LPC-KO} mice are highly susceptible to DGal/LPS challenge.

OTUB1^{LPC-KO} and OTUB1^{FL} mice were injected with 700 mg/kg of DGal and 2.5 μ g/kg LPS i.p. (A) Survival was determined after 24 h of challenge (n = 7 per group). (B) Representative macroscopic liver images of DGal/LPS-treated OTUB1^{LPC-KO} and OTUB1^{FL} mice at 6 h after injection (n = 5 per experimental group). (C) Histological examinations of liver sections dissected from OTUB1^{LPC-KO} and OTUB1^{FL} mice after 6 h of DGal/LPS treatment. In OTUB1^{LPC-KO} livers, sharply demarcated liver necrosis was present which was absent in OTUB1^{FL} livers (H&E staining, scale bar indicates 50 μ m). Representatives are shown (n = 5 per group). (D) 6 h after DGal/LPS challenge, serum was collected and the ALT activity was measured. Data are pooled from three individual experiments with each 3 - 4 mice per experimental group. (E) Quantitative RT-PCR analysis for TNF mRNA expression in DGal/LPS-treated livers at 6 h post challenge. Data of two experiments are represented (n = 6 - 7 per group). (F) Levels of the indicated cytokines were determined in serum collected from DGal/LPS-treated (6 h) OTUB1^{LPC-KO} and OTUB1^{FL} mice. Data from three representative experiments are depicted (n = 9 per group). Bar graphs indicate the mean values + SEM. (D, E) Student's *t*-test, * p \leq 0.05.

Next, we investigated whether the enhanced hepatocellular death was a consequence of the excessive hepatic TNF production. Therefore, LPS was substituted by TNF and equal amounts of TNF were injected in combination with DGal i.p. into the OTUB1^{LPC-KO} and OTUB1^{FL} mice. In line with the DGal/LPS experiments, the survival of the OTUB1^{LPC-KO} mice was reduced by 70 % as compared to the OTUB1^{FL} mice after 24 h of DGal/TNF injection (Figure 15 A). Similarly, the surviving OTUB1^{LPC-KO} mice displayed excessive liver damage whereas the livers of OTUB1^{FL} mice appeared to be normal macroscopically (Figure 15 B).

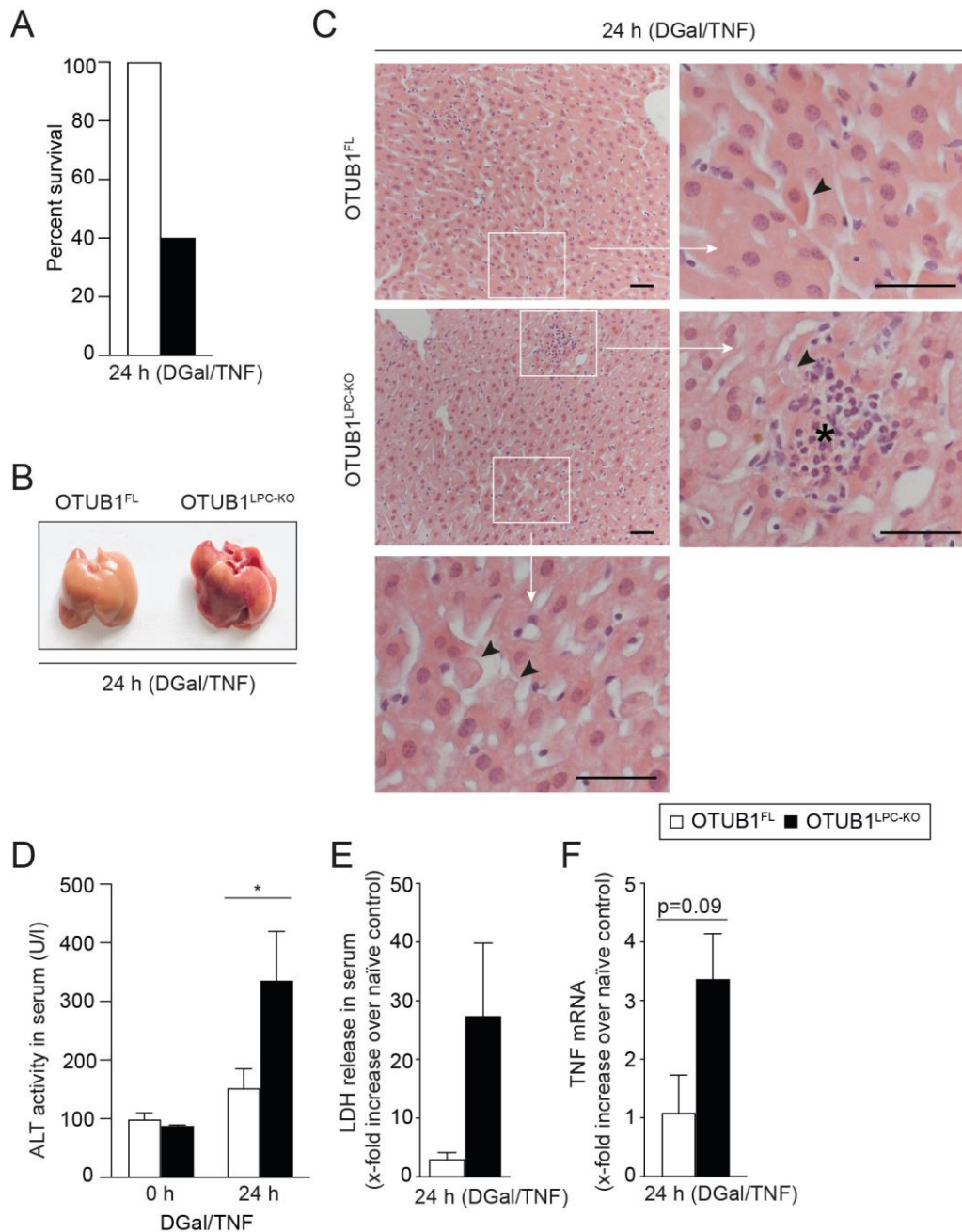


Figure 15: OTUB1^{LPC-KO} mice develop acute hepatitis upon DGal/TNF challenge.

Mouse strains were challenged with 400 mg/kg DGal and 40 μ g/kg murine recombinant TNF i.p. (A) After 24 h of challenge, the number of surviving mice were determined. One representative data set with $n = 5$ mice per experimental group is depicted. (B) Macroscopic analysis of DGal/TNF-treated livers at 24 h post challenge ($n = 3$ per group). (C) Histopathology of OTUB1^{LPC-KO} and OTUB1^{FL} mice at 24 h after DGal/TNF injection ($n = 3$ per group). Histopathological analysis revealed an inflammatory infiltrate associated to a damaged hepatocyte (upper white box, asterisk) in OTUB1^{LPC-KO} livers. High-power magnifications of the marked areas showed multiple damaged hepatocytes characterized by swelling, an eosinophilic cytoplasm and the lack of nuclei (arrowheads). In contrast, OTUB1^{FL} mice harbored a normal liver architecture and only single hepatocytes with a swollen, eosinophilic cytoplasm (arrowhead, high-power magnification, H&E staining, scale bars indicate 50 μ m). (D, E) At 24 h post challenge, serum was harvested and analyzed for (D) ALT activity and (E) LDH levels. Data of three experiments with each 4 - 5 mice were combined. (F) TNF mRNA expression was quantified in liver tissue from 24 h DGal/TNF-treated OTUB1^{LPC-KO} and OTUB1^{FL} mice by qRT-PCR. One representative experiment is displayed ($n = 4$ per experimental group). Data are means + SEM, (D - F) Student's *t*-test, * $p \leq 0.05$.

Histologically, the liver pathology in the OTUB1^{LPC-KO} mice was characterized by many swollen eosinophilic hepatocytes which partially lacked nuclei and small inflammatory infiltrates which were associated with damaged hepatocytes (Figure 15 C). In contrast to liver of OTUB1^{LPC-KO} mice, inflammatory infiltrates were absent in the livers of OTUB1^{FL} mice. In addition, OTUB1^{FL} mice harbored only single slightly swollen hepatocytes which were accompanied by a prominent eosinophilic cytoplasm (Figure 15 C). Accordingly, serum ALT levels and LDH release into the serum were pronounced in these mice, although the differences for LDH were not significant (Figure 15 D, E). Importantly, the injection of equal amounts of TNF resulted in an enhanced liver-intrinsic production of TNF in the OTUB1^{LPC-KO} mice 24 h after challenge suggesting a liver-intrinsic function of OTUB1 in restricting hepatic TNF production (Figure 15 F). Taken together, these findings indicate that OTUB1 inhibits TNF-dependent hepatocellular death *in vivo*.

4.3 OTUB1 regulates TNF-induced signaling pathways

4.3.1 OTUB1 regulates TNF-triggered ERK but not NF- κ B activation

TNF is a pleiotropic pro-inflammatory cytokine which can regulate cell survival by triggering NF- κ B-dependent gene transcription of the anti-apoptotic molecules Bcl-2 and c-FLIP (Brenner *et al.*, 2015). Since OTUB1 has been reported to influence NF- κ B signaling under inflammatory conditions (Mulas *et al.*, 2020), we analyzed the NF- κ B pathway in Lm-infected liver tissue of OTUB1^{LPC-KO} and OTUB1^{FL} mice by WB. As shown in Figure 16 A, the NF- κ B subunit p65 was phosphorylated and the NF- κ B subunit p100 was processed to p52 equally in both mouse strains illustrating that both canonical and non-canonical NF- κ B activation are independent of hepatocyte-specific OTUB1 expression. Consequently, NF- κ B-dependent gene transcription of the pro-apoptotic molecule Bax (Figure 16 B) and the anti-apoptotic molecules Bcl-2 and c-FLIP (Figure 16 C, D) was equally upregulated in OTUB1^{LPC-KO} livers upon infection with Lm as compared to OTUB1^{FL} livers.

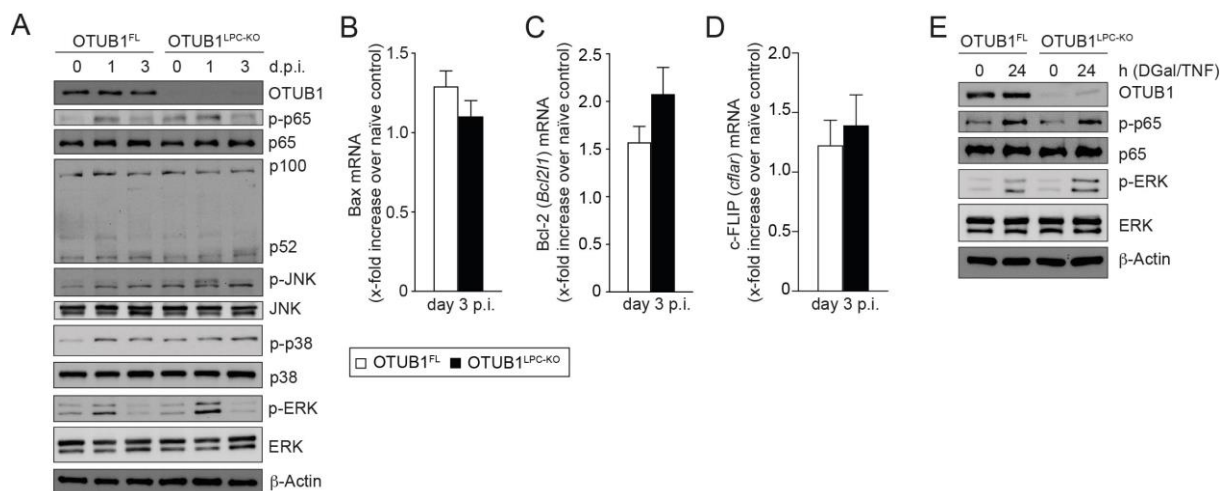


Figure 16: Augmented activation of ERK in OTUB1-deficient livers.

(A) WB analysis for the indicated proteins from total liver lysates obtained from uninfected and Lm-infected OTUB1^{LPC-KO} and OTUB1^{FL} mice at day 1 and day 3 p.i., respectively. β -Actin was used as loading control. Representative blots are displayed. Experiment was repeated three times. (B - D) At day 3 post infection with 5×10^4 CFU of Lm, relative gene expression of *Bax*, *Bcl2l1*, *cflar*, respectively, were quantified by qRT-PCR. Bar graphs are representatives from one out of two independent experiments ($n = 4$ mice per experimental group). Mean + SEM are shown. (E) The indicated mice strains were injected with 400 mg/kg DGal and 40 μ g/kg murine recombinant TNF i.p. Whole liver lysates were harvested at 24 h post injection and immunoblotted with antibodies for OTUB1, p-p65, p65, p-ERK, ERK and β -Actin as loading control. Blots are representatives. (B - D) Student's *t*-test.

In addition to NF- κ B, comparable protein levels of phosphorylated JNK and p38 were detected. However, ERK was more activated in the livers of OTUB1^{LPC-KO} mice as compared OTUB1^{FL} mice as indicated by its enhanced phosphorylation at day 1 p.i. which was followed by a decline in both strains of mice (Figure 16 A). Similar results were obtained after DGal/TNF challenge with a comparable activation of the canonical NF- κ B pathway but a pronounced activation of ERK (Figure 16 E).

4.3.2 OTUB1 blocks TNF-induced necroptotic cell death

Beside its role in NF- κ B signaling, ligation of TNF to the TNFR1 can also lead to apoptosis and necroptosis, respectively. With respect to OTUB1, it has been shown that OTUB1 can block apoptosis by stabilizing c-IAP1 (Goncharov *et al.*, 2013). In agreement with Goncharov *et al.*, we detected an accelerated degradation of c-IAP1 in livers of Lm-infected OTUB1^{LPC-KO} mice (Figure 17 A, B) starting at day 1 p.i. At day 3 p.i., protein levels of c-IAP1 were reduced by 60 % in OTUB1^{LPC-KO} livers while only being reduced by 30 % in the OTUB1^{FL} livers. Importantly, c-IAP1 mRNA levels did not differ between both genotypes (Figure 17 C) at day 3 p.i. as quantified by RT-PCR suggesting its post-translational modification. Apoptotic signaling is associated with cleavage of caspase-8 which in turn either directly cleaves the effector caspases-3, -6 and -7 or indirectly via cleaving BID to tBID and the subsequent activation of Bax (Feltham *et al.*, 2017). Surprisingly, the reduced levels of c-IAP1 did not result in an enhanced apoptotic signaling since cleavage of procaspase-8 to its active form was even diminished in the Lm-infected OTUB1^{LPC-KO} livers at day 1 and day 3 p.i., respectively (Figure 17 A). Accordingly, the downstream effector caspases, caspases-3, -6, and -7 were also reduced at day 1 and at day 3 p.i., respectively, as indicated by their cleaved products (Figure 17 A). In contrast, processing of BID to tBID and the activation of Bax occurred similarly in the livers of both genotypes (Figure 17 A). Since the massive hepatocellular death in the OTUB1^{LPC-KO} mice might not be attributed to caspase cleavage, we next studied RIPK1/RIPK3-mediated necroptosis. As shown in Figure 17 A, expression of RIPK1 was slightly upregulated and the expression of RIPK3 remained unchanged in the liver of both mouse strains. However, necroptosis requires the interaction of RIPK1 and RIPK3, a complex termed as necrosome (Schwabe & Luedde, 2018). To study RIPK1/RIPK3 complex formation, RIPK1-associated complexes were immunoprecipitated in total liver lysates before and after infection with Lm. As shown by WB, the RIPK1 immunoprecipitates contained very low amounts of RIPK3 before infection which increased upon Lm infection only in OTUB1-deficient livers but not in OTUB1-sufficient livers (Figure 17 D).

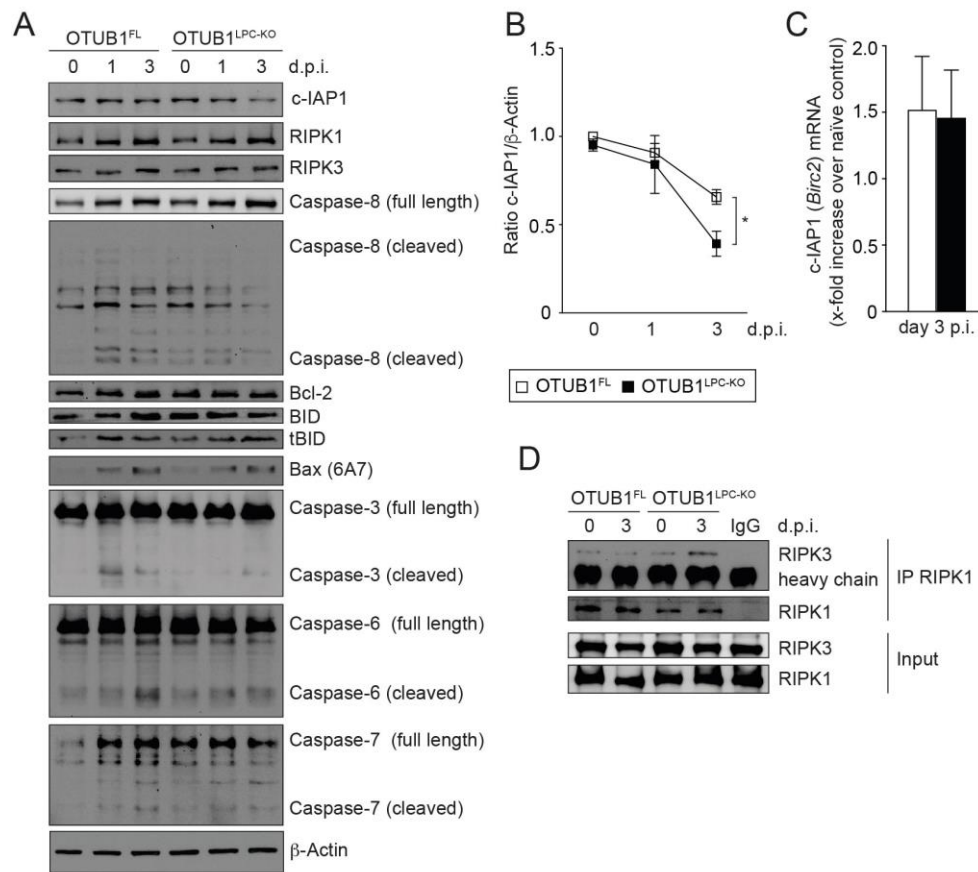


Figure 17: Accelerated degradation of c-IAP1 and enhanced necrosome formation in the absence of OTUB1.

(A) Total protein lysates of uninfected and with 5×10^4 CFU of Lm-infected OTUB1^{LPC-KO} and OTUB1^{FL} mice at day 1 and day 3 p.i., respectively, were analyzed by WB. (B) Based on WB data, c-IAP1 expression levels were quantified and normalized to β -Actin. Data of 4 independent experiments were analyzed and are shown as mean ratio c-IAP1/ β -Actin. (C) Relative gene expression of c-IAP1 mRNA was determined in liver tissue at day 3 p.i. One experiment with 4 mice per experimental group is presented. (D) Whole liver lysates from uninfected and Lm-infected (day 3 p.i.) OTUB1^{LPC-KO} and OTUB1^{FL} mice were immunoprecipitated with α -RIPK1. Immunoprecipitates and inputs were analyzed by WB using antibodies for RIPK1 and RIPK3. All WBs are representatives of at least two analyzed mice per group. (B, C) Error bars indicate +SEM, * $p \leq 0.05$.

To further validate whether the inhibitory effect of OTUB1 on necroptosis is restricted to bacterial infections, we analyzed apoptotic and necroptotic cell death signaling in DGal/TNF-induced liver injury. In line with the listeriosis, OTUB1 also preserved c-IAP1 stability upon DGal/TNF challenge. After 24 h of DGal/TNF injection, c-IAP1 levels dropped around 60 % in OTUB1-deficient livers and only 20 % in the OTUB1-sufficient livers (Figure 18 A). WB analysis for apoptotic signaling revealed similar data as seen upon infection with Lm with decreased levels of the cleaved caspases, caspase-8 and -3 (Figure 18 A) but increased RIPK3-containing RIPK1 complexes (Figure 18 B). Taken together, these data demonstrate that the hepatocellular death of OTUB1^{LPC-KO} mice is independent of caspase cleavage but is associated with RIPK1/RIPK3 complex formation.

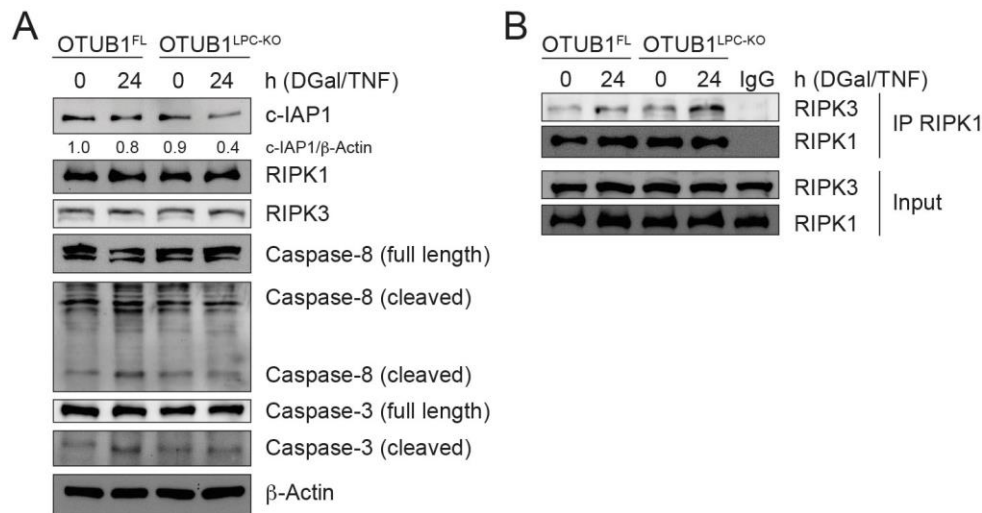


Figure 18: Cell death in OTUB1^{LPC-KO} mice is RIPK1/RIPK3-mediated.

OTUB1^{LPC-KO} and OTUB1^{FL} mice were challenged with 400 mg/kg DGal plus 40 μ g/kg murine recombinant TNF i.p. Total proteins were isolated from untreated and 24 h DGal/TNF-treated livers of the indicated mouse strains. (A) WB analysis were performed for c-IAP1, RIPK1, RIPK3, caspase-8 and caspase-3 with the respective antibodies. β -Actin served as loading control. (B) After immunoprecipitating RIPK1-complexes using α -RIPK1 antibody, immunoprecipitates were assessed for RIPK1 and RIPK3 by WB. Experiments were repeated two times and representative blots are depicted.

4.4 Inhibition of necroptosis but not of apoptosis rescues OTUB1^{LPC-KO} mice from *Listeria*-induced mortality

4.4.1 RIPK1 inhibition preserves liver function in Lm-infected OTUB1^{LPC-KO} mice

Given that necroptosis requires kinase activity of RIPK1, we studied the impact of RIPK1 kinase inhibition on necroptosis in OTUB1^{LPC-KO} mice. Therefore, the OTUB1^{LPC-KO} mice and OTUB1^{FL} mice were treated with the RIPK1 inhibitor, Necrostatin-1s (Nec-1s). Figure 19 A illustrates the experimental design. Mice received Nec-1s i.v. 90 min prior to infection with 5×10^4 CFU of Lm and thereafter daily up to day 2 p.i. Separate groups of both mouse strains were treated with the pan-caspase inhibitor zVAD-FMK (zVAD) and left untreated, respectively.

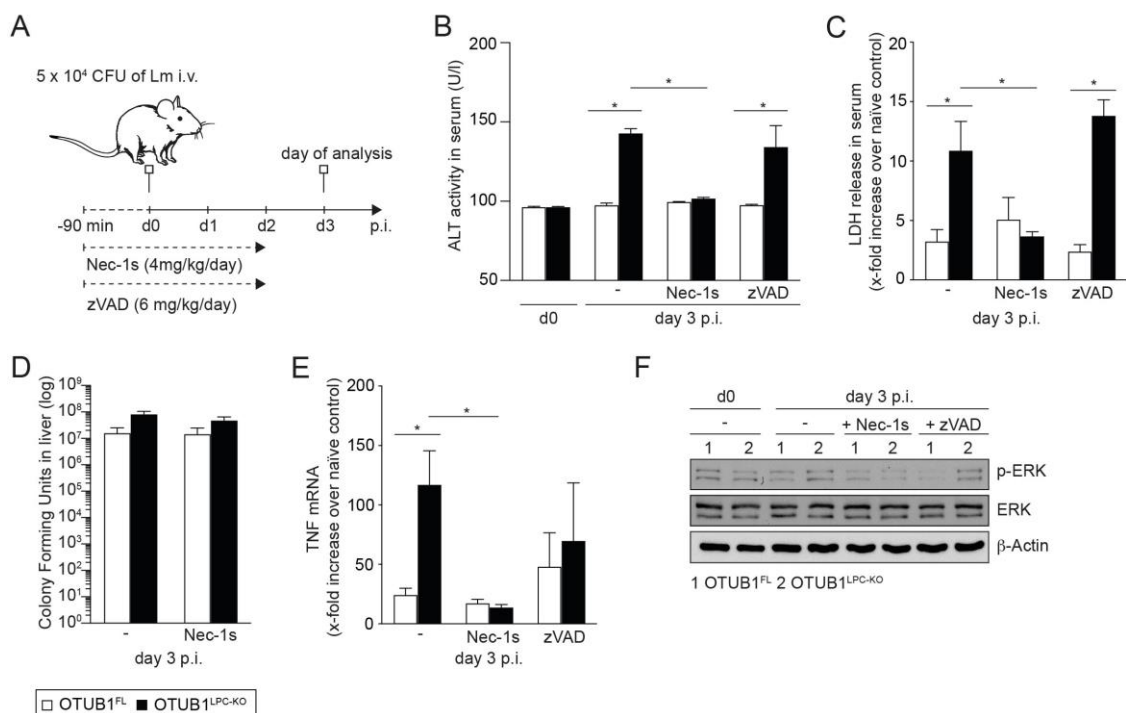


Figure 19: Nec-1s but not zVAD limits liver failure and TNF production in Lm-infected OTUB1^{LPC-KO} mice.

(A) Scheme illustrating the experimental design. Beginning 90 min before i.v. infection with 5×10^4 CFU of Lm, OTUB1^{LPC-KO} and OTUB1^{FL} mice received daily i.v. injections with 4 mg/kg Nec-1s or 6 mg/kg zVAD. Nec-1s and zVAD were administrated up to day 2 p.i. At day 3 p.i., mice were sacrificed and examined. (B) Serum analysis was performed for the liver enzyme ALT (n = 3 per experimental). (C) LDH was measured in serum of the indicated mice groups (n = 3 per experimental group). (D) CFUs were determined in liver. Compiled data of two experiments with each 3 - 4 mice per experimental group are shown. (E) qRT-PCR analysis for the relative hepatic TNF expression (n = 3 per group). (F) Total liver lysates were probed with antibodies for p-ERK, ERK and β-Actin. Data represents one experiment with n = 3, means +SEM are shown, (B, C, E) two-way Anova, (D) Kruskal-Wallis test, * p ≤ 0.05.

As shown in Figure 19 B and C, ALT as well as LDH levels declined significantly in serum of OTUB1^{LPC-KO} mice in the presence of Nec-1s without affecting the bacterial loads in liver. While Nec-1s treatment abolished the differences between the both groups of mice completely, zVAD treatment showed no effect. In contrast, LDH levels were even enhanced upon zVAD treatment indicating an increased necroptosis induction by combined OTUB1 deficiency and caspase inhibition. Noteworthy, Nec-1s also completely abolished the excessive TNF production in the liver of the OTUB1^{LPC-KO} mice whereas zVAD administration resulted only in a minor decrease in TNF mRNA levels. Additional WB analysis revealed that the augmented ERK activation as seen in Lm-infected OTUB1^{LPC-KO} livers could be blocked by Nec-1s but not by zVAD treatment indicating that the enhanced TNF production might be associated with enhanced ERK activation.

Based on these results, we studied whether Nec-1s also conferred protection against *Listeria*-induced lethality in OTUB1^{LPC-KO} mice. For studying survival, Nec-1s treatment was extended up to day 5 p.i., when OTUB1^{LPC-KO} mice started to succumb to the infection (Figure 20 A). In fact, Nec-1s treatment completely prevented mortality of OTUB1^{LPC-KO} mice equally to OTUB1^{FL} mice. In contrast, all OTUB1^{LPC-KO} mice without Nec-1s treatment succumbed to the infection around day 5 p.i. (Figure 20 B). These findings demonstrate that activation of RIPK1 is responsible for necroptosis and lethality in *Listeria*-infected OTUB1^{LPC-KO} mice.

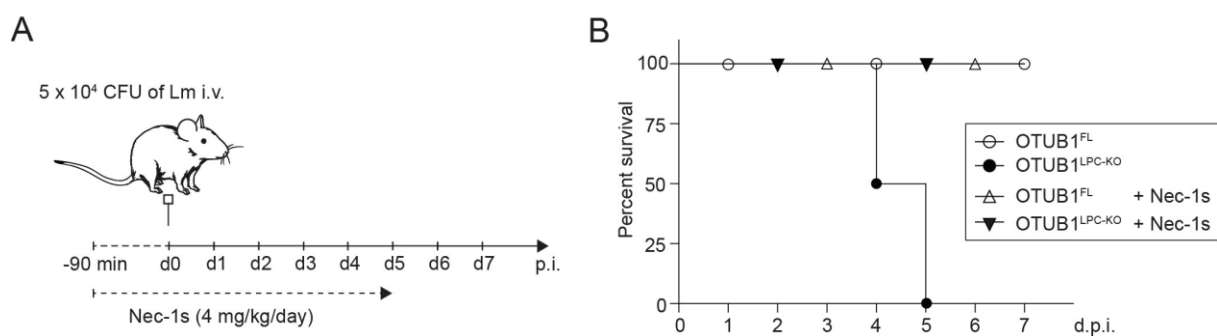


Figure 20: Improved survival of OTUB1^{LPC-KO} mice in the presence of Nec-1s.

(A) Experimental design for survival experiment. 4 mg/kg Nec-1s was injected i.v. 90 min before infecting the OTUB1^{LPC-KO} and OTUB1^{FL} mice with 5 x 10⁴ CFU of Lm i.v., followed by daily i.v. injections of 4 mg/kg Nec-1s up to day 5 p.i. (B) Survival rates were monitored daily up to day 7 p.i. (n = 3 - 4 per group).

4.4.2 Deletion of MLKL prevents Lm-induced liver damage in OTUB1^{LPC-KO} mice

Association of RIPK1 to RIPK3 initiates necroptosis by serving as signaling platform for the subsequent activation of MLKL (Holbrook *et al.*, 2019). Thereafter, MLKL translocates to the plasma membrane where it causes rupture of the plasma membrane (Hildebrand *et al.*, 2014). Since MLKL has been identified as terminal executor of necroptosis, we hypothesized that genetic deletion of MLKL might abrogate necroptosis in OTUB1^{LPC-KO} mice. Thus, we crossed OTUB1^{LPC-KO} mice with MLKL-deficient mice (MLKL^{del/del}) to generate double knockout mice (MLKL^{del/del} OTUB1^{LPC-KO}) lacking OTUB1 and MLKL expression in the liver parenchymal cells.

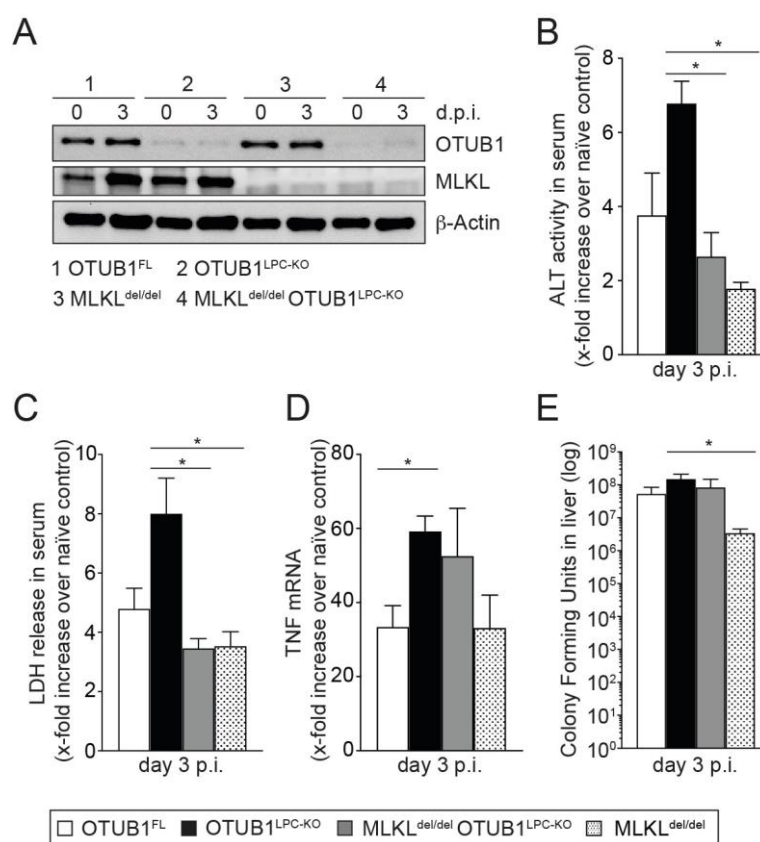


Figure 21: Genetic ablation of MLKL reduces liver damage in OTUB1^{LPC-KO} mice.

OTUB1^{FL}, OTUB1^{LPC-KO}, MLKL^{del/del} and MLKL^{del/del} OTUB1^{LPC-KO} were infected with 5×10^4 CFU of Lm i.v. At day 3 p.i., the mice were sacrificed. (A) For protein expression, total liver lysates were probed with α -OTUB1, α -MLKL and α - β -Actin antibodies. Blots are representatives. Serological analysis for (B) ALT activity and (C) LDH release were performed (D) Quantification of the relative TNF mRNA expression in liver tissue. (E) Bacterial loads were determined in the Lm-infected livers (day 3 p.i.). Data of two independent experiments with three mice per group were pooled. Mean values are shown. Error bars indicate + SEM, (B - D) two-way Anova, (E) Kruskal-Wallis-test, * $p \leq 0.05$.

WB analysis confirmed the deletion of both OTUB1 and MLKL in the livers of uninfected and Lm-infected MLKL^{del/del} OTUB1^{LPC-KO} mice (Figure 21 A). Upon infection with Lm, MLKL^{del/del} OTUB1^{LPC-KO} mice were characterized by reduced levels of ALT and LDH in serum at day 3 p.i. However, deletion of MLKL had no impact on TNF mRNA transcription as quantified by qRT-PCR (Figure 21 D) and the pathogen clearance from liver as determined by the CFUs at day 3 p.i. (Figure 21 E).

4.5 OTUB1 prevents TNF-triggered necroptosis via c-IAP1 stabilization

4.5.1 OTUB1 interacts with c-IAP1 upon *Listeria*-infection and DGal/TNF challenge

In 2013, Goncharov et al. uncovered that OTUB1 interacts with c-IAP1, thereby regulating TWEAK-induced apoptosis in human cell lines *in vitro* (Goncharov *et al.*, 2013). Considering, the accelerated degradation of hepatic c-IAP1 without affecting its mRNA levels upon infection with Lm and DGal/TNF challenge (Figure 17 A - C, Figure 18 A), we further investigated whether OTUB1 targets c-IAP1 upon *Listeria* infection and DGal/TNF challenge *in vivo*. As illustrated in Figure 22 A - D, c-IAP1 was co-immunoprecipitated with OTUB1 and vice versa in OTUB1-sufficient livers after both *Listeria* infection and after DGal/TNF challenge. Of note, this interaction occurred only under stimulatory conditions.

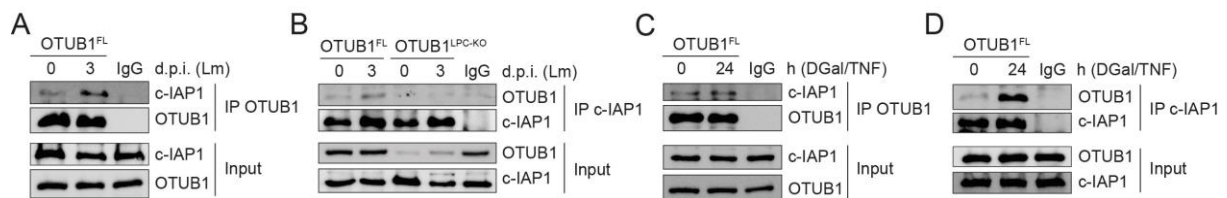


Figure 22: *Listeria*- and DGal/TNF-induced interaction of OTUB1 and c-IAP1 in the liver.

Liver homogenates obtained from untreated and (A, B) Lm-infected or (C, D) DGal/TNF-treated OTUB1^{LPC-KO} and OTUB1^{FL} mice were analyzed for OTUB1-c-IAP1 interaction. Protein complexes were immunoprecipitated with either (A, C) α -OTUB1 or (B, D) α -c-IAP1 antibodies and thereafter probed with α -OTUB1 and α -c-IAP1, respectively. All blots are representatives. Experiments were repeated two times.

4.5.2 OTUB1 cleaves K48-linked polyubiquitin chains from c-IAP1

Mechanistically, Goncharov et al. identified that OTUB1 regulates c-IAP1 stability in a ubiquitin-dependent manner by disassembling its K48-linked polyubiquitin chains upon TWEAK stimulation *in vitro*. Consequently, TWEAK-induced accumulation of K48-linked polyubiquitin chains targeted c-IAP1 for proteasomal degradation which caused apoptotic cell death in the absence of OTUB1 (Goncharov *et al.*, 2013). In accordance, we observed strong K48-linked polyubiquitination of c-IAP1 in OTUB1-deficient livers which was nearly absent in the OTUB1-sufficient livers at day 3 post Lm infection (Figure 23). These findings illustrate removal of K48-linked polyubiquitin chains from c-IAP1 by OTUB1.

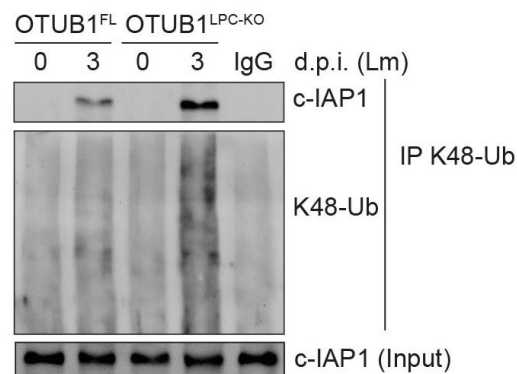


Figure 23: OTUB1 deficiency causes accumulation of K48-linked polyubiquitination on c-IAP1.

K48-linked polyubiquitination was analyzed in liver tissue of uninfected and Lm-infected OTUB1^{LPC-KO} and OTUB1^{FL} mice. Whole liver lysates were immunoprecipitated with α -ubiquitin (Lys48-specific) and stained with antibodies against c-IAP1 and K48-Ub, respectively. Data represents results from one mouse analyzed per group. Experiment was repeated two times.

4.5.3 OTUB1-mediated stabilization of c-IAP1 increases K63-linked polyubiquitination of RIPK1

Signaling of TNF through TNFR1 critically involves the coordinative assembling of RIPK1-containing signaling complexes. Concomitantly, the activity of RIPK1 itself is regulated by the E3 ligase c-IAP1 which adds K63-linked polyubiquitin chains on RIPK1. K63-linked polyubiquitination of RIPK1 functions as an adaptor for recruiting the NF- κ B-activating complex while blocking the activity of RIPK1 required for necroptosis. Thus, we investigated whether the reduced c-IAP1 stability results in an impaired K63-linked polyubiquitination of RIPK1 in Lm-infected OTUB1^{LPC-KO} mice. Infection induced interaction of c-IAP1 and RIPK1 which resulted in strong K63-linked polyubiquitination of RIPK1 in OTUB1^{FL} mice. In contrast, c-IAP1/RIPK1 complex formation and K63-linked polyubiquitination of RIPK1 were impaired in livers of OTUB1^{LPC-KO} mice suggesting that reduced c-IAP1 levels in the absence of OTUB1 impaired K63-linked polyubiquitination of RIPK1 which initiated hepatocyte necroptosis in OTUB1^{LPC-KO} mice (Figure 24).

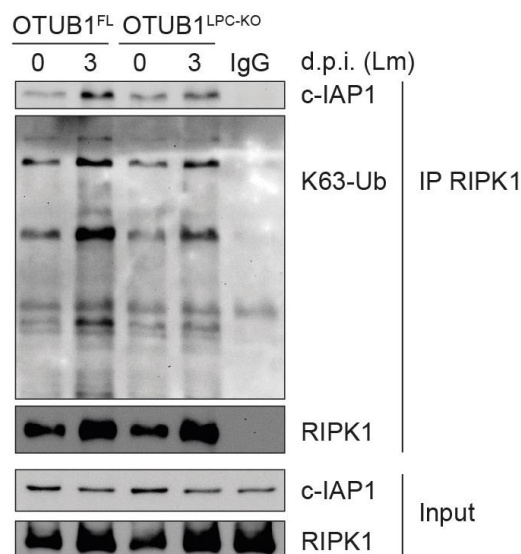


Figure 24: Impaired K63-linked polyubiquitination of RIPK1 in the absence of OTUB1.

Total liver proteins were isolated from uninfected and Lm-infected OTUB1^{LPC-KO} and OTUB1^{FL} mice and immunoprecipitated with α -RIPK. Immunoprecipitates were analyzed for c-IAP1, K63-Ub and RIPK1 by WB using the respective antibodies. Representative blots of two individual experiments are depicted.

4.6 Hepatocyte-intrinsic OTUB1 limits necroptosis and TNF production

The previously shown data that OTUB1 (i) limited TNF-dependent hepatocellular death and (ii) also limited TNF mRNA expression *in vivo* as well as *in vitro* following *Listeria* infection without affecting the pathogen control revealed a hepatocyte-intrinsic function of OTUB1 which was further supported in the DGal/TNF shock model. To extend our investigation of the molecular function of hepatocyte-specific OTUB1, we performed *Listeria* infection and TNF stimulations in a human hepatocyte cell line deficient in OTUB1 expression.

4.6.1 OTUB1 exhibits a similar phenotype in human and mice

Preliminary data were obtained with siRNA-transfected HepG2 cells. Thereafter, all experiments were performed with lentiviral transduced HepG2 cells, in which OTUB1 was stably knocked down. As illustrated by WB analysis in Figure 25 A and B, OTUB1 expression was successfully downregulated in both siRNA-transfected and lentiviral-transduced HepG2 cells, although the knockdown seemed to be more efficient with lentiviral transduction. The OTUB1-sufficient and -deficient HepG2 cells were infected with *Listeria* and analyzed for pro-inflammatory and cell death pathways. As observed in mice, OTUB1 did not regulate NF- κ B signaling, since I κ B α and p65 were phosphorylated equally following *Listeria*-infection (Figure 25 A, B). However, OTUB1 limited the phosphorylation of ERK, in particular early after Lm infection (60 min p.i.) (Figure 25 A, B). With respect to cell death signaling, OTUB1 deficiency caused destabilization of c-IAP1 leading to its rapid degradation starting 60 min after Lm infection and further progressing until 24 h after Lm infection (Figure 25 A, B). After 24 h of infection, c-IAP1 levels were decreased by 90 % in OTUB1-deficient HepG2 cells and only by 30 % in OTUB1-sufficient HepG2 cells. Similar to Lm infection in mice, cleavage of caspase-8 and -3 was slightly reduced in OTUB1-deficient HepG2 cells as compared to OTUB1-sufficient cells while levels of RIPK1 and RIPK3 remained unchanged upon Lm infection in both groups (Figure 25 A, B).

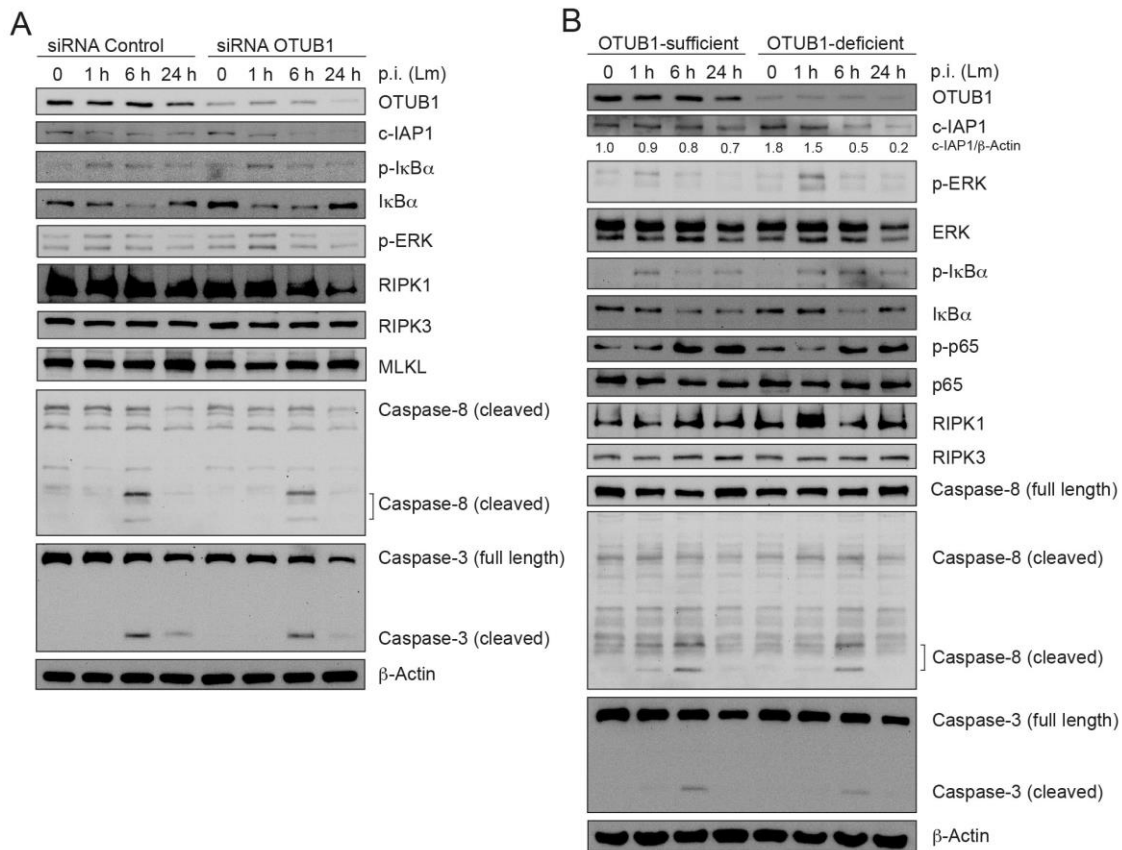


Figure 25: Knockdown of OTUB1 destabilizes c-IAP1, augments ERK activation but does not affect NF-κB activation and caspase cleavage.

(A) HepG2 cells were transfected with siRNA targeting OTUB1 or nonsense (control), respectively. After 24 h of transfection, cells were left untreated or infected with Lm with a MOI of 10 for the indicated time points. Proteins were isolated and analyzed by WB. (B) OTUB1 was knocked down using lentiviral transduction. OTUB1-sufficient and -deficient HepG2 cells were infected with Lm (MOI of 10). At the indicated time points, cells were harvested for protein isolation. Proteins from uninfected and Lm-infected cells were probed with the indicated antibodies. β-Actin was used as loading control. Representative blots are shown.

In addition, we detected association of OTUB1 with c-IAP1. In Lm-infected OTUB1-sufficient HepG2 cells K48-linked polyubiquitination of c-IAP1 was reduced as compared to OTUB1-deficient HepG2 cells (Figure 26 B). Consequently, reduction of c-IAP1 in OTUB1-deficient HepG2 cells diminished K63-linked polyubiquitination on RIPK1 was detected in OTUB1-deficient HepG2 cells resulting in enhanced phosphorylation of RIPK1 (p-Ser) and enhanced RIPK1/RIPK3 necrosome formation 6 h.p.i. (Figure 26 C). Microscopically, OTUB1-deficient HepG2 cells showed increased numbers of phosphorylated MLKL⁺ and phosphorylated MLKL puncta per cell (Figure 26 D).

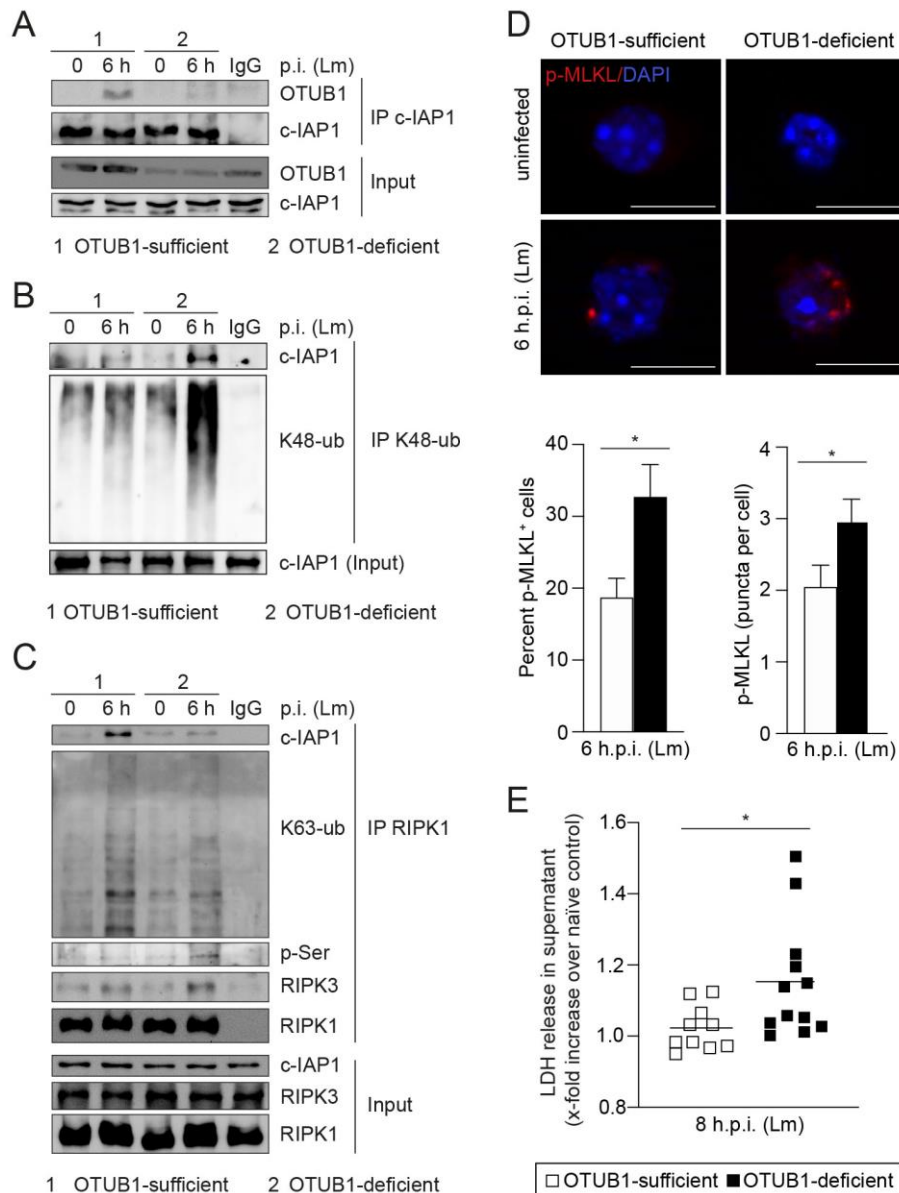


Figure 26: Interaction of OTUB1 with c-IAP1 inhibits necroptosis in HepG2 cells.

OTUB1-sufficient and -deficient HepG2 cells were infected with 10:1 Lm for 6 h in the presence (B) or absence (A, C, D) of MG132. Whole cell lysates were immunoprecipitated with (A) α -c-IAP1, (B) α -ubiquitin, Lys48-specific (K48-Ub) or (C) α -RIPK1 and thereafter analyzed for the indicated proteins by WB using the respective antibodies. Blots are representatives of at least two individually performed experiments. (D) Representative immunofluorescence images from uninfected and Lm-infected (6 h.p.i.) OTUB1-sufficient and -deficient HepG2 cells. Cells were stained for p-MLKL (red) and the nucleus (DAPI, blue), scale bar represents 20 μ m. The number of p-MLKL⁺ and the puncta per cell were determined microscopically by counting a total of 100 cells per experimental group. Bar graphs are representatives from a single experiment. Mean values + SEM are shown. (E) At 8 h.p.i., the LDH release into the supernatant was measured and calculated as x-fold increase over the respective uninfected controls. A single experiment is depicted (n = 10 - 12). (D, E) Student's *t*-test, * $p \leq 0.05$.

To complement our *in vivo* findings from DGal/TNF challenged mice, we next analyzed pro-inflammatory and cell death signaling upon stimulation with TNF/CHX. Supporting our *in vivo* observations, TNF/CHX stimulation triggered a rapid decline in c-IAP1 levels in

OTUB1-deficient HepG2 cells early after stimulation (Figure 27 A). In contrast, c-IAP1 levels remained stable in OTUB1-sufficient HepG2 cells (Figure 27 A). Upon TNF/CHX stimulation, OTUB1 did not affect the degradation of the NF- κ B inhibitor I κ B α indicating a normal NF- κ B activation, whereas phosphorylation of ERK was pronounced in OTUB1-deficient HepG2 cells upon TNF-stimulation (Figure 27 A). Additionally, cleavage of caspase-8 and -3 was reduced in OTUB1-deficient HepG2 cells but RIPK1/RIPK3 complex formation as well as phosphorylation of MLKL were higher as compared to OTUB1-sufficient HepG2 cells (Figure 27 B, C).

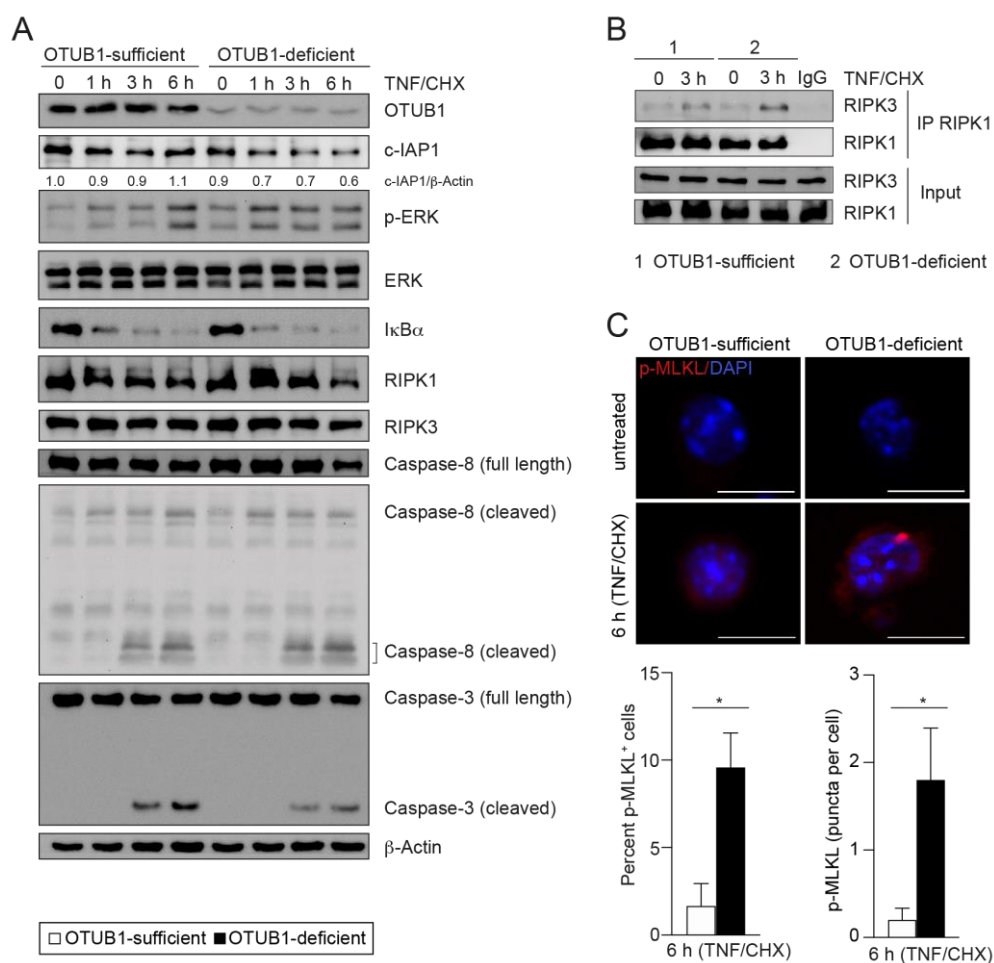


Figure 27: TNF/CHX-induced degradation of c-IAP1 and necroptosis in OTUB1-deficient HepG2 cells.

(A) OTUB1-sufficient and OTUB1-deficient HepG2 cells were left untreated or stimulated with TNF (20 ng/ml, human recombinant TNF) plus CHX (10 μ g/ml) for 1, 3 and 6 h. Protein lysates were harvested at the indicated time points and analyzed by WB. Loading of equal protein amounts was controlled with β -Actin. (B) Protein lysates from unstimulated and 3 h TNF + CHX stimulated HepG2 cells were immunoprecipitated with α -RIPK1 antibody and stained for RIPK1 and RIPK3 by WB. Blots represent one out of two independent experiments. (C) p-MLKL⁺ cells (red) were assessed by immunofluorescence. Cells were counterstained with DAPI for the nucleus (blue). Representative images are shown, scale bars indicate 20 μ m. Based on the microscopic images, the number of p-MLKL⁺ cells and the number of puncta per cell were quantified. A total of 100 cells per experimental group were counted. Mean values with +SEM are indicated, Student's *t*-test, * $p \leq 0.05$.

4.6.2 Hepatocyte TNF production is enhanced by the RIPK1/ERK axis in the absence of OTUB1

In vivo, hepatocellular death in OTUB1^{LPC-KO} mice was accompanied by increased TNF mRNA expression after Lm infection and DGal/TNF challenge. Therefore, we analyzed TNF mRNA expression in OTUB1-deficient HepG2 cells. Quantitative RT-PCR analysis revealed that OTUB1-deficient HepG2 cells expressed significantly higher amounts of TNF mRNA as compared to OTUB1-sufficient HepG2 cells. Comparable to *in vivo* infection, Nec-1s treatment attenuated TNF mRNA expression in Lm-infected OTUB1-sufficient and -deficient HepG2 cells but to a greater extent in OTUB1-deficient HepG2 cells which abolished the differences (Figure 28 A). Inflammatory cytokine responses might be induced by RIPK1 by association to ERK (Najjar *et al.*, 2016). Considering the augmented RIPK1-dependent ERK activation upon OTUB1 deletion in hepatocytes *in vivo* and *in vitro*, we hypothesized that RIPK1 may associate with ERK upon Lm infection. In fact, *Listeria* induced association of RIPK1 to ERK in both OTUB1-sufficient and OTUB1-deficient HepG2 cells. However, this interaction was more prominent in OTUB1-deficient HepG2 cells, especially early after Lm infection at 60 min p.i. (Figure 28 B). To further validate the contribution of ERK to TNF mRNA expression, we infected the HepG2 cells with Lm in the presence of an ERK inhibitor. As depicted in Figure 28 D, ERK inhibition with SCH772984 reduced the TNF expression in both groups but more effectively in OTUB1-deficient HepG2 cells, thereby abolishing differences between both groups.

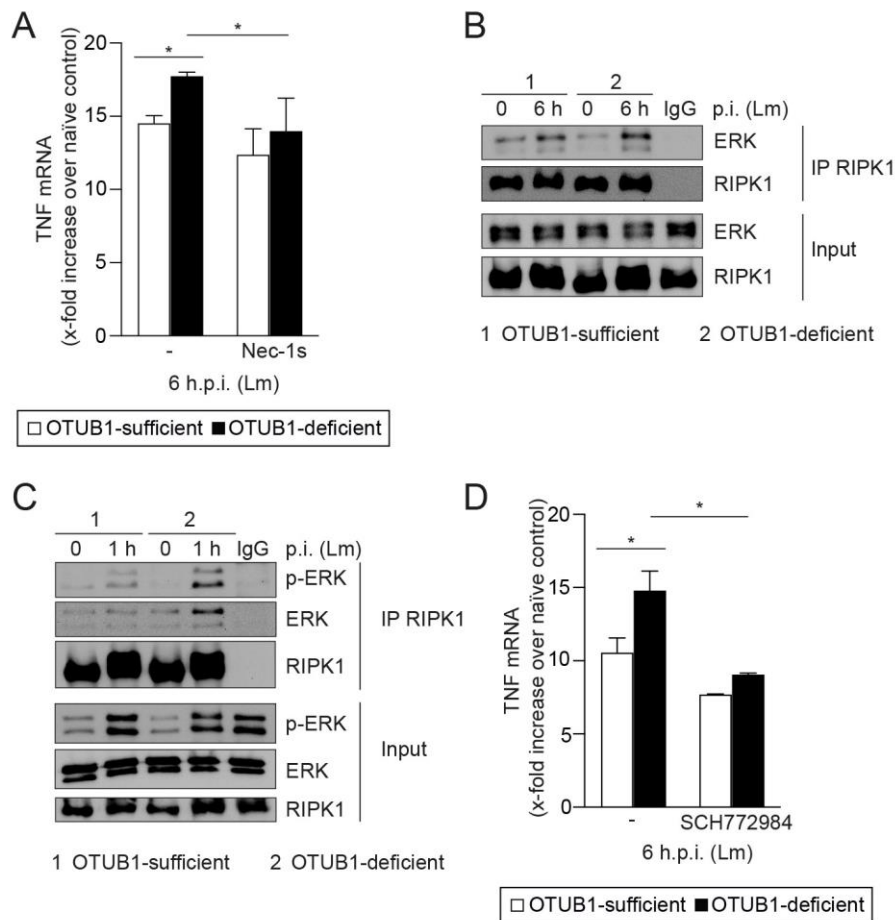


Figure 28: Augmented RIPK1-ERK interaction triggers TNF production in OTUB1-deficient HepG2 cells.

OTUB1-sufficient and OTUB1-deficient HepG2 cells were infected with Lm (MOI of 10) for 6 h. (A) HepG2 cells were either left untreated or treated with Nec-1s (50 μ M) starting 30 min before Lm infection. At 6 h post infection, relative TNF mRNA expression was quantified by RT-PCR ($n = 3$). (B, C) Immunoprecipitation was performed for RIPK1, thereafter protein complexes were probed with antibodies for RIPK1 and ERK and p-ERK, respectively. In (B) the same IP was analyzed as in Figure 26 C. (D) qRT-PCR analysis of TNF mRNA in OTUB1-sufficient and -deficient HepG2 cells infected with Lm for 6 h with or without ERK inhibition (0.5 μ M, starting 30 min before infection, $n = 6$). In (A) and (D) data represents means + SEM as fold increase over the respective untreated controls, two-way Anova, * $p \leq 0.05$. In (B) and (D) Blots are representative for one experiment.

Additionally, TNF/CHX stimulation of HepG2 cells also resulted in an association of RIPK1 with ERK which was more pronounced in the absence of OTUB1 (Figure 29 A). Moreover, TNF mRNA expression was increased in OTUB1-deficient HepG2 cells and could be blocked by ERK inhibition (Figure 29 B). Taken together, these data demonstrate that OTUB1 limits hepatic TNF production by inhibition of the RIPK1/ERK axis.

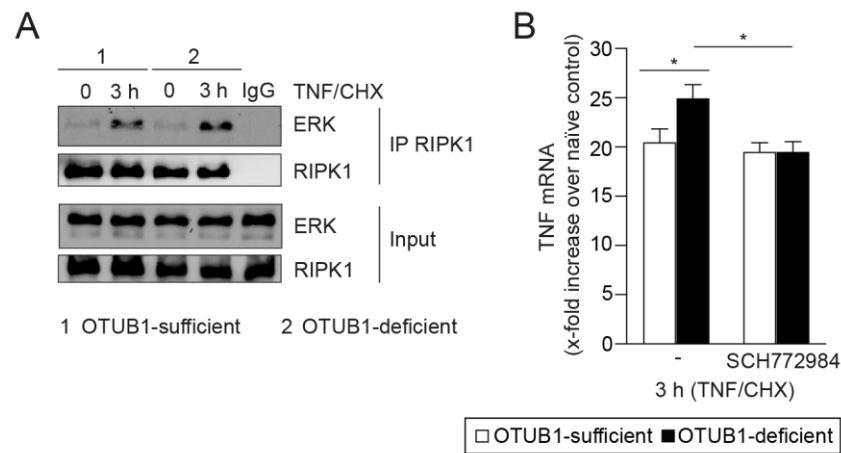


Figure 29: Interaction of RIPK1 and ERK mediates TNF mRNA expression.

OTUB1-sufficient and -deficient HepG2 cells were left unstimulated or stimulated with TNF (20 ng/ml human recombinant TNF) plus CHX (10 μ g/ml) for 3 h. (A) Whole cell lysates were immunoprecipitated with α -RIPK1 and then immunoblotted for RIPK1 and ERK. The same IP samples as in Figure 27 B were analyzed. (B) Relative TNF mRNA expression in OTUB1-sufficient and -deficient HepG2 cells after 3 h of TNF/CHX stimulation with or without the ERK inhibitor SCH772984 (0.5 μ M, starting 30 min before TNF/CHX stimulation). One data set is illustrated as mean values + SEM (n = 6), two-way Anova, * p \leq 0.05.

5 DISCUSSION

In the present study, we identified the deubiquitinating enzyme OTUB1 as a novel inhibitor of TNF-dependent necroptosis and hepatocyte-intrinsic TNF production, thereby preventing bacterial- and toxin-induced mortality of mice *in vivo*. On a molecular level, OTUB1 targeted c-IAP1 after infection with *Listeria monocytogenes* and DGal/TNF challenge.

Hepatocyte-protective role of OTUB1 during liver inflammation Liver inflammation is often caused by invading pathogens or hepatotoxic substances which can lead to excessive hepatocellular death and finally to liver failure. Therefore, liver inflammation has to be tightly controlled by the host to prevent liver damage. Here, we demonstrate that hepatocyte-specific expression of OTUB1 critically regulates hepatocyte necroptosis during *Listeria*- and DGal/TNF- induced liver inflammation *in vivo*. To study the hepatocyte-specific function of OTUB1, we generated conditional OTUB1 knockout mice lacking OTUB1 specifically in the hepatocytes (OTUB1^{LPC-KO}). Similar to the astrocytes in the brain (Wang *et al.*, 2019), deficiency of OTUB1 did not alter liver architecture or function under physiological conditions indicating that OTUB1 is dispensable for liver homeostasis. However, hepatocyte-specific OTUB1 expression protected mice from mortality upon low and high dose infections with the Gram-positive, intracellular bacterium *Listeria monocytogenes*. Upon high dose infection, all OTUB1^{LPC-KO} mice succumbed within 6 days p.i. whereas 90 % of the OTUB1^{FL} control mice survived. Disease progression in OTUB1^{LPC-KO} mice was characterized by (i) a more severe liver pathology with widespread inflammation and necrotic hepatocytes which finally yielded in liver dysfunction and (ii) pronounced mRNA expression of the pro-inflammatory cytokine TNF in the liver. Of note, OTUB1 did not affect pathogen control in liver and spleen. Interestingly, OTUB1 deficiency only augmented TNF mRNA expression but not the expression of other pro-inflammatory cytokines, since mRNA levels of IL-6, IFN γ and IL- β were not significantly increased in OTUB1-deficient livers as compared to OTUB1-sufficient livers at day 3 p.i. In addition, serum cytokines circulating in the periphery were comparable between OTUB1^{LPC-KO} and OTUB1^{FL} control mice arguing against a systemic inflammation in these mice. In liver, *Listeria* primarily utilizes the hepatocytes as host for replication (Gregory *et al.*, 1992). However, the liver-resident macrophages (Kupffer cells) are considered as the first line of host defense which secrete various cytokines, in particular TNF, in response to LLO-producing *Listeria* (Vazquez *et al.*, 1995). Consequently, the innate and adaptive immune cells are activated and recruited to the site of infection. The anti-listerial capacity of TNF during acute listeriosis has been addressed in several studies using TNFR1 and TNF knockout mice as

well as TNF neutralizing antibodies (Rothe *et al.*, 1993; Slifman *et al.*, 2003; Torres *et al.*, 2005; Wroblewski *et al.*, 2016). Defects in TNF signaling resulted in a high *Listeria*-induced lethality due to bacteremia (Pfeffer *et al.*, 1993). However, excessive production of TNF, as observed in OTUB1^{LPC-KO} mice, may lead to immunopathology and hepatocyte cell death without improved pathogen clearance. Noteworthy, the enhanced liver-intrinsic TNF production was not attributed to liver-resident macrophages or infiltrating macrophages and monocytes but to hepatocytes. Additionally, leukocyte infiltration to the *Listeria*-infected livers was not impaired in the absence of OTUB1. Thus, lethality in the OTUB1^{LPC-KO} mice was not caused by a defective immune response against *Listeria*. Considering the severe pathology and the increased TNF levels in the liver, it is likely that TNF overproduction leads to the excessive hepatocellular death in context of OTUB1 deficiency. In line with that, *in vitro* infection of primary hepatocytes with *Listeria* resulted in enhanced cell death and higher expression of TNF in the absence of OTUB1 without affecting pathogen control. These findings reveal a hepatocyte-intrinsic mechanism of OTUB1 for limiting TNF production which may cause the inflammation and subsequently the death of the hepatocytes in OTUB1-deficient livers. Given that OTUB1-deficiency did not affect bacterial loads *in vivo* as well as *in vitro*, both hepatocellular death and TNF production seem to be triggered independently from listerial LLO which is known to induce both (Vazquez *et al.*, 1995; Carrero *et al.*, 2004; González-Juarbe *et al.*, 2015). In good agreement to listeriosis, hepatocyte-specific OTUB1 expression conferred protection against DGal/LPS- and DGal/TNF-induced liver injury. Previous reports demonstrated that acute liver injury induced by DGal/LPS entirely depends on hepatocyte TNFR-signaling (Josephs *et al.*, 2000; Nowak *et al.*, 2000). Similar to infection with *Listeria*, OTUB1 reduced liver damage and limited hepatocyte TNF production, thereby preserving liver function upon both DGal/LPS and DGal/TNF challenge. Therefore, we conclude that the hepatocellular death is correlated to the TNF levels and confirmatively both are pathogen-independent. Of note, when challenging the mice with equal amounts of TNF combined with DGal, these mice still displayed enhanced hepatocellular death and increased liver-intrinsic TNF expression compared to the OTUB1^{FL} control mice indicating that the increased cell death is primarily attributed to sensitivity of the OTUB1-deficient hepatocytes towards TNF per se and might be further amplified by the pronounced TNF synthesis.

OTUB1 as a regulator of TNF-dependent necroptosis TNF can induce both apoptosis and necroptosis in various cell types and tissues. TNF signal transduction via TNFR1 involves the coordinative assembling of distinct signaling complexes either directing survival signaling through NF- κ B activation or death signaling via caspase cleavage (apoptosis) or RIPK1/RIPK3 complex formation (necroptosis) (Micheau & Tschopp, 2003; Schwabe & Luedde, 2018). However, in context of hepatocellular death, necroptotic signaling and its initiating factors are controversially discussed. In most cases, hepatocytes are considered as necroptosis resistant since necroptosis is only observed when apoptosis was experimentally blocked or an abnormal RIPK3 expression is induced (Ramachandran *et al.*, 2013; Kondylis & Pasparakis, 2019). Here, we demonstrate that OTUB1 inhibits the switch from TNF-induced apoptosis to necroptosis in hepatocytes. Upon deletion of this inhibitory mechanism, hepatic failure was induced by *Listeria*-infection and DGal/TNF challenge as observed in OTUB1^{LPC-KO} mice. Within TNFR1 signaling, c-IAP1 plays a critical role, since genetic ablation or pharmacological degradation of c-IAP1 shifts survival canonical NF- κ B signaling towards death signaling (Tenev *et al.*, 2011). As demonstrated by Goncharov *et al.*, the deubiquitinating enzyme OTUB1 stabilizes c-IAP1 and thereby blocks TNF-mediated cell death in a ubiquitin-dependent manner (Goncharov *et al.*, 2013). Mechanistically, OTUB1 disassembled K48-linked polyubiquitin chains from c-IAP1 following TWEAK stimulation *in vitro*. Thus, knockdown of OTUB1 resulted in an accelerated degradation of c-IAP1 and diminished TWEAK-induced NF- κ B and MAPK signaling which increased the sensitivity towards TNF-induced apoptosis. TWEAK, however, enhances cell death signaling but requires cooperation with the TNFR1 for cell death induction (Wicovsky *et al.*, 2009; Ikner & Ashkenazi, 2011). In the present study, we demonstrate that OTUB1 directly interferes with the TNFR1 signaling by maintaining hepatic c-IAP1 levels following TNF-stimulation *in vivo* as well as *in vitro*. In contrast to Goncharov *et al.*, deficiency of OTUB1 augmented hepatic RIPK1/RIPK3 necrosome formation upon TNF stimulation but not caspase cleavage. In fact, caspase cleavage was even reduced in the absence of OTUB1 pointing to a shift towards necroptotic signaling, since loss of c-IAP1 combined with impaired caspase-8 activation has been shown to promote necroptosis (Feltham *et al.*, 2017). Considering that the c-IAP1 levels dropped drastically after stimulation of the TNFR1 as seen in our studies but remained unchanged upon TWEAK stimulation as revealed by Goncharov *et al.*, the different mode of cell death might be explained by the different levels of c-IAP1 within TNFR1 signaling. These findings highlight that the function of OTUB1 is in part dependent on the stimulus. Furthermore, these data illustrate that OTUB1 is important in blocking necroptosis *in vivo* and *in vitro* without preventing apoptosis. Following TNFR1

stimulation, c-IAP1 acts as an E3 ubiquitin ligase adding K63-linked polyubiquitin chains on RIPK1 which may serve as a signaling platform for NF- κ B activation while restricting its kinase activity (Delanghe *et al.*, 2020). Several studies on RIPK1 suggested its kinase-dependent and kinase-independent mode of action. Necroptosis is considered to be dependent on its kinase activity, since RIPK1 inactive mice are protected from TNF-induced necroptosis *in vivo* and *in vitro* (Polykratis *et al.*, 2014) whereas RIPK1 deficient hepatocytes are sensitized towards TNF-induced apoptosis (Suda *et al.*, 2016). This concept was further extended by using RIPK1 mutant cells harboring a mutated lysine residue (Lys376, K376) on a ubiquitination site. In this study, Zhang *et al.* uncovered that the K63-linked polyubiquitin chains on Lys376 are catalyzed by c-IAP1 and are essential for limiting RIPK1-kinase dependent cell death as well as inflammation (Zhang *et al.*, 2019). In accordance with the published data, we observed that the increased lethality of OTUB1^{LPC-KO} mice compared to control mice upon *Listeria* infection and DGal/TNF challenge was a consequence TNF-mediated (i) pronounced degradation of c-IAP1, (ii) impaired K63-linked polyubiquitination of RIPK1 and (iii) RIPK1/RIPK3 dependent necroptosis. Interestingly, viability of RIPK1 mutant cells was further reduced upon TNF stimulation in the presence of SMAC mimetic, which inhibits c-IAP1, and could be prevented by Nec-1s but not by zVAD treatment (Zhang *et al.*, 2019). This is in line with our *in vivo* findings illustrating that Nec-1s administration completely rescued the OTUB1^{LPC-KO} mice from death during *Listeria*-infection. We observed that Nec-1s administration efficiently prevented excessive liver damage and TNF production while zVAD failed to prevent both. These data illustrate that the activity of RIPK1 is not only responsible for the necroptosis induction but is also involved in the inflammatory response during *Listeria*-infection in the OTUB1-deficient livers. Likewise, deletion of MLKL, the executioner of necroptotic cell death, conferred protection from cell death in the OTUB1^{LPC-KO} mice similarly to Nec-1s treatment. However, deletion of MLKL had no impact on the liver-intrinsic TNF production indicating that the hepatocyte-intrinsic TNF production is independent of necroptosis. Although OTUB1 has been identified to interfere with NF- κ B signaling (Mulas *et al.*, 2020), our data further show that the susceptibility of the OTUB1^{LPC-KO} mice to TNF-induced lethality was not caused by defects in canonical or non-canonical NF- κ B signaling and the subsequent transcription of anti-apoptotic genes, since degradation of the NF- κ B inhibitor, I κ B α , the phosphorylation of the NF- κ B subunit p65 and the processing of p100 to p52 as well as the transcription of the anti-apoptotic genes Bcl-2 and c-FLIP were similar in both genotypes following *Listeria* infection. In addition to NF- κ B, OTUB1-deficiency did not influence the activation of p38 and JNK but promoted the phosphorylation of ERK. These findings are in line with the previous

published studies and support the hypothesis that RIPK1 kinase activity is dispensable for NF- κ B activation (Festjens *et al.*, 2007; Polykratis *et al.*, 2014). However, in contrast, ERK activation was reported to require RIPK1 activity (Devin *et al.*, 2003; Festjens *et al.*, 2007). This might explain the enhanced phosphorylation of ERK as observed in OTUB1-deficient livers upon *Listeria* infection and DGal/TNF treatment *in vivo*. Of note, this ERK hyperactivation could be prevented by Nec-1s treatment.

OTUB1 as a regulator of hepatic TNF-production Given that ERK activation and TNF expression were augmented in the absence of OTUB1 in a RIPK1-dependent manner, we questioned whether the increased TNF synthesis is amplified by the RIPK1/ERK axis. Inhibition of IAP-proteins have already been reported to trigger inflammatory cytokine responses, in particular autocrine TNF synthesis, leading to cell death (Wong *et al.*, 2014). Contrary to this report, Najjar *et al.* proposed that the RIPK1/RIPK3 necrosome can associate with ERK to trigger TNF synthesis upon LPS stimulation in the presence of zVAD (Najjar *et al.*, 2016). To address this, we knocked down OTUB1 in HepG2 using lentiviral transduction. Notably, OTUB1-deficient HepG2 cells showed similar characteristics upon *Listeria*-infection and TNF/CHX treatment as seen in mice with a normal NF- κ B signaling but an augmented ERK signaling. With respect to cell death signaling, OTUB1-deficient HepG2 cells showed reduced cleavage of caspases but enhanced RIPK1/RIPK3 complex formation which resulted in an increased phosphorylation of MLKL. Therefore, our data support the functional role of OTUB1 as molecular switch preventing necroptosis but still allowing apoptosis. Similar to the *in vivo* model, the enhanced necroptosis in OTUB1-deficient HepG2 cells was a consequence of the enhanced degradation of c-IAP1 caused by accumulation of K48-linked polyubiquitin chains on c-IAP1 and the subsequent insufficient K63-linked polyubiquitination of RIPK1. In good agreement with the hypothesis that the hepatic TNF expression is amplified in a RIPK1/ERK-mediated autocrine loop when OTUB1 is absent, RIPK1 complexed to ERK upon infection with *Listeria* and TNF/CHX stimulation. Although this interaction occurred both in the presence and in the absence of OTUB1 it was more pronounced in OTUB1-deficient HepG2 cells, especially at early time points after infection. Therefore, we conclude that difference in TNF expression between the OTUB1-sufficient and -deficient HepG2 cells is mainly driven by the RIPK1/ERK axis. In accordance to that, treatment with an ERK inhibitor could efficiently downregulate the TNF expression in the OTUB1-deficient HepG2 cells, similar to Nec-1s treatment and was less efficient in OTUB1-sufficient HepG2 cells. Taken together, the current study demonstrates that OTUB1 critically regulates not only the sensitivity towards

TNF-induced cell death, in particular necroptosis, but also the hepatocyte-intrinsic TNF production which further amplifies the hepatocellular death. Thus, OTUB1 plays an important role in inhibiting TNF-induced necroptosis and liver inflammation, thereby preventing acute liver failure during inflammatory liver diseases *in vivo* and *in vitro*.

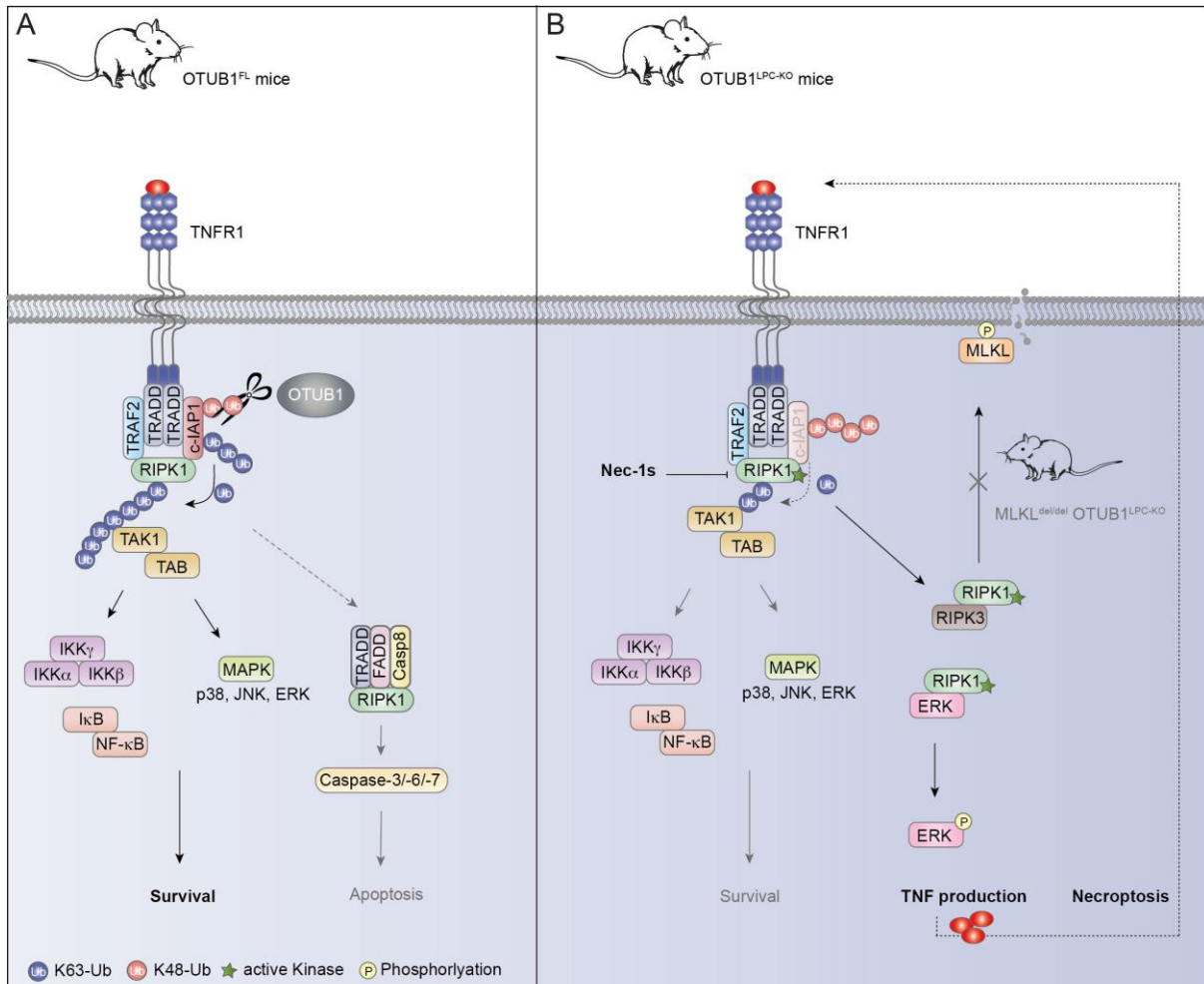


Figure 30: Schematic summary of the present study.

Scheme illustrating the TNF signaling in the presence (A) or absence of OTUB1 (B) in the liver. Following TNF-TNFR1 ligation, c-IAP1 which is stabilized by OTUB1 auto-ubiquitinates first itself and thereafter RIPK1 in K63. K63-linked polyubiquitination of RIPK1 in turn primarily leads to the activation of pro-survival NF-κB when OTUB1 is present. (B) In the absence of OTUB1, accumulation of K48-linked polyubiquitin chains on c-IAP1 cause the rapid TNF-induced degradation of c-IAP1. Consequently, K63-linked polyubiquitination of RIPK1 is impaired leading to the RIPK1 kinase-dependent necroptosis induction which is further enhanced by autocrine RIPK1/ERK-mediated TNF production. Nec-1s administration blocks both necroptotic signaling and RIPK1/ERK-mediated TNF production while knockout of MLKL only prevents necroptosis execution.

REFERENCES

- Annibaldi, A. & Meier, P. (2018) Checkpoints in TNF-Induced Cell Death: Implications in Inflammation and Cancer. *Trends in Molecular Medicine*, **24**, 49–65.
- Balakirev, M.Y., Tcherniuk, S.O., Jaquinod, M., & Chroboczek, J. (2003) Otubains: A new family of cysteine proteases in the ubiquitin pathway. *EMBO Reports*, **4**, 517–522.
- Bentires-alj, M., De Jardin, E., Viatour, P., Lint, C. van, Froesch, B., Reed, J.C., Merville, M., & Bours, V. (2001) Inhibition of the NF- κ B transcription factor increases Bax expression in cancer cell lines. *Oncogene*, **53**.
- Blériot, C., Dupuis, T., Jouvion, G., Eberl, G., Disson, O., & Lecuit, M. (2015) Liver-Resident Macrophage Necroptosis Orchestrates Type 1 Microbicidal Inflammation and Type-2-Mediated Tissue Repair during Bacterial Infection. *Immunity*, **42**, 145–158.
- Bogdanos, D.P., Gao, B., & Gershwin, M.E. (2013) Liver immunology. *Comprehensive Physiology*, **3**, 567–598.
- Brenner, C., Galluzzi, L., Kepp, O., & Kroemer, G. (2013) Decoding cell death signals in liver inflammation. *Journal of Hepatology*, **59**, 583–594.
- Brenner, D., Blaser, H., & Mak, T.W. (2015) Regulation of tumour necrosis factor signalling: Live or let die. *Nature Reviews Immunology*, **15**, 362–374.
- Carrero, J.A., Calderon, B., & Unanue, E.R. (2004) Listeriolysin O from *Listeria monocytogenes* Is a Lymphocyte Apoptogenic Molecule. *The Journal of Immunology*, **172**, 4866–4874.
- Chen, X., Li, W., Ren, J., Huang, D., He, W.T., Song, Y., Yang, C., Li, W., Zheng, X., Chen, P., & Han, J. (2014) Translocation of mixed lineage kinase domain-like protein to plasma membrane leads to necrotic cell death. *Cell Research*, **24**, 105–121.
- Cossart, P. (2011) Illuminating the landscape of host-pathogen interactions with the bacterium *Listeria monocytogenes*. *Proceedings of the National Academy of Sciences of the United States of America*, **108**, 19484–19491.
- Cousens, L.P. & Wing, E.J. (2000) Innate defenses in the liver during *Listeria* infection. *Immunological Reviews*, **174**, 150–159.
- Dammer, E.B., Na, C.H., Xu, P., Seyfried, N.T., Duong, D.M., Cheng, D., Gearing, M., Rees, H., Lah, J.J., Levey, A.I., Rush, J., & Peng, J. (2011) Polyubiquitin linkage profiles in three models of proteolytic stress suggest the etiology of alzheimer disease. *Journal of Biological Chemistry*, **286**, 10457–10465.

-
- Dara, L., Liu, Z.X., & Kaplowitz, N. (2016) Questions and controversies: the role of necroptosis in liver disease. *Cell Death Discovery*, **2**, 1–10.
- de Almagro, M.C., Goncharov, T., Izrael-Tomasevic, A., Duttler, S., Kist, M., Varfolomeev, E., Wu, X., Lee, W.P., Murray, J., Webster, J.D., Yu, K., Kirkpatrick, D.S., Newton, K., & Vucic, D. (2017) Coordinated ubiquitination and phosphorylation of RIP1 regulates necroptotic cell death. *Cell Death and Differentiation*, **24**, 26–37.
- de Oliveira, J.R., Rosa, J.L., Ambrosio, S., & Bartrons, R. (1992) Effect of galactosamine on hepatic carbohydrate metabolism: Protective role of fructose 1,6-bisphosphate. *Hepatology*, **15**, 1147–1153.
- Delanghe, T., Dondelinger, Y., & Bertrand, M.J.M. (2020) RIPK1 Kinase-Dependent Death: A Symphony of Phosphorylation Events. *Trends in Cell Biology*, **30**, 189–200.
- Devin, A., Lin, Y., & Liu, Z.G. (2003) The role of the death-domain kinase RIP in tumour-necrosis-factor-induced activation of mitogen-activated protein kinases. *EMBO Reports*, **4**, 623–627.
- Dondelinger, Y., Darding, M., Bertrand, M.J.M., Walczak, H., Ripk, Á., Lubac, I.A.P.Á., & Cyld, Á.A.Á. (2016) Poly-ubiquitination in TNFR1-mediated necroptosis. *Cellular and Molecular Life Sciences*, **73**, 2165–2176.
- D’Orazio, S.E.F. (2019) Innate and Adaptive Immune Responses during *Listeria monocytogenes* Infection. *Microbiology Spectrum*, **7**, 1–40.
- Dynek, J.N., Goncharov, T., Dueber, E.C., Fedorova, A. v., Izrael-Tomasevic, A., Phu, L., Helgason, E., Fairbrother, W.J., Deshayes, K., Kirkpatrick, D.S., & Vucic, D. (2010) C-IAP1 and UbcH5 promote K11-linked polyubiquitination of RIP1 in TNF signalling. *EMBO Journal*, **29**, 4198–4209.
- Edelmann, M.J., Iphöfer, A., Akutsu, M., Altun, M., di Gleria, K., Kramer, H.B., Fiebiger, E., Dhe-Paganon, S., & Kessler, B.M. (2009) Structural basis and specificity of human otubain 1-mediated deubiquitination. *Biochemical Journal*, **418**, 379–390.
- Feltham, R., Vince, J.E., & Lawlor, K.E. (2017) Caspase-8: Not so silently deadly. *Clinical and Translational Immunology*, **6**, 1–13.
- Feoktistova, M., Geserick, P., Kellert, B., Dimitrova, D.P., Langlais, C., Hupe, M., Cain, K., MacFarlane, M., Häcker, G., & Leverkus, M. (2011) CIAPs Block Ripoptosome Formation, a RIP1/Caspase-8 Containing Intracellular Cell Death Complex Differentially Regulated by cFLIP Isoforms. *Molecular Cell*, **43**, 449–463.
- Festjens, N., vanden Berghe, T., Cornelis, S., & Vandenabeele, P. (2007) RIP1, a kinase on the crossroads of a cell’s decision to live or die. *Cell Death and Differentiation*, **14**, 400–410.

-
- Goncharov, T., Niessen, K., de Almagro, M.C., Izrael-Tomasevic, A., Fedorova, A. v., Varfolomeev, E., Arnott, D., Deshayes, K., Kirkpatrick, D.S., & Vucic, D. (2013) OTUB1 modulates c-IAP1 stability to regulate signalling pathways. *EMBO Journal*, **32**, 1103–1114.
- González-Juarbe, N., Gilley, R.P., Hinojosa, C.A., Bradley, K.M., Kamei, A., Gao, G., Dube, P.H., Bergman, M.A., & Orihuela, C.J. (2015) Pore-Forming Toxins Induce Macrophage Necroptosis during Acute Bacterial Pneumonia. *PLoS Pathogens*, **11**, 1–23.
- Gonzalvez, F., Lawrence, D., Yang, B., Yee, S., Pitti, R., Marsters, S., Pham, V.C., Stephan, J.P., Lill, J., & Ashkenazi, A. (2012) TRAF2 Sets a Threshold for Extrinsic Apoptosis by Tagging Caspase-8 with a Ubiquitin Shutoff Timer. *Molecular Cell*, **48**, 888–899.
- Gregory, S.H., Barczynski, L.K., & Wing, E.J. (1992) Effector function of hepatocytes and Kupffer cells in the resolution of systemic bacterial infections. *Journal of Leukocyte Biology*, **51**, 421–424.
- Hamon, M., Bierne, H., & Cossart, P. (2006) *Listeria monocytogenes*: A multifaceted model. *Nature Reviews Microbiology*, **4**, 423–434.
- Harhaj, E.W. & Dixit, V.M. (2011) Deubiquitinases in the regulation of NF- κ B signaling. *Cell Research*, **21**, 22–39.
- He, M., Zhou, Z., Shah, A.A., Zou, H., Tao, J., Chen, Q., & Wan, Y. (2016) The emerging role of deubiquitinating enzymes in genomic integrity, diseases, and therapeutics. *Cell and Bioscience*, **6**, 1–15.
- Herhaus, L., Al-salihi, M., Macartney, T., Weidlich, S., & Sapkota, G.P. (2013) OTUB1 enhances TGF β signalling by inhibiting the ubiquitylation and degradation of active SMAD2/3. *Nature Communications*, 1–13.
- Hildebrand, J.M., Tanzer, M.C., Lucet, I.S., Young, S.N., Spall, S.K., Sharma, P., Pierotti, C., Garnier, J.M., Dobson, R.C.J., Webb, A.I., Tripaydonis, A., Babon, J.J., Mulcair, M.D., Scanlon, M.J., Alexander, W.S., Wilks, A.F., Czabotar, P.E., Lessene, G., Murphy, J.M., & Silke, J. (2014) Activation of the pseudokinase MLKL unleashes the four-helix bundle domain to induce membrane localization and necroptotic cell death. *Proceedings of the National Academy of Sciences of the United States of America*, **111**, 15072–15077.
- Holbrook, J., Lara-Reyna, S., Jarosz-Griffiths, H., & McDermott, M. (2019) Tumour necrosis factor signalling in health and disease. *F1000Research*, **8**, 1–12.
- Iglesias-Gato, D., Chuan, Y.C., Jiang, N., Svensson, C., Bao, J., Paul, I., Egevad, L., Kessler, B.M., Wikström, P., Niu, Y., & Flores-Morales, A. (2015) OTUB1 de-ubiquitinating

-
- enzyme promotes prostate cancer cell invasion in vitro and tumorigenesis in vivo. *Molecular Cancer*, **14**, 1–14.
- Ikner, A. & Ashkenazi, A. (2011) TWEAK induces apoptosis through a death-signaling complex comprising receptor-interacting protein 1 (RIP1), Fas-associated Death Domain (FADD), and caspase-8. *Journal of Biological Chemistry*, **286**, 21546–21554.
- Jahan, A.S., Biquand, E., Muñoz-Moreno, R., le Quang, A., Mok, C.K.P., Wong, H.H., Teo, Q.W., Valkenburg, S.A., Chin, A.W.H., Man Poon, L.L., te Velthuis, A., García-Sastre, A., Demeret, C., & Sanyal, S. (2020) OTUB1 Is a Key Regulator of RIG-I-Dependent Immune Signaling and Is Targeted for Proteasomal Degradation by Influenza A NS1. *Cell Reports*, **30**, 1570-1584.e6.
- Jin, Z., Li, Y., Pitti, R., Lawrence, D., Pham, V.C., Lill, J.R., & Ashkenazi, A. (2009) Cullin3-Based Polyubiquitination and p62-Dependent Aggregation of Caspase-8 Mediate Extrinsic Apoptosis Signaling. *Cell*, **137**, 721–735.
- Josephs, M.D., Fukuzuka, K., Ksontini, R., Solorzano, C.C., Edwards, C.K., Tannahill, C.L., Mackay, S.L.D., Copeland, E.M., & Moldawer, L.L. (2000) Lipopolysaccharide and D-galactosamine-induced hepatic injury is mediated by TNF- α and not by Fas ligand. *American Journal of Physiology - Regulatory Integrative and Comparative Physiology*, **278**, 1196–1201.
- Karunarathna, U., Kongsema, M., Zona, S., Gong, C., Cabrera, E., Gomes, A.R., Man, E.P.S., Khongkow, P., Tsang, J.W.H., Khoo, U.S., Medema, R.H., Freire, R., & Lam, E.W.F. (2016) OTUB1 inhibits the ubiquitination and degradation of FOXM1 in breast cancer and epirubicin resistance. *Oncogene*, **35**, 1433–1444.
- Keppler, D., Lesch, R., Reutter, W., & Decker, K. (1968) Experimental hepatitis induced by d-galactosamine. *Experimental and Molecular Pathology*, **9**, 279–290.
- Keppler D., Rudigier J.F.M., Bischoff E., D.K.F.A. (1970) The Trapping of Uridine Phosphates. *European Journal of Biochemistry*, **17**, 246–253.
- Kim, S.J. & Lee, S.M. (2017) Necrostatin-1 Protects Against d-Galactosamine and Lipopolysaccharide-Induced Hepatic Injury by Preventing TLR4 and RAGE Signaling. *Inflammation*, **40**, 1912–1923.
- Komander, D., Clague, M.J., & Urbé, S. (2009) Breaking the chains: Structure and function of the deubiquitinases. *Nature Reviews Molecular Cell Biology*, **10**, 550–563.
- Kondylis, V. & Pasparakis, M. (2019) RIP Kinases in Liver Cell Death, Inflammation and Cancer. *Trends in Molecular Medicine*, **25**, 47–63.

-
- Li, Y., Yang, J.Y., Xie, X., Jie, Z., Zhang, L., Shi, J., Lin, D., Gu, M., Zhou, X., Li, H.S., Watowich, S.S., Jain, A., Yun Jung, S., Qin, J., Cheng, X., & Sun, S.C. (2019) Preventing abnormal NF- κ B activation and autoimmunity by Otub1-mediated p100 stabilization. *Cell Research*, **29**, 474–485.
- Lim, M.C.C., Maubach, G., Sokolova, O., Feige, M.H., Diezko, R., Buchbinder, J., Backert, S., Schlüter, D., Lavrik, I.N., & Naumann, M. (2017) Pathogen-induced ubiquitin-editing enzyme A20 bifunctionally shuts off NF- κ B and caspase-8-dependent apoptotic cell death. *Cell Death and Differentiation*, **24**, 1621–1631.
- Lin, J., Kumari, S., Kim, C., Van, T.M., Wachsmuth, L., Polykratis, A., & Pasparakis, M. (2016) RIPK1 counteracts ZBP1-mediated necroptosis to inhibit inflammation. *Nature*, **540**, 124–128.
- Liu, X., Shi, F., Li, Y., Yu, X., Peng, S., Li, W., Luo, X., & Cao, Y. (2016) Post-translational modifications as key regulators of TNF-induced necroptosis. *Cell death & disease*, **7**, e2293.
- Livak, K.J. & Schmittgen, T.D. (2001) Analysis of relative gene expression data using real-time quantitative PCR and the $2^{-\Delta\Delta CT}$ method. *Methods*, **25**, 402–408.
- Luedde, T., Kaplowitz, N., & Schwabe, R.F. (2014) Cell death and cell death responses in liver disease: Mechanisms and clinical relevance. *Gastroenterology*, **147**, 765-783.e4.
- Macías-Rodríguez, R.U., Inzaugarat, M.E., Ruiz-margáin, A., Nelson, L.J., Trautwein, C., & Cubero, F.J. (2020) Reclassifying hepatic cell death during liver damage: Ferroptosis—a novel form of non-apoptotic cell death? *International Journal of Molecular Sciences*, **21**.
- Mevissen, T.E.T. & Komander, D. (2017) Mechanisms of Deubiquitinase Specificity and Regulation. *Annual Review of Biochemistry*, **86**, 159–192.
- Micheau, O. & Tschopp, J. (2003) Induction of TNF receptor I-mediated apoptosis via two sequential signaling complexes. *Cell*, **114**, 181–190.
- Mulas, F., Wang, X., Song, S., Nishanth, G., Yi, W., Brunn, A., Larsen, P.K., Isermann, B., Kalinke, U., Barragan, A., Naumann, M., Deckert, M., & Schlüter, D. (2020) The deubiquitinase OTUB1 augments NF- κ B-dependent immune responses in dendritic cells in infection and inflammation by stabilizing UBC13. *Cellular and Molecular Immunology*.
- Muriel, P., Ramos-Tovar, E., Montes-Páez, G., & Buendía-Montaño, L.D. (2017) Experimental Models of Liver Damage Mediated by Oxidative Stress. *Liver Pathophysiology: Therapies and Antioxidants*, 529–546.

-
- Najjar, M., Saleh, D., Zelic, M., Nogusa, S., Shah, S., Tai, A., Finger, J.N., Polykratis, A., Gough, P.J., Bertin, J., Whalen, M.J., Pasparakis, M., Balachandran, S., Kelliher, M., Poltorak, A., & Degterev, A. (2016) RIPK1 and RIPK3 Kinases Promote Cell-Death-Independent Inflammation by Toll-like Receptor 4. *Immunity*, **45**, 46–59.
- Nakada, S., Tai, I., Panier, S., Al-Hakim, A., Iemura, S.I., Juang, Y.C., O'Donnell, L., Kumakubo, A., Munro, M., Sicheri, F., Gingras, A.C., Natsume, T., Suda, T., & Durocher, D. (2010) Non-canonical inhibition of DNA damage-dependent ubiquitination by OTUB1. *Nature*, **466**, 941–946.
- Ni, Q., Chen, J., Li, X., Xu, X., Zhang, N., Zhou, A., Zhou, B., Lu, Q., & Chen, Z. (2017) Expression of OTUB1 in hepatocellular carcinoma and its effects on HCC cell migration and invasion. *Acta Biochimica et Biophysica Sinica*, **49**, 680–688.
- Nijman, S.M.B., Luna-Vargas, M.P.A., Velds, A., Brummelkamp, T.R., Dirac, A.M.G., Sixma, T.K., & Bernards, R. (2005) A genomic and functional inventory of deubiquitinating enzymes. *Cell*, **123**, 773–786.
- Nowak, M., Gaines, G.C., Rosenberg, J., Minter, R., Bahjat, F.R., Rectenwald, J., Kay, S.L.D.M.A.C., Iii, C.K.E., Moldawer, L.L., Oaks, T., Gaines, G.C., Rosen-, J., Minter, R., Bahjat, F.R., Rectenwald, J., Mackay, S.L.D., Iii, C.K.E., & Lyle, L. (2000) LPS-induced liver injury in D -galactosamine-sensitized mice requires secreted TNF- α and the TNF-p55 receptor. *Am J Physiol Regulatory Integrative Comp Physiol*, 1202–1209.
- Orozco, S., Yatim, N., Werner, M.R., Tran, H., Gunja, S.Y., Tait, S.W.G., Albert, M.L., Green, D.R., & Oberst, A. (2014) RIPK1 both positively and negatively regulates RIPK3 oligomerization and necroptosis. *Cell Death and Differentiation*, **21**, 1511–1521.
- Pamer, E.G. (2004) Immune responses to *Listeria monocytogenes*. *Nature Reviews Immunology*, **4**, 812–823.
- Pasupala, N., Morrow, M.E., Que, L.T., Malynn, B.A., Ma, A., & Wolberger, C. (2018) OTUB1 non-catalytically stabilizes the E2 ubiquitin-conjugating enzyme UBE2E1 by preventing its autoubiquitination. *Journal of Biological Chemistry*, **293**, 18285–18295.
- Peltzer, N., Darding, M., & Walczak, H. (2016) Holding RIPK1 on the Ubiquitin Leash in TNFR1 Signaling. *Trends in Cell Biology*, **26**, 445–461.
- Pfeffer, K., Matsuyama, T., Kündig, T.M., Wakeham, A., Kishihara, K., Shahinian, A., Wiegmann, K., Ohashi, P.S., Krönke, M., & Mak, T.W. (1993) Mice deficient for the 55 kd tumor necrosis factor receptor are resistant to endotoxic shock, yet succumb to *L. monocytogenes* infection. *Cell*, **73**, 457–467.

-
- Pickart, C.M. & Eddins, M.J. (2004) Ubiquitin: Structures, functions, mechanisms. *Biochimica et Biophysica Acta - Molecular Cell Research*, **1695**, 55–72.
- Polykratis, A., Hermance, N., Zelic, M., Roderick, J., Kim, C., Van, T.-M., Lee, T.H., Chan, F.K.M., Pasparakis, M., & Kelliher, M.A. (2014) Cutting Edge: RIPK1 Kinase Inactive Mice Are Viable and Protected from TNF-Induced Necroptosis In Vivo. *The Journal of Immunology*, **193**, 1539–1543.
- Ramachandran, A., McGill, M.R., Xie, Y., Ni, H.M., Ding, W.X., & Jaeschke, H. (2013) Receptor interacting protein kinase 3 is a critical early mediator of acetaminophen-induced hepatocyte necrosis in mice. *Hepatology*, **58**, 2099–2108.
- Rauert, H., Wicovsky, A., Müller, N., Siegmund, D., Spindler, V., Waschke, J., Kneitz, C., & Wajant, H. (2010) Membrane Tumor Necrosis Factor (TNF) induces p100 processing via TNF receptor-2 (TNFR2). *Journal of Biological Chemistry*, **285**, 7394–7404.
- Robinson, M.W., Harmon, C., & O’Farrelly, C. (2016) Liver immunology and its role in inflammation and homeostasis. *Cellular and Molecular Immunology*, **13**, 267–276.
- Rothe, J., Lesslauer, W., Lötscher, H., Lang, Y., Koebel, P., Köntgen, F., Althage, A., Zinkernagel, R., Steinmetz, M., & Bluethmann, H. (1993) Mice lacking the tumour necrosis factor receptor 1 are resistant to IMF-mediated toxicity but highly susceptible to infection by *Listeria monocytogenes*. *Nature*, **364**, 798–802.
- Saldana, M., VanderVorst, K., Berg, A.L., Lee, H., & Carraway, K.L. (2019) Otubain 1: A non-canonical deubiquitinase with an emerging role in cancer. *Endocrine-Related Cancer*, **26**, R1–R14.
- Santos, S.A. dos, Andrade Júnior, D.R. de, & Andrade, D.R. de (2011) Tnf- α production and apoptosis in hepatocytes after *Listeria monocytogenes* and *Salmonella typhimurium* invasion. *Revista do Instituto de Medicina Tropical de São Paulo*, **53**, 107–112.
- Schlech, W.F. (2019) Epidemiology and Clinical Manifestations of *Listeria monocytogenes* Infection. *Gram-Positive Pathogens*, 793–802.
- Schümann, J., Mühlen, K., Kiemer, A.K., Vollmar, A.M., & Tiegs, G. (2003) Parenchymal, But Not Leukocyte, TNF Receptor 2 Mediates T Cell-Dependent Hepatitis in Mice. *The Journal of Immunology*, **170**, 2129–2137.
- Schwabe, R.F. & Luedde, T. (2018) Apoptosis and necroptosis in the liver: a matter of life and death. *Nature Reviews Gastroenterology and Hepatology*, **15**, 738–752.
- Shen, Y., Naujokas, M., Park, M., & Ireton, K. (2000) InIB-dependent internalization of *Listeria* is mediated by the Met receptor tyrosine kinase. *Cell*, **103**, 501–510.

-
- Slifman, N.R., Gershon, S.K., Lee, J.H., Edwards, E.T., & Braun, M.M. (2003) Listeria monocytogenes infection as a complication of treatment with tumor necrosis factor α -neutralizing agents. *Arthritis and Rheumatism*, **48**, 319–324.
- Soares, L., Seroogy, C., Skrenta, H., Anandasabapathy, N., Lovelace, P., Chung, C.D., Engleman, E., & Fathman, C.G. (2004) Two isoforms of otubain 1 regulate T cell anergy via GRAIL. *Nature Immunology*, **5**, 45–54.
- Stavru, F., Archambaud, C., & Cossart, P. (2011) Cell biology and immunology of Listeria monocytogenes infections: Novel insights. *Immunological Reviews*, **240**, 160–184.
- Suda, J., Dara, L., Yang, L., Aghajan, M., Song, Y., Kaplowitz, N., & Liu, Z.-X. (2016) Knockdown of RIPK1 Markedly Exacerbates Murine Immune-Mediated Liver Injury through Massive Apoptosis of Hepatocytes, Independent of Necroptosis and Inhibition of NF- κ B. *The Journal of Immunology*, **197**, 3120–3129.
- Sun, J.C. & Bevan, M.J. (2003) Defective CD8 T cell memory following acute infection without CD4 T cell help. *Science*, **300**, 339–342.
- Sun, X.X., Challagundla, K.B., & Dai, M.S. (2012) Positive regulation of p53 stability and activity by the deubiquitinating enzyme Otubain 1. *EMBO Journal*, **31**, 576–592.
- Szalay, G., Hess, J., & Kaufmann, S.H.E. (1995) Restricted replication of Listeria monocytogenes in a gamma interferon- activated murine hepatocyte line. *Infection and Immunity*, **63**, 3187–3195.
- Tacke, F., Luedde, T., & Trautwein, C. (2009) Inflammatory pathways in liver homeostasis and liver injury. *Clinical Reviews in Allergy and Immunology*, **36**, 4–12.
- Tang, Y., Joo, D., Liu, G., Tu, H., You, J., Jin, J., Zhao, X., Hung, M.C., & Lin, X. (2018) Linear ubiquitination of cFLIP induced by LUBAC contributes to TNF-induced apoptosis. *Journal of Biological Chemistry*, **293**, 20062–20072.
- Tenev, T., Bianchi, K., Darding, M., Broemer, M., Langlais, C., Wallberg, F., Zachariou, A., Lopez, J., MacFarlane, M., Cain, K., & Meier, P. (2011) The Ripoptosome, a Signaling Platform that Assembles in Response to Genotoxic Stress and Loss of IAPs. *Molecular Cell*, **43**, 432–448.
- Tiegs, G., Wolter, M., & Wendel, A. (1989) Tumor necrosis factor is a terminal mediator in galactosamine/endotoxin-induced hepatitis in mice. *Biochemical Pharmacology*, **38**, 627–631.
- Ting, A.T. & Bertrand, M.J.M. (2016) More to Life than NF- κ B in TNFR1 Signaling. *Trends in Immunology*, **37**, 535–545.

-
- Torres, D., Janot, L., Quesniaux, V.F.J., Grivennikov, S.I., Maillet, I., Sedgwick, J.D., Ryffel, B., & Erard, F. (2005) Membrane tumor necrosis factor confers partial protection to *Listeria* infection. *American Journal of Pathology*, **167**, 1677–1687.
- Vazquez, M.A., Sicher, S.C., Wright, W.J., Proctor, M.L., Schmalzried, S.R., Stallworth, K.R., Crowley, J.C., & Lu, C.Y. (1995) Differential regulation of TNF- α production by listeriolysin-producing versus nonproducing strains of *Listeria monocytogenes*. *Journal of Leukocyte Biology*, **58**, 556–562.
- Wajant, H., Pfizenmaier, K., & Scheurich, P. (2003) Tumor necrosis factor signaling. *Cell Death and Differentiation*, **10**, 45–65.
- Wajant, H. & Siegmund, D. (2019) TNFR1 and TNFR2 in the control of the life and death balance of macrophages. *Frontiers in Cell and Developmental Biology*, **7**, 1–14.
- Wang, S., Ni, H.M., Dorko, K., Kumer, S.C., Schmitt, T.M., Nawabi, A., Komatsu, M., Huang, H., & Ding, W.X. (2016) Increased hepatic receptor interacting protein kinase 3 expression due to impaired proteasomal functions contributes to alcohol-induced steatosis and liver injury. *Oncotarget*, **7**, 17681–17698.
- Wang, T., Yin, L., Cooper, E.M., Lai, M.Y., Dickey, S., Pickart, C.M., Fushman, D., Wilkinson, K.D., Cohen, R.E., & Wolberger, C. (2009) Evidence for Bidentate Substrate Binding as the Basis for the K48 Linkage Specificity of Otubain 1. *Journal of Molecular Biology*, **386**, 1011–1023.
- Wang, X., Mulas, F., Yi, W., Brunn, A., Nishanth, G., Just, S., Waisman, A., Brück, W., Deckert, M., & Schlüter, D. (2019) OTUB 1 inhibits CNS autoimmunity by preventing IFN- γ -induced hyperactivation of astrocytes. *EMBO Journal*, 1–17.
- Wang, Y., Zhou, X., Xu, M., Weng, W., Zhang, Q., Yang, Y., Wei, P., & Du, X. (2016) OTUB1-catalyzed deubiquitination of FOXM1 facilitates tumor progression and predicts a poor prognosis in ovarian cancer. *Oncotarget*, **7**, 36681–36697.
- Wertz, I.E. & Dixit, V.M. (2008) Ubiquitin-mediated regulation of TNFR1 signaling. *Cytokine and Growth Factor Reviews*, **19**, 313–324.
- Wicovsky, A., Salzman, S., Roos, C., Ehrenschrwender, M., Rosenthal, T., Siegmund, D., Henkler, F., Gohlke, F., Kneitz, C., & Wajant, H. (2009) TNF-like weak inducer of apoptosis inhibits proinflammatory TNF receptor-1 signaling. *Cell Death and Differentiation*, **16**, 1445–1459.
- Wiener, R., Zhang, X., Wang, T., & Wolberger, C. (2012) The mechanism of OTUB1-mediated inhibition of ubiquitination. *Nature*, **483**, 618–622.

-
- Wong, W.W.L., Vince, J.E., Lalaoui, N., Lawlor, K.E., Chau, D., Bankovacki, A., Anderton, H., Metcalf, D., O'Reilly, L., Jost, P.J., Murphy, J.M., Alexander, W.S., Strasser, A., Vaux, D.L., & Silke, J. (2014) cIAPs and XIAP regulate myelopoiesis through cytokine production in an RIPK1- And RIPK3-dependent manner. *Blood*, **123**, 2562–2572.
- Wroblewski, R., Armaka, M., Kondylis, V., Pasparakis, M., Walczak, H., Mittrücker, H.W., Schramm, C., Lohse, A.W., Kollias, G., & Ehlken, H. (2016) Opposing role of tumor necrosis factor receptor 1 signaling in T cell–mediated hepatitis and bacterial infection in mice. *Hepatology*, **64**, 508–521.
- Wu, Y., Hu, S., Liu, J.U.N., Cao, H., Xu, W.E.I., Li, Y., & Li, L. (2014) Nature and mechanisms of hepatocyte apoptosis induced by D -galactosamine / lipopolysaccharide challenge in mice. *International Journal of Molecular Medicine*, 1498–1506.
- Ye, Y. & Rape, M. (2009) Building ubiquitin chains: E2 enzymes at work. *Nature Reviews Molecular Cell Biology*, **10**, 755–764.
- Yi, X., Yin, X.M., & Dong, Z. (2003) Inhibition of Bid-induced apoptosis by Bcl-2. tBid insertion, Bax translocation, and Bax/Bak oligomerization suppressed. *Journal of Biological Chemistry*, **278**, 16992–16999.
- Zenewicz, L.A. & Shen, H. (2007) Innate and adaptive immune responses to *Listeria monocytogenes*: a short overview. *Microbes and Infection*, **9**, 1208–1215.
- Zhang, X., Zhang, H., Xu, C., Li, X., Li, M., Wu, X., Pu, W., Zhou, B., Wang, H., Li, D., Ding, Q., Ying, H., Wang, H., & Zhang, H. (2019) Ubiquitination of RIPK1 suppresses programmed cell death by regulating RIPK1 kinase activation during embryogenesis. *Nature Communications*, **10**.
- Zhao, L., Wang, X., Yu, Y., Deng, L., Chen, L., Peng, X., Jiao, C., Gao, G., Tan, X., Pan, W., Ge, X., & Wang, P. (2018) OTUB1 protein suppresses mTOR complex 1 (mTORC1) activity by deubiquitinating the mTORC1 inhibitor DEPTOR. *Journal of Biological Chemistry*, **293**, 4883–4892.
- Zhou, H., Liu, Y., Zhu, R., Ding, F., Cao, X., Lin, D., & Liu, Z. (2018) OTUB1 promotes esophageal squamous cell carcinoma metastasis through modulating Snail stability. *Oncogene*, **37**, 3356–3368.
- Zhou, X., Yu, J., Cheng, X., Zhao, B., Manyam, G.C., Zhang, L., Schluns, K., Li, P., Wang, J., & Sun, S.C. (2019) The deubiquitinase Otub1 controls the activation of CD8⁺ T cells and NK cells by regulating IL-15-mediated priming. *Nature Immunology*, **20**, 879–889.

DECLARATION OF ORIGINALITY

Hiermit erkläre ich, dass ich die von mir eingereichte Dissertation zu dem Thema

Hepatocyte-specific role of the deubiquitinating enzyme OTUB1 during inflammatory liver diseases

selbstständig verfasst, nicht bereits als Dissertation verwendet habe und die benutzten Hilfsmittel und Quellen vollständig angegeben wurden.

Weiterhin erkläre ich, dass ich weder diese noch eine andere Arbeit zur Erlangung des akademischen Grades doctor rerum naturalium (Dr. rer. nat.) an anderen Einrichtungen eingereicht habe.

Magdeburg, 23.06.2020

Josephin Koschel

DECLARATION OF CRIMINAL CONVICTIONS

Ich erkläre hiermit, nicht wegen einer Straftat verurteilt worden zu sein, die Wissenschaftsbezug hat.

Magdeburg, 23.06.2020

Josephin Koschel

DECLARATION OF HONOR

Ich versichere hiermit, dass ich die vorliegende Arbeit ohne unzulässige Hilfe Dritter und ohne Benutzung anderer als der angegebenen Hilfsmittel angefertigt habe, verwendete fremde und eigene Quellen sind als solche kenntlich gemacht.

Ich habe insbesondere nicht wissenschaftlich:

- Ergebnisse erfunden oder widersprüchlich verschwiegen,
- statistische Verfahren absichtlich missbraucht, um meine Daten in ungerechtfertigter Weise zu interpretieren,
- fremde Ergebnisse oder Veröffentlichungen plagiiert,
- fremde Forschungsergebnisse verzerrt wiedergegeben.

Mir ist bekannt, dass Verstöße gegen das Urheberrecht Unterlassungs- und Schadenersatzansprüche des Urhebers sowie eine strafrechtliche Ahndung durch die Strafverfolgungsbehörden begründen kann.

Ich erkläre mich damit einverstanden, dass die Arbeit ggf. mit Mitteln der elektronischen Datenverarbeitung auf Plagiate überprüft werden kann.

Die Arbeit wurde bisher weder im Ausland in gleicher oder ähnlicher Form als Dissertation eingereicht und ist als Ganzes auch noch nicht veröffentlicht.

Magdeburg, 23.06.2020

Josephin Koschel